POLITECNICO DI TORINO

MASTER's Degree in ENERGY AND NUCLEAR ENGINEERING

MASTER's Degree Thesis

Investigation of variance reduction methods based on weight-windows for radiation transport simulation in deep penetration problems

Supervisors

Prof. Sandra DULLA

Dr. Nicolò ABRATE

M.Sc. Matteo ZAMMATARO

Dr. Matteo FALABINO

Candidate

Gianluca CANNILLO

NOVEMBER 2024

Acknowledgement

The thesis work was performed in collaboration with *new*cleo S.p.A. during an internship programme. Then I would like to express my gratitude to *new*cleo for the great opportunity that has been given to me, in particular the thanks go to my company supervisor, Dr. Daniele Tomatis (Head of Codes and Methods (C&M) Unit), for the very important advice and suggestions that has given for the planning of the work.

I would also like to thank Matteo Zammataro (research engineer) and Dr. Matteo Falabino (computational physicist) for the support they gave me, for explaining the methodologies I used during the internship and for their constant availability during the months of the internship.

From the academic point of view I would like to thanks my academic supervisor Prof. Sandra Dulla for the collaboration and the knowledge that she gave me during Nuclear Fission Reactor Physics and Transport Theory course and during Monte Carlo Methods course. Lastly, I would like to thank Dr. Nicolò Abrate, my academic co-supervisor, for his support and his ability to be a fundamental link between the Politecnico di Torino and *new*cleo during my time in the company and also for the suggestions I received while writing my thesis.

Abstract

In the nuclear field, radiation protection is crucial to prevent harm to the environment and human health. The most significant challenges in radiation protection are those associated with deep penetration, which have been studied in a very large set of applications, e.g, in the frame of nuclear reactor operation. The ultimate goal of radiation shielding calculations is the estimate of the dose delivered to workers; this calculation requires a set of different steps. To assess the dose estimation, it is necessary knows the particle distribution with a certain accuracy using deterministic or MC approaches. The main issue encountered with these kinds of calculations is that the simulated particles may not be able to reach the detector regions. This negatively contributes to the estimation of the particle flux, increasing the variance.
Over the years, considerable research and development efforts have been devoted to improve Monte Carlo codes with methodologies to reduce the statistical uncertainty associated with the results.
Variance Reduction (VR) methods based on weight-windows have been analyzed in this work. VR methods use statistical artifices to score statistically rare events, e.g., the particles reaching the detectors, still preserving the expected value of the statistical phenomena. The work demonstrated that one method called MAGIC (Method of Automatic Generation of Importances by Calculation) can be considered for different studies without the use of deterministic and quasi-deterministic solutions coupled with MC codes. In addition, a methodological improvement has been designed in the work. The performances of MAGIC has been optimized from the computational point of view using new stopping criteria that allow a better estimation of the particle flux in a reduced time.

Keywords: Deep penetration problems, Particle flux estimation, Variance Reduction (VR) methods, Weight-windows, MAGIC method, New optimization

Contents

List of Figures

List of Tables

Chapter 1

Introduction

Among the Generation-IV concepts, Lead-cooled Fast Reactors (LFRs) are excellent candidates to meet the current requirements of the nuclear energy sector in terms of economic, environmental and safety sustainability. The features of LFRs, which encompass the adoption of a fast neutron spectrum and of liquid lead as coolant, allows to minimise long-term radioactive wastes and the proliferation risk while enhancing the overall safety level and economic competitiveness. The design calculations for developing the LFR concept at *new*cleo include a series of radiation transport simulations performed using Monte Carlo (MC) codes. MC codes are based on statistical sampling techniques for simulating many replicas of the particles, with the goal of estimating averaged macroscopic quantities (e.g. the neutron flux). The main issue is that particles simulated using MC codes may not reach the detector zones to perform dose rate assessment, typically situated far from the radioactive source. This set of problems are called deep penetration problems and with the slow convergence of MC methods it can be difficult to obtain a reliable estimate of the particle flux in all reactor regions (low statistical uncertainty associated with the estimation).
Even if the particles reach the detectors regions, their number could be not enough to get reliable results.
Variance Reduction (VR) techniques, which artificially increase the probability of rare events while maintaining the same expected value, are commonly used to overcome these issues. The statistical artifice allows for a larger statistical sample in deep regions to reduce the variance associated with the particle flux estimation.

Standard VR methods are used to give greater importance to specific regions of the reactor, favouring the transport of the particles towards these regions.
Global Variance Reduction (GVR) methods aim at equally populating each region of the model. This allows physical observables to be estimated with an acceptable level of accuracy over the entire model [1].
The focus of the thesis is the investigation of one of these VR methods for the preliminary reactor design based on the Weight Windows (WW) approach [2].
One of the possible statistical artifices is the assignment of a weight to the particles, a quantity that allows to favor the penetration of the particles. Each particle is born with a unitary weight, which changes after each collision according to a formula that will be analyzed in the next chapters. This assignment is introduced to prevent the end of their

simulations in case of capture. In this way, they can reach detectors in deep regions of the domain for the estimation of the flux.
The use of the weight is a standard VR methodology but in the detector regions, the particles could have a very low weight compared to the average weight. Consequently the life (history) of the particles can increase the computational time without giving an effective contribution to the particle flux estimation.
On the other hand, some particles could have a high weight relatively to the average one that contribute to a high variance. A population control is necessary to fix these issues and the WW approach offers the possibility to avoid overpopulated or underpopulated regions. The domain under investigation is divided into phase-space regions. For each region a WW is assigned consisting of an upper and lower limit. When a particle enters in a weight window, its weight is compared with the weight window bounds. A particle is split if its weight is above the upper limit of the window, and Russian roulette is played if the particle's weight is below the lower limit. If the particle's weight is within the weight window, it can continue its history without any weight change.

Over the years, many proposals have been considered to properly set the weight window bounds. A suitable approach is to set the WW bounds using the particle flux as proposed by Cooper and Larsen in 2001 [3]. The flux can be calculated using deterministic or quasi-deterministic solutions that could be difficult to obtain in complex geometries. In 2011 A.Davis and A.Turner suggested an alternative method called MAGIC (Method of Automatic Generation of Importances by Calculation). The fundamental principle is using an initial analog MC run (with poor accuracy and without variance reduction techniques) to determine an approximate flux distribution in the system.
The flux estimation is used to compute Monte Carlo weight windows with better precision and the process is iterated until the entire system is not fully covered. The use of the MAGIC coupled with the WW is useful to perform a GVR method, that estimate reliable neutron flux for subsequent analysis and dose rate assessments.

During the work, further investigation of different options for MAGIC to optimize the simulation results will be carried out. A new suggestion for a proper use of the WW and the MAGIC will be provided with a new algorithm that automatically stops the MAGIC algorithm. Some results are shown also for the MAGIC-GPS improvement proposed in 2023 [4]. Furthermore a comparison with other VR methods will be considered to verify the effectiveness of the method during the analysis of the results.

The Chapter 2 describes the theoretical background starting from the Neutron Transport Equation (NTE) [5] that is necessary to quantify the neutron distribution in the reactor. Moreover the MC methods are linked with the resolution of the NTE with a brief investigation on the implementation of OpenMC, MC code. After a brief historical review, a basic overview will be given about the others VR methods used to assess the performance with the MAGIC (Chapter 3). To test WW and MAGIC different models in Continuous and in Multi-group mode will be presented and tested in Chapters 4, 5.
At the end of the work different conclusions have been collected aims to offer a proper validation of MAGIC in a wide range of models and unfavorable situations.

Chapter 2

Theoretical Background

The physical phenomena that occur in the universe are based on the interactions of the particles [6][7]. In nuclear physics the particles can be subdivided into:

- Neutral particles that include neutrons (n) produced by fission, fusion or other energetic reactions, and photons (γ) emitted by nuclear reactions, radioactive decay and activated nuclides.
- Charged particles such as electrons, positrons and heavy ions concerned with alpha/beta decay, accelerator applications and space physics.

The development and the design of nuclear fission reactors is based on the interactions of particles with matter. The physics of the neutrons and their behavior can be described by the Neutron Transport Equation (NTE) [5]:

$$\begin{aligned} &\frac{1}{v}\frac{\partial\phi(\mathbf{r},\mathbf{\Omega},E,t)}{\partial t} + \Omega\cdot\nabla\phi(\mathbf{r},\mathbf{\Omega},E,t) + \Sigma(\mathbf{r},E)\phi(\mathbf{r},\mathbf{\Omega},E,t) = \\ &\oint_{4\pi}\int_0^\infty \Sigma_s(\mathbf{r},E')f_s(\mathbf{r},\mathbf{\Omega}'\cdot\mathbf{\Omega},E'\rightarrow E)\phi(\mathbf{r},\mathbf{\Omega}',E',t)d\mathbf{\Omega}'dE' + \\ &\frac{\chi(\mathbf{r},E)}{4\pi}\int_0^\infty \nu(\mathbf{r},E')\Sigma_f(\mathbf{r},E')\phi(\mathbf{r},\mathbf{\Omega}',E',t)dE' + S(\mathbf{r},\mathbf{\Omega},E,t) \end{aligned} \tag{2.1}$$

where $\phi(\mathbf{r},\mathbf{\Omega},E,t)$ is the neutron flux defined in a six-dimensional space called phase-space. It describes the n population, and its evolution in time is evaluated through the first term of Eq. (2.1).
In the left-hand side of the NTE the "loss terms" are defined, i.e the streaming term and the collision term. To take into account the collisions, the total reaction rate is introduced into the NTE ($\Sigma\phi$) where Σ is the probability that a neutron collides per unit path and is called total cross section.

The right hand side of the NTE contains the "source terms":

- The "Scattering source", where Σ_s (scattering cross-section) is the probability that a neutron makes a scattering per unit path and this also contains information about the type of scattering (elastic or inelastic), and f_s is the scattering probability density function that depends on the position of the neutron. Moreover, it depends on the energy and direction before ($\mathbf{\Omega}$',E') and after the collision ($\mathbf{\Omega}$,E). The scattering

function integrated on the angle and the energy becomes the probability that a neutron are emitted in dE' and d$\mathbf{\Omega}$' interval after a scattering.

- The "Fission source" takes into account the neutrons emitted in the system by fissions. $\chi(\mathbf{r}, E)$ is a probability density function called "Fission spectrum", which describes the probability of a neutron being emitted at a given energy (E). The fissions can be considered isotropic, which means that a factor $1/4\pi$ is introduced to enfore the normalisation condition for flying direction. ν is the number of neutrons emitted per fission, and Σ_f is the probability of a neutron making a fission per unit path, defined as fission cross-section.

- S is an external source of neutrons acting in the system.

A similar equation can be formulated for the photons, where the cross sections are specific for photons interactions.
To solve the NTE, a set of initial and Boundary Conditions (BCs) is necessary. The initial conditions, in general are introduced as a fixed neutron flux value at t=0.

$$\phi(\mathbf{r}, \mathbf{\Omega}, E, t = 0) = \phi_0(\mathbf{r}, \mathbf{\Omega}, E) \tag{2.2}$$

The Boundary conditions require a bigger attention because they can modify the results of the system. First of all, it is necessary to assume that the space domain is a non-returning (convex) and simply connected one. This is physically translated into a void/vacuum state in which neutrons can leave the system but cannot re-enter because they cannot collide anymore [7]. The assumption is fair because the neutron in air has almost the same behavior as in the vacuum. Mathematically , it is possible define the boundary of the domain as a point of the phase-space:

$$x = (\mathbf{r}, \mathbf{\Omega}, E) \qquad \mathbf{r} \in \partial D, \mathbf{\Omega} \cdot n(\mathbf{r})^+ < 0 \tag{2.3}$$

The incoming direction ($\mathbf{\Omega}_{incoming}$) is described by the negative product of $\mathbf{\Omega}$ with the normal vector $n(\mathbf{r})^+$ (it is defined as exiting from the boundary of the domain) in Eq. (2.3). The vacuum condition can be written as the incoming flux equal to 0 at the boundaries:

$$\phi(x, \mathbf{\Omega}_{incoming}, E, t) = 0 \tag{2.4}$$

From the practical point of view the steady-state NTE can be cast in two ways:

- Eigenvalue problem: let's consider a system without source and in steady-state condition. Eq. (2.1) can be rewritten as follows:

$$\hat{T}\phi = \hat{\theta_s}\phi + \frac{1}{k}\hat{F}\phi \tag{2.5}$$

  where $\hat{T}$, $\hat{\theta_s}$, and $\hat{F}$ are the Transport, Scattering and Fission operators applied on the neutron flux in steady state condition. To find a non-zero solution for the Eq. (2.5), an eigenvalue k is introduced.
  If k = 1, the system is called critical, meaning that the neutron population is self-sustaining.

If $k < 1$ means that the fission process is not able to compensate the leakage, the system is not self-sustaining and the system is called subcritical.
If $k > 1$ means that the neutrons emitted by fissions are larger than the neutron lost for leakage, the system is called supercritical.

The quantity of interest are k and ϕ, and to solve this equation an iterative procedure called "Power method" is performed. The first step is the introduction of a guess value for k and ϕ defined as $k^{(0)}$ and $\phi^{(0)}$. These guess can used in the Fission operator:

$$\frac{1}{k^{(0)}}\hat{F}\phi^{(0)} = S_f^{(0)} \tag{2.6}$$

$S_f^{(0)}$ in Eq. (2.6) can be seen as a source and we can apply it in Eq. (2.1) in a non multiplicative medium form (without fission operator because it is considered inside S_f):

$$\hat{T}\phi^{(1)} = \hat{\theta}_s\phi^{(1)} + S_f^{(0)} \tag{2.7}$$

From the Eq. (2.7) is possible find $\phi^{(1)}$ and use it into Eq. (2.6) to define a new $S_f^{(1)}$. The iterative process is repeated until the flux and the eigenvalue have been found with a lower relative error. For k the error should be in the order of 10^{-5} (P.C.M.). The Eq. (2.6) for n-th iteration can be written as follows:

$$\hat{T}\phi^{(n+1)} = \hat{\theta}_s\phi^{(n+1)} + \frac{1}{k^{(n)}}\hat{F}\phi^{(n)} \tag{2.8}$$

- Fixed source problem, the system in this case is considered heterogeneous due to introduction of an external fixed source S, the Eq. (2.1) can be written as:

$$\hat{T}\phi = \hat{\theta}_s\phi + S \tag{2.9}$$

The resulting equation is considered as a differential equation in space and as an integral over energy and direction. To solve the fixed source calculation, different approximations of the integral and a numerical scheme have to be introduced.
In addition, the integral term is coupled to the solution for each angular direction, and the coupling problems are typically handled by the iterative Gauss-Seidel method [8].

These problems aim to calculate the neutron flux through iterative methodologies and they can be solved with different approaches:

- Deterministic approach [5], in which some approximations are necessary to reduce the complexity of the NTE:

  1. The geometry is discretized into a small number of homogeneous material regions. For instance a standard approach considers the fuel assembly of the reactor as homogeneous, even if inside the region there are different materials. The geometry approximations allow to reduce the number of cross sections inside the NTE.

2. The continuous energy dependence of the cross sections. The whole energy spectrum is condensed into a number of discrete energy groups (Multi-group theory [9]).
3. The angular dependence in the scattering probability density function and in the neutron flux can be difficulty to evaluate. To overcome these issues, the approximations uses the functional expansions (Legendre Polynomials) or discrete directions. The handling of the angular dependence is what distinguishes the approximation methods (S_N, P_N, method of characteristics and diffusion theory).

- Monte Carlo (MC) methods do not introduce any approximations to solve the NTE. They are used to provide a statistical estimations of the integrals in the scattering and fission terms. The possibility of avoiding approximations is one of the reasons why MC methods have been studied over the years, despite the solution of the problem is featured by statistical uncertainty [10].

2.1 MC background

The following paragraph gives a theoretical introduction to MC methods. The resolution of the integrals in the scattering and fission source term is fundamental to handle the NTE. The methods perform a statistical sampling on a computer to estimate the physical observables of interest.

Using the Probability Density Functions (PDFs), it is possible to investigate the evolution and the occurrence probability of some events, for instance how many times a neutron collides during its lifetime.
The PDF, indicates as f(x), depends on an independent variable (x) and contains all the information about the probability that any event happens. The space in which the density function is defined is called "Sample Space" (S) [10]. In the nuclear physics the sample space is called Phase-space (3 variables in the space and 1 variable in energy) and the density function describes the physics of the problem containing all the operators (Collision, Transport, Fission and Scattering) of the NTE.

The MC methods require the definition of Random Variable ξ (RV) to perform statistical sampling starting from the PDF. ξ is an application that starts from the Sample Space and for each outcome/event of the PDF returns a real number.
The RVs can be defined "discrete" when the probability of occurrence of an event is fixed or "continuous" when they can take any value in a specified interval in the continuum.
The properties of the PDF ($f_\xi(x)$) are described by the probability theory: it is always positive and normalised (i.e. its integral over the sample space is 1).

From the practical point of view MC methods aim at doing something the integral form inside of the NTE. The mean value can be calculated for each distribution as the first order moment:

$$E[x] = \int_a^b x f_\xi(x) dx \ (Mean\ value) \tag{2.10}$$

where x is distributed according to $f_\xi(x)$. The statistical sampling techniques are useful to perform an estimation of the mean value defined as:

$$\bar{\xi}^{(N)} = \frac{1}{N}\sum_{i=1}^{N}\xi_i,\ (Sample\ average) \tag{2.11}$$

where N is the number of experiments. For each experiment a random variable ξ_i is assigned, generated according to the PDF of the problem. The ξ_i are statistically independent and identically distributed and this is a fundamental hypothesis. Statistically independent means that each RV is generated independently by the others. The RVs are identically distributed when they follow the same statistical law/distribution (PDF).
If the number of experiments is sufficiently large ($\rightarrow \infty$), the sample average tends to the mean value.
It is possible rewrite the general integral as follows:

$$R = \int_D \xi(x) f_\xi(x) \tag{2.12}$$

where $\xi(x)$ is an estimator of the function f of the Eq. (**??**) and it depends on the integral under consideration, and D is the domain over which the integral is evaluated. For instance, if we consider the scattering integral, the estimator function is an estimator of the scattering cross section that returns an estimate of the average number of times a neutron makes a scattering.
A finite integral is equivalent to the expected value of its integrand, then it is possible use the Eq. 2.11 to estimate the value of any integral in the NTE.

However, the estimation of the average behavior of a physical phenomenon using a statistical sampling has an associated uncertainty, which depends mainly on the number of experiments performed for the evaluation. In general statistics it is called variance, the expected value of the squared deviation from the mean of a random variable.
The variance of the distribution depends by the characteristics of the PDF and it can be calculated using the second order of the moment of the distribution:

$$E[x^2] = \int_a^b x^2 f_\xi(x)dx,\ (Second\ order\ moment) \tag{2.13}$$

$$\sigma^2(x) = E[x^2] - E[x]^2,\ (Variance\ of\ the\ distribution) \tag{2.14}$$

In the statistical sampling process, a variance can be associated with the sample average:

$$\bar{\sigma}_x^2 = \frac{1}{N-1}\sum_{i=1}^{N}(\xi_i - \bar{\xi}^{(N)})^2\ (Sample\ variance) \tag{2.15}$$

Also for the sample variance, if the number of experiments is sufficiently large its value tends to the variance of the distribution. The lower the value of the sample variance is in our estimation, the more accurate the estimation of the mean value will be. Moreover, it is possible to define other two useful quantities from Eq. (2.15):

- The Standard Deviation (SD) $\bar{\sigma}_x = \sqrt{\bar{\sigma}_x^2}$
- The Relative Standard Deviation (RSD) , obtained by dividing the standard deviation by the sample mean.

The key point is the convergence of the variance, which in the case of MC methods is inversely proportional to the square root of experiments N. To have a good statistics (low variance) the number of samples have to increase and it is proportional to the computational time.

2.2 Monte Carlo Methods for Particle Transport

The statistical sampling is a technique that can be applied to a wide set of problems. For *new*cleo purposes, MC methods are applied to simulate the transport of neutral particles, i.e., neutrons and photons. The transport equation contains a term for the displacement of the particles and other terms for the different events that can happen during their life. The displacement in the space is studied through the exponential distribution [10] probability density function. In general, the PDF is defined in $[0, \infty)$ as follows:

$$f(x) = \Sigma_t(x) \cdot e^{-\int_0^\infty \Sigma_t(x)dx} \; for \; x >= 0, \tag{2.16}$$

where $\Sigma_t(x)$ $[cm^{-1}]$ is the total cross-section introduced in the NTE (Eq. (2.1)) and it depends by the medium in which the particles stream.
If the total cross section does not depend by the space, i.e. for a homogeneous medium, the distribution can be simplified:

$$f(x) = \Sigma_t \cdot e^{-\Sigma_t \cdot x} \tag{2.17}$$

The mean value of this distribution can be easily calculated using Eq. (2.10): $1/\Sigma_t$. It physically represents the mean free path travelled by the particles in a homogeneous medium having Σ_t.
However, each particle travels a different path and the final goal is to understand where the particles can arrive (inside and outside the system). To evaluate their path, for each particle a Random Walk (RW) [11] is generated through a MC code using the "direct sampling method" [12] or the "inverse transform method". This approach correlates a random number for the statistical sample to the Cumulative Density Function (CDF or F(x)) that is strictly related to the PDF:

$$F(x) = \int_{-\infty}^{x} f(x')dx' \tag{2.18}$$

The CDF have some important properties according to the probability theory:

- $0 \leq$ F(x) $\leq$ 1
- Monotonically not decreasing
- $\lim_{x \to -\infty} F(x) = 0, \lim_{x \to \infty} F(x) = 1$

For the exponential distribution, the CDF in the case of a homogeneous medium is the following:

$$F(x) = e^{-\Sigma_t \cdot x} \tag{2.19}$$

Applying the inverse transform method, we can generate randomly the random variable for the path traveled by each particle:

$$F(x) = e^{-\Sigma_t \cdot x} = \rho, \tag{2.20}$$

the random number ρ is generated uniformly between [0,1) and we can invert Eq. (2.20) to find "l" parameter, the distance traveled by a particle until the next collision (its transport in a medium having Σ_t):

$$l = -\frac{ln(\rho)}{\Sigma_t} \tag{2.21}$$

The MC codes are useful to simulate a large number of particle paths or experiments (N). The path of the particle from its starting position to its end is called "history". MC codes simulate the histories of many particles generating the random numbers. In the fixed source mode, an initial population of particles is considered and the starting positions are generated from the specified source. Using this mode, the MC code estimates the particle flux in a region of interest, or other quantities such as reaction rates, as a response to a user-defined source.
In the eigenvalue problem, the MC code simulates the nuclear chain reaction and applies the power iteration method for the criticality problem (the main output is the eigenvalue k).

2.2.1 Simulation of the Particles Transport using OpenMC

In the thesis, the OpenMC, will be used in fixed source mode because the main scope is a reliable estimation of the particle flux. OpenMC is an open-source code that simulates the particle histories with different steps [13]:

1. The source is initialized and also cross section data in case of multi-group mode (MG) or continuous-energy mode (CE) are obtained.

2. The domain is divided in spatial cells and for each cell a material is assigned with associated properties.
   The simulation of a particle starts, the first control is if spatial position is inside the geometry and inside the energy interval considered.

3. The distance to the next collision is sampled according to Eq (2.21).

4. If the distance to the nearest boundary of a cell is lower than the distance between 2 collisions, the particle is moved to the boundary. The particle will collide and the type of collision will be sampled.

5. For continuous-energy simulations, different nuclides compose our materials. OpenMC samples the probability that the particles collides with a certain nuclide:

$$P(i) = \frac{\Sigma_{t,i}}{\Sigma_t}, \tag{2.22}$$

where P_i is the probability that collision occurs with nuclide i, $\Sigma_{t,i}$ is the total cross section of the nuclide i at particle's energy. In MG mode, the above formula is not used because nuclides are not specified. Cross sections data are defined by the user for each energy group.

6. For the sampled nuclide, OpenMC samples also the reaction that occurs as collision:

$$P(k)_i = \frac{\sigma_k}{\sigma_t}, \tag{2.23}$$

where $P(k_i)$ is the probability that reaction k occurs for the nuclide sampled i, σ_x is the microscopic cross section for each reaction k, and σ_t is the total one. Subsequently, if the particles is not captured a new pseudo random number is generated and a new path is calculated. The steps 3 to 6 are repeated until all the particles history are not simulated.

7. When a particle enters in a detector region, typically MC code estimators increase a counter (called tally). OpenMC accumulates sum and sum of squares for each detector region. Using sum the sample mean and the variance is calculated according to the Eqs. (2.11) and (2.15).

2.2.2 OpenMC Estimators

The estimation of macroscopic quantities in Monte Carlo codes is based on the random generations of particles path. To evaluate the macroscopic quantities, Monte Carlo codes use the concept of "Tally". A tally is a counter that gives us information about any quantity of interest. In each Monte Carlo code a Tally can be defined as follows:

$$X = \int d\mathbf{r} \int d\mathbf{\Omega} \int dE\, f(\mathbf{r}, \mathbf{\Omega}, E)\phi(\mathbf{r}, \mathbf{\Omega}, E), \tag{2.24}$$

where the integrals are the filters that the user can assign during the tally definition for each region of the phase-space, f is the scoring function that depends by the quantity to be estimated. ϕ is the flux dependent by space, angle and energy. For example in case of scattering reaction rate ($\Sigma_s \cdot \phi$) the scoring function will be an estimator of the scattering cross section. The counter is increased when a scattering occurs in the detector region. The Eq. (2.24) introduced in OpenMC is equivalent to the one proposed in the MC theory [10].
There are 3 different estimator which tallies in OpenMC [13] estimate the reaction rates or other macroscopic quantities:

1. Analog Estimator, the simplest one. Essentially, we count the number of actual reactions taking place and use this as our estimate of the reaction rate.

$$R_x = \frac{1}{W} \sum_{i \in A} w_i, \tag{2.25}$$

where R_x is the reaction x, i denotes an index for each event, A is the set of all events resulting in reaction x, and W is the total starting weight of the particles (typically is 1), and w_i is the pre-collision weight of the particle as it enters event i.

2. Collision Estimator: the analogue estimator is very simple but it can be insufficient in estimating some rare events. Another estimator can be considered to allow us to score the tally in a more probable way.
   It is based on the contribution, in fact in this case each collision contributes to the score, different from the Analog Estimator in which we only consider when a reaction happens.

   For example, if we want to estimate the neutron flux, we can start from the total reaction rate $R = \Sigma_t \phi$, where ϕ is the scalar flux. The flux can be calculated through the estimation of the total reaction rate divided by the total macroscopic cross section:
   $$\phi = \frac{1}{W} \sum_{i \in C} \frac{w_i}{\Sigma_t(E_i)}. \tag{2.26}$$
   C is the set of all events resulting in a collision with a nucleus, and $\Sigma_t(E_i)$ is the total macroscopic cross section of the target material at the incoming energy of the particle E_i.

3. Track-length Estimator, which increases the possibility to have a score to the tally is based on the length traveled by the particles.
   $$V\phi = \frac{1}{W} \sum_{i \in T} w_i l_i, \tag{2.27}$$
   where V is the volume, T is the set of all T is the set of all the particle's trajectories within the desired volume and l_i is the length of the i-th trajectory.

In the calculations (in fixed source mode) that we have performed the choice is the Track-length estimator, the default OpenMC estimator.

Chapter 3

Variance Reduction methods review

The MC background (section 2.1) showed that the variance associated with the mean value of physical observables needs to be as low as possible. To obtain a low variance, it is necessary to increase the number of simulated particles / histories. In deep penetration problems, the number of histories can be very large, but a higher number of simulated particles leads to a higher computational time and the reliability of the results may take a long time.
For these kind of problems the tally does not score enough contributions/random variables and the estimation of the physical quantities (e.g. particle flux) may have a high variance.

The estimation of the sample mean and sample variance converges as $\sqrt{1/N}$ as shown in Eqs. (2.11) and (2.15). The estimation of the particle flux requires an accurate estimation in order to correctly perform the dose rate assessment (a very important step during the reactor design process).
To reduce the variance associated with the particle flux estimation, different Variance Reduction (VR) methods have been proposed during the years.

VR methods favor some rare events through some statistical artifice. In this way, the particles could reach more easily the tally and can contribute to the sample variance estimation. Their use is fair because they maintain the same mean value of the physical phenomenon. The VR methods can be performed locally or globally in the domain, the choice depends on the problem to be solved [1]:

- *Local Variance Reduction methods*, the idea is to assign an importance to each phase space region. The importance will be higher, where the detectors are located. The particles tend to move in the regions of higher importance, to make the estimation of the tally more accurate in the detector region. The local VR methods are very useful if the user knows the exact position of the detector and the geometry of the reactor. This VR family is not usually used during the design process, and assigning importance could lead to statistical biases (e.g., the particles tends to stream in specified regions but the VR method does not preserve the same mean value of the physical phenomenon).

- *Global Variance Reduction (GVR) methods*, it attempts to transport particles everywhere in the model. The idea is trying to have an estimation of the particle flux with a lower variance in the whole domain. The user can obtain a reliable estimation

of the particle flux in the regions near the source but also in deep regions, where typically the detectors are placed.

The statistical artifice introduced maintains the same sample mean using different strategies that can be applied to Local and Global VR methods:

1. *Modified Sampling Methods*, it adjusts radiation transport using different probability density functions in order to direct particles in high-importance zones. Introducing a new probability density function in the mean value calculation the rare events in the tally zone can be sampled more easily. In general it is considered multiply and divide for a new PDF, the random variables are generated according to new probability density function.
   To reduce the variance maintaining the same mean value and to avoid distortion of the statistics, the concept of particle weight is introduced. The mean value in Eq. (2.10) can be modified as follows:

$$E[x] = \int_a^b x \frac{f(x)}{f^*(x)} \cdot f^*(x) dx \tag{3.1}$$

   where the ratio between the 2 probability density function is defined as the average weight of the particles (w^*). The new probability density function can be chosen with different criteria, for example changing the cross sections of the medium or the particles direction to facilitate the score.
   One possibility is the exponential transform, which is performed through the adjustment of the macroscopic cross section. In zones with higher importance, the total cross section is decreased in order to have less capture while in zone with lower importance zone, the cross section is increased. The total cross section and the particle weight (w^*) are adjusted/calibrated as follows to preserve the statistics:

$$\Sigma_t^* = \Sigma_t (1 - p \cdot \mu) \tag{3.2}$$

$$w^* = \frac{\Sigma_t e^{-\Sigma_t s}}{\Sigma_t^* e^{-\Sigma_t^* s}}, \tag{3.3}$$

   where Σ_t^* is the adjusted total macroscopic cross section, Σ_t is the total cross section from nuclear data, p is the transform parameter that is difficult to choice properly and $\cos\theta$ is the cosine of the angle between preferred and particle direction.
   Another way to adjust radiation transport with new probability density function is considering the particles' directionality (Source Biasing method). The advantage is that the probability to bias particles in function of energy, direction and space can be performed separately. However Exponential Transform and Source Biasing are very dependent on the user's choice of parameters and for these reason, other methods have been investigated.

2. *Truncation methods*, it is based on stopping of the tracked particles in regions of the phase space that have a minor importance for the tally. This truncation can be performed in the space (when a particle reaches a certain low importance zone, it is eliminated), or in energy (when its energy is too low to contribute to the tally score, its history ends). The main issue of these methods is that the user need to

pay attention to the criteria used in the truncation of the particles history. If the truncation criteria are set in a wrong way, the particles histories important for the estimation could end prematurely.

3. *Partially deterministic methods*, it typically uses a response function that is calculated with the deterministic approaches (section 2), which makes stochastic Monte Carlo unnecessary in certain regions of the problem. In these regions, the probability of scattering in the region of interest is deterministically calculated and recorded by an associated tallying at each step of the Monte Carlo random walk. The use of a deterministic solution introduces a series of approximations, which can strongly affect the results.

4. *Population control methods*. It adjusts the density of the particles in the problem to achieve better sampling in the domain by preferentially increasing or decreasing the particle population in different regions. The approach of these methods is based on Splitting, Rouletting, and Weight Windows which were proposed by Booth and Hendricks [14]. In the next sections one of these Population control methods will be investigated.

3.1 Population control method based on the weight windows

3.1.1 Historical review

Many VR methods assign importance to each phase-space cell. In this case, the importance represents the interest for the phase-space region and mapping the entire domain, it is possible favor the particle transport in higher importance regions. Estimating the importance map is the key to using these methods correctly. In 1984 Booth and Hendricks proposed a first approach to achieve this scope based on the theoretical MC principles [15]. They started considering the idea of MacDonald [16] & Cashwell [17], and Deutsch & Carter approach [18].
Figure 3.1 shows the Booth and Hendricks study during the years. MacDonald and Cashwell shown that the MC code can split surfaces using pattern recognition. However, this automated splitting may be unreliable in case of complex geometry. For this reason, Booth and Hendricks studied Deutsch and Carter's work, in which the estimation of the importances at geometry surfaces is performed during forward MC calculations. Between 1981 and 1984, Booth and Hendricks proposed a different approach for estimating importances and controlling population subdividing the domain in cells.

A Cell is a region of the phase-space which is defined in energy and space. Its importance can then be defined as the expected score generated by a unit weight particle after entering the cell.

The weight of the particle is the score that considers the particle's collision and it changes for any kind of collision. Booth suggested a way to estimate the Cell importance using the

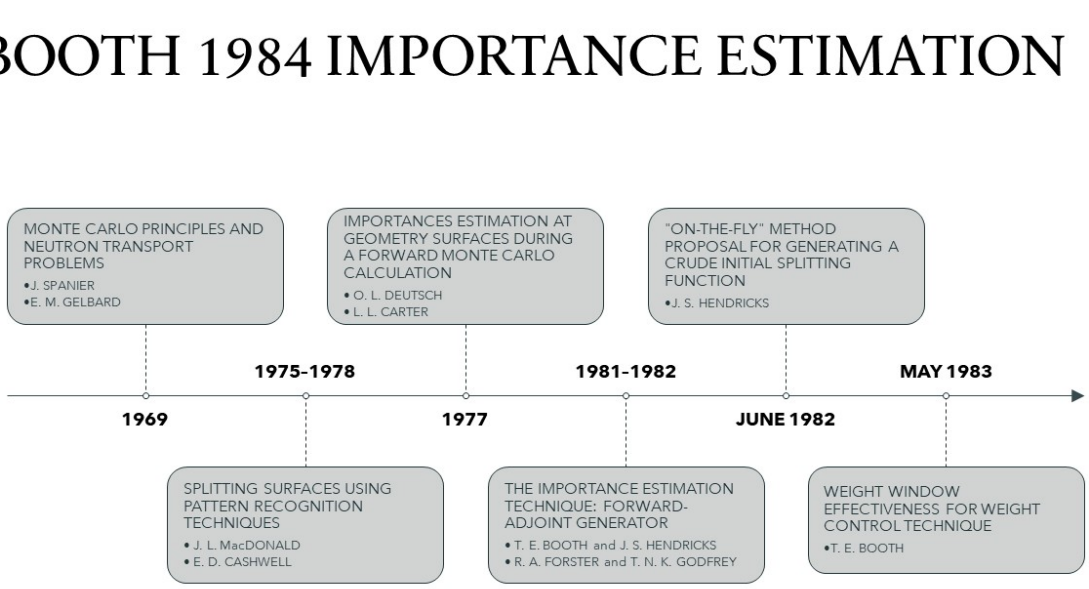

Figure 3.1: Timeline for importance estimation in forward Monte Carlo calculations of Booth-Hendricks

score of the particles and the weight concept:

$$Importance = \frac{total\ weight\ due\ to\ particles\ (and\ their\ progeny)\ entering\ the\ cell}{total\ weight\ entering\ the\ cell} \tag{3.4}$$

Its generator is based on a forward-adjoint method[19] that estimates the optimal importance function for subsequent runs and generate space-energy dependent weight windows. The Forward-adjoint method is not correlated to the adjoint flux estimation, the main problem encountered is a bad estimation of the importance function due to the statistical nature of the generator. Further analysis confirm that often the unreliable estimation is correlated to the importance function guess.

The difference between MacDonald-Cashwell's technique and Booth's generator is the subdivision of the phase-space. The Forward-adjoint generator is not capable to learn how the phase-space should have been divided but only the average importance of the given phase-space regions.
To fix the importance guess problem, in 1982 J. Hendricks [20] presented an "On-the-Fly" method that does not need any initial importance function. The weights of the particles entering and leaving each cell are different, generally because there are different collisions/splittings/roulettings. The splitting parameter is inversely proportional to the average cell weight, and this is suitable to cover the system uniformly [21] [22].
Differently from the Forward-Adjoint Method, the On-the-Fly method has an update for the splitting parameters during the run.
The final goal of the generator is an importance function that will improve the computa-

tional efficiency of the problem.

On-the-Fly Method	Forward-Adjoint Method
1. Starts with no initial importance function.	1. Requires crude initial importance function.
2. Continually changes its splitting parameters during the course of a calculation.	2. Does not affect the calculation; produces an importance function for subsequent use.
3. Resulting splitting parameters tend to populate space uniformly, which is good for some problems, crude for most.	3. Resulting importance function tends to optimize the efficiency of a particular tally by emphasizing important phase-space regions and deemphasizing unimportant regions.

Figure 3.2: Comparison of the Forward-Adjoint Method and "On-the-Fly" Method [14]

3.1.2 Use of the weight windows in the VR methods

Without a VR method in deep penetration problems, the simulated particles may arrive very close to the detectors but their life usually end before reaching the detector due to capture, even if the number of histories is very large. When this happens, the contribution to the tally is lost, the statistical sample is smaller and the sample variance increases.

To avoid increasing the number of histories and the computational time, a VR method based on the weight is considered. A weight is assigned to each particle. In general new particles gave a unitary weight that changed after each collision. In this way, the particles that would not able to reach the detectors can contributes to the sample average and the sample variance estimation, despite with a small contribution
To be fair with the statistics and, hence, with the physics of the problem, in Eqs. (2.11) and (2.15) the weight of the particles is taken into account in the estimation:

$$E[x] = \int_a^b x \frac{f(x)}{f^*(x)} \cdot f^*(x)dx - - > \bar{\xi}^{(N)} = \frac{1}{N}\sum_{i=1}^{N} \xi_i \cdot w_i \tag{3.5}$$

The ratio between the 2 probability density functions is defined like the weight. For the sample average, the weight (w_i) is assigned for each random variable (ξ_i). The approach in which a capture does not terminate the particles history is called implicit capture and it is the kernel of the VR method. The change of the weight occurs independently on the kind of the collision according to the following formula [13] in OpenMC:

$$w_i^* = w_i \cdot \left(1 - \frac{\sigma_a(E)}{\sigma_t(E)}\right), \tag{3.6}$$

where the absorption cross section σ_a and the total microscopic cross section σ_t depend on the nuclide involved in the collision. The quantity in the brackets represents the probability to have a scattering at a given particle energy.
Using the implicit capture, the simulations of the particles end only if they leak by the control volume or when their weight falls below a weight cut-off (in OpenMC the default value is 10^{-38}).

The VR method based on the weight seems to be very powerful because each particle simulated can contributes to the sampling without any statistical lose, however some issues can appear using the weight approach. The sample mean is estimated with the particles weight. Therefore, if the w_i are very different between them in a phase space region the sample variance increases, being the squared distance of each RV to the sample average.
For example, near to the source, there are particles with a weight close to 1 and others particles that collided multiple times with a lower weight. A similar problem occurs in the regions of the detectors, where the population can have a very wide range of weights.
For the *new*cleo purposes, a GVR method is considered to provide a reliable particle flux estimation in the whole domain, then a uniform particle distribution is necessary to avoid underpopulated or overpopulated regions.
The use of the Weight Windows (WW), analyzed by Booth and Hendricks during their study, offers a way to perform a control of the weight. The domain of interest is divided in spatial cells, and for each cell a weight window is assigned.
A weight window is a region of the phase-space delimited by a upper bound (ww_u) and a lower bound (ww_l). When a particle enters in a weight window after a collision, its weight (w_i) is compared with the WW bounds.
If its weight is inside the window, the particle continues its life. Otherwise if the weight is above the WW upper bound, the particle is splitted in N copies. The split is necessary to reduce the number of particles with a very high weight as compared to the mean weight in the same WW, this avoiding sharp variations in the variance.
If the particle weight is below the lower bound a Russian Roulette game is played. If the particle wins, it survives and its weight is adjusted. If it loses, it is killed and its history ends.

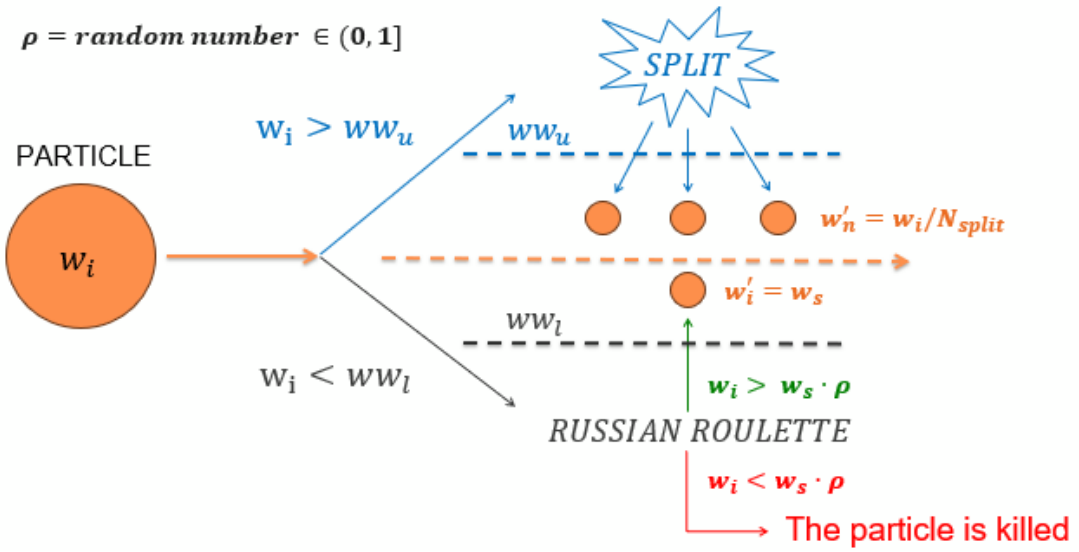

Figure 3.3: Weight window scheme

To preserve the same mean value and the physics of the problem, the sum of the weights of the child particles after the splitting is equal to the weight of the particle before the split.

The number of split N_{split} in OpenMC depends on the following formula:

$$N_{split} = min(N_{max}, [w_i/ww_u]), \tag{3.7}$$

where N_{max} is the maximum number of particles from a split, and it is a user-defined parameter (in OpenMC default value of N_{max} is 10). For the Russian Roulette probability shown in Figure 3.3, a new parameter is introduced, the survival weight w_s.
If the particle weight is higher than the product between the survival weight and a random number ρ generated, the weight is adjusted to the survival weight. If the particle loses the game (weight lower than the product) its simulation ends. The survival weight should be set within the weight window to avoid an additional splitting/rouletting that increases the computational effort.
In OpenMC the survival weight is defined as:

$$w_s = min([N_{max} \cdot w_i], [f_s \cdot ww_l]) \tag{3.8}$$

where f_s is the ratio of the survival weight (w_s) to the lower weight window bound (ww_l). The Rouletting avoids to maintain alive particles with a very low weight that continue their history and increase the computational time pointlessly.
To achieve the goal of the GVR method the set of the WW bounds is fundamental, for this reason Booth and Thompson [23][24][25] worked to understand and test the weight windows. They offers some recommendation parameters for the weight windows that are used nowadays also in OpenMC:

1. The weight window always does an integer split because an integer split differently by the Russian roulette do not introduce variance in the total weight post-split.

2. The weight window must be at least a factor of 2 wide because otherwise after a particle split, the post-split particles could be below the ww_l. Consequently a Russian Roulette could be played after a splitting, it increases the computational time and there is the possibility that the particles are rouletted.

3. The upper weight window bound is recommended to be at least 5 times the lower weight window bound. Also in this case to avoid the Roulette game after a split, this phenomena is called "thrashing" and it appears more frequently if the system has a substantial amount of scatterings. Moreover the roulettings introduce variance after the game, so the Roulette must be performed only if is strictly necessary.

4. The roulette survival weight (w_s) was recommended to be 3 times the ww_l. This does not increase sample variance but increases the computational time for useless particle cycles because if the survival weight is too low, for small changes in particle weight Russian roulette is played.

5. The maximum split/roulette factor was recommended to be 5 in order to avoid over splitting in case of large importance variations.

6. The ratio between 2 adjacent weight windows is recommended to be almost the same for the entire domain, and Booth suggested a maximum ratio of 4.

3.1.3 The set of the weight windows

A deeper investigation was performed in the years to find a suitable way to set the WW bounds.
Cooper and Larsen [3] have demonstrated that the weight windows based on the forward transport problem are suitable from the particles distribution point of view.
For the determination of robust weight windows typically the scalar flux is used [20]. The use of S_N, P_N methods [5] is not recommended due to the computational cost inaccurate for challenging problems and the approximation introduced. To improve the accuracy, Cooper and Larsen decided to change the weight window based on the diffusion theory with the quasi-diffusion method [26][27].
Quasi-diffusion method is a non-linear particle method proposed by Gol'din, and it is based on transport correction terms known as Eddington factors.
The use of quasi-diffusion solution coupled the deterministic approach to the Monte Carlo problem.
To understand if the link between deterministic transport and weight window approach is reliable, it is necessary to identify the final objective.

From the practical point of view, a uniform distribution of particles in the system has to be obtained in order to avoid a too low population far from the source and a too large population close to the sources. Larsen and Cooper fixed these issues linking the density of physical particles in cell j (N_j) with the mean weight in cell j (w_j):

$$N_j \propto \frac{total\ weight\ of\ all\ Monte\ Carlo\ particles\ in\ cell\ j}{volume\ of\ cell\ j} = \frac{\bar{w_j} \cdot M_j}{V_j} = \bar{w_j} \cdot \rho_j \tag{3.9}$$

where V_j is volume of the j-th cell and M_j is number of Monte Carlo particles in the j-th cell and ρ_j is the density of MC particles in j-th cell.
To obtain the uniform distribution in the whole domain ρ_i has to be roughly constant in each cell j. The Cooper and Larsen's idea was to set $\bar{w_j}$ (it is also defined as the center of the weight window j) proportional to the density of the physical particles in cell j:

$$\bar{w_j} \propto Nj \rightarrow \rho_j \approx constant\ (independent\ by\ the\ cell\ j) \tag{3.10}$$

To get this proportionality the proposal was correlate the center of the WW with the scalar flux (deterministic solutions could be used to set properly WW in the entire domain). In general Cooper and Larsen defined the isotropic weight window in a mono-energetic transport problem as follows:

$$\bar{w_j} = ww(\vec{r}) = C \cdot \frac{\phi_j(\vec{r})}{max\ \phi(\vec{r})} \tag{3.11}$$

where $\phi(\vec{r})$ is the particle flux evaluated for a region of space (r), $ww(\vec{r})$ represents the center of the weight window in a cell j and C is a factor ≥ 1. Using the Eq. (3.14) is possible to define the WW bounds in each cell of the domain for each energy group:

$$ww_u(\vec{r}) = \rho \cdot ww(\vec{r}) \tag{3.12}$$

$$ww_l(\vec{r}) = \frac{ww(\vec{r})}{\rho} \tag{3.13}$$

where $\rho \geq 1$ is a user-defined scale factor. The weight windows follow the behavior of the flux and they are normalized over the maximum flux.
A weight window can be assigned to each region of the phase-space. This means that if a energy structure is considered, it is possible to assign a weight window to each energy group and to each spatial cell.
The total number of the weight windows is the Cartesian product between spatial cells and energy bins. The weight window lower bounds in spatial-energy mesh are set for each energy group. The Eq. (3.14) is modified with the energy flux of the group g for each j-th cell:

$$\bar{w}_{j,g} = ww_g(\vec{r}) = \frac{\phi_{j,g}(\vec{r})}{max\ \phi_g(\vec{r})}, \tag{3.14}$$

The weight comparison method can be different: the energy of the particle is evaluated, and its weight is compared with the energetic WW in which the particle is, as shown in Figure 3.4:

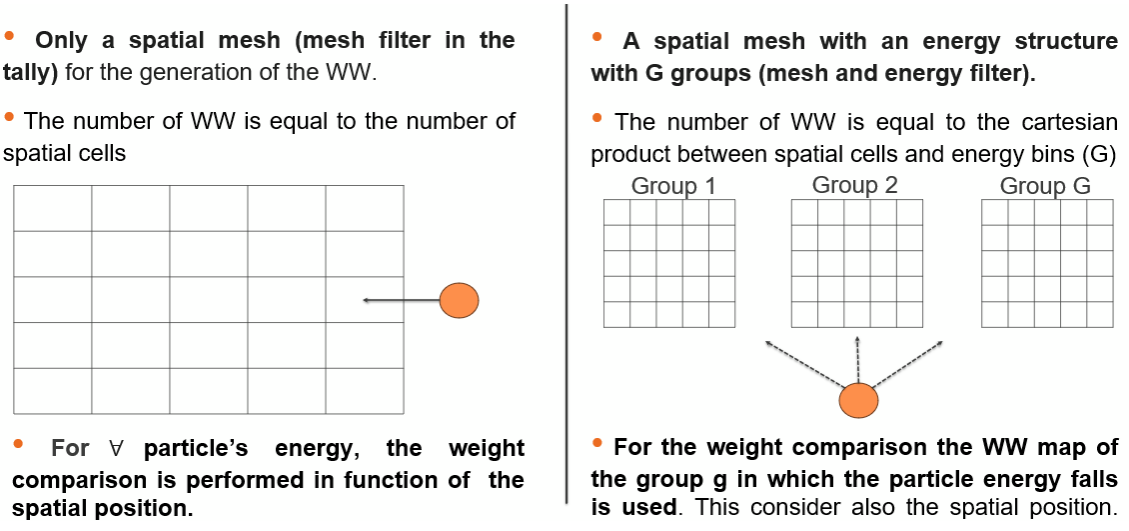

Figure 3.4: Generation of the WW with spatial or with spatial-energy mesh

However the scalar flux necessary to set the WW is the unknown of our problem, then an input scalar flux have to provided. During the evolution of Variance Reduction Methods, a difference between deterministic methods and non-deterministic methods were considered to get an approximate solution for the particle flux.
In 1997, Wagner and Haghighat [28] introduced the Consistent Adjoint Driven Importance Sampling (CADIS) [29][28] method based on an adjoint source defined at the problem boundary. The CADIS is typically used for enhance Local VR performance. In 2007, Peplow proposed a method known as Forward-Weighted Consistent Adjoint-Driven Importance Sampling (FW-CADIS) [30].
FW-CADIS [31][32] uses the adjoint solution from the deterministic calculation to generate consistent source biasing and the weight windows. However in some deep penetration problems, deterministic solutions are difficult to calculate, then non-deterministic approaches have been investigated to set automatically the weight windows during MC simulations. One of these methods is the Method of Automatic Generation of Importances by Calculation (MAGIC)[33].

3.2 The MAGIC method

MAGIC is a method that does not use a deterministic/adjoint solution to provide a WW map. The method determines an approximated particle flux distribution from an initial Analog Run (AR) without the WWs introduction.
The standard AR in which the particles are killed when an absorption occurs is not used in recent MC codes because many particles are absorbed and the statistical information are not enough to provide reliable results.
For example, in OpenMC an Analog Run uses only Russian Roulette, after a collision if the weight of the particle is lower than a cut-off weight w_c, then the particle is killed with probability $1 - w_i/w_s$.
If it survives, the weight is adjusted to w_s. It can be confirmed that the average weight after the Russian roulette game is simply w_i so the game is fair from the statistical point of view. By default, the cutoff weight in OpenMC is w_c=0.25 and the survival weight is w_s=1.0 [13].

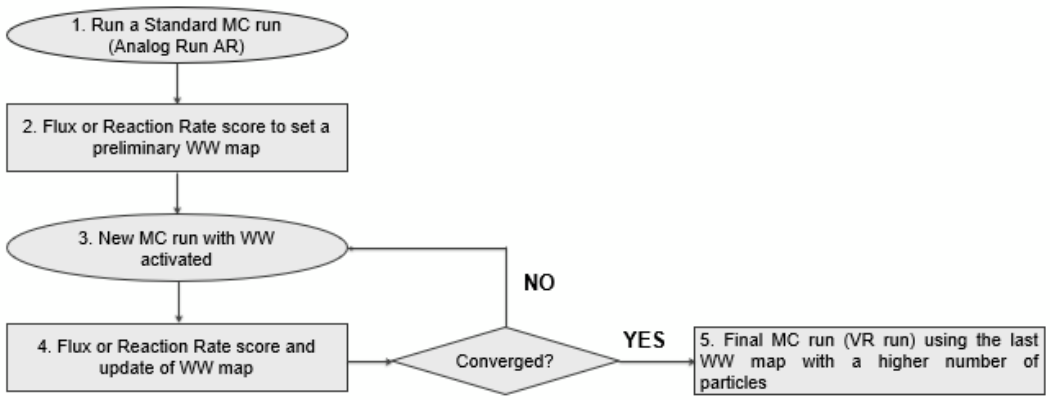

Figure 3.5: MAGIC Steps

Typically, in deep penetrations problems the AR is not able to give flux score in the entire domain, but it is possible set a preliminary WW map for the next calculations as shown in Figure 3.5 (Step 2).
At this point MAGIC iterative process starts. MAGIC uses the WW map of the i-th iteration as input in a Non-Analog Run (WW approach is used as described in section 3.1.2). The new MC run is able to populate better the different regions of the domain. The process is iterated until the number of iterations, a user-defined parameter, is not reached. The last step of the MAGIC is to use the last generated WW map as input for a MC run, increasing the number of particles. The run is typically called Variance Reduction run (VR run) and it allows us to get the flux estimation with a lower variance.

The gain of the method using the WWs and the MAGIC to set the WW bounds can be evaluated through a new parameter called Figure Of Merit (FOM) proportional to the computational performance:

$$FOM = \frac{1}{\sigma^2 \cdot T} \tag{3.15}$$

where σ is the Sample Standard Deviation derived from the Eq. (2.15), and T is the computational time of the simulation that is proportional to the number of histories.
The FOM allows to compare different MC methods with the possibility to compare the MC run with and without the VR techniques. Figure Of Merit takes into account also the reliability of the results because it is calculated using the sample variance. In general, the higher the FOM, the more efficient the MC simulation is.

Davis and Turner analyzed different VR methods in "Fusion applications" using the Average FOM and the Average error (Average RSD) [34]. They compare Analog Run (AR), MAGIC weight window in cell (MWIC), MAGIC Weight Window in mesh (MWIM), and FW-CADIS to understand the effectivness of the method. The MWIC uses the exiting weight information to set properly the WWs, while the MWIM uses the flux information as presented by Cooper and Larsen [3] [35].

Parameter	AN	FW-CADIS	MWIC	MWIM
CPU Time (mins)	13468	12511	10672	12522
Av. error	92.52%	13.80%	20.50%	11.16%
%age not scoring	86.90%	0.86%	10.90%	0.03%
Av. FOM	8.67×10^{-5}	4.20×10^{-3}	2.28×10^{-3}	6.41×10^{-3}

Figure 3.6: Comparison between VR methods in ITER problem [33]

In Figure 3.6, it is possible appreciate that the MWIM has an average error lower than the FW-CADIS that need a deterministic solution to provide results. The Average FOM is higher than the FW-CADIS, therefore the MAGIC can be an alternative reliable method to avoid the use of deterministic solutions.

3.3 MAGIC-GPS the evolution of the method

The FOM (Figure 3.6) shows a gain, but during the years different researchers tried to enhance the performance of the method. A new method have been proposed called MAGIC-GPS [4], where GPS is a Growth Population Scheme (GPS) in which the number of particles simulated increases for each iteration of the MAGIC. Before to enter in the detail the mathematical proof of the gain using the MAGIC-GPS than the MAGIC is provided. The MAGIC iterative step can be written using the NTE (Eq. (2.1)):

$$(L + C) \cdot \phi = (S + F) \cdot \phi + Q_s \tag{3.16}$$

where the operators L, C, S, and F represent the leakage, collision, scattering, and fission operators respectively; ϕ is the neutron flux, and Q_s is the external neutron source.

From the Cooper and Larsen idea the weight window center needs to be proportional to the neutron flux as described in Eq. (3.14).

$$\begin{aligned} \phi^{(1)} &= [L(w^{(0)}) + C(w^{(0)}) - S(w^{(0)}) - F(w^{(0)})]^{-1} \cdot Q_s \\ w^{(1)} &= C \cdot \frac{\phi^{(1)}(\vec{r})}{max\ [\phi^{(1)}(\vec{r})]} = K \cdot \phi^{(1)}(\vec{r}) \end{aligned} \tag{3.17}$$

where Eq. (3.17) is the first iteration and an estimation of the first neutron flux for each phase-space cell is performed and the MAGIC iterative process using these information is described as follows:

$$\begin{aligned} \phi^{(k+1)} &= [L(w^{(k)}) + C(w^{(k)}) - S(w^{(k)}) - F(w^{(k)})]^{-1} \cdot Q_s \\ w^{(k+1)} &= C \cdot \frac{\phi^{(k+1)}(\vec{r})}{max\ [\phi^{(k+1)}(\vec{r})]} = K \cdot \phi^{(K+1)}(\vec{r}) \\ & for\ k = 2, 3, ... \end{aligned} \tag{3.18}$$

If we consider k as the k^{th} iterative step we can rewrite the iterative equations:

$$\phi^{(k+1)} = H^{(k)} Q_s = constant \cdot H^{(k)} = H \cdot \phi^{(k)} \tag{3.19}$$

H is the iterative matrix/operator, while $H^{(k)}$ is a k^{th} order iterative operator of H. If we consider that operator H has eigenvalue λ_j and eigenvectors a_j for j= 1,2,3,... For the properties of eigenvectors:

$$Ha_i = \lambda_i a_i\ , i = 1, 2, 3, ... \tag{3.20}$$

The eigenvalues are ordered $|\lambda_1| > |\lambda_2| > |\lambda_3|$.... The global flux distribution to be solved is the fundamental mode a_1.
The initial flux distribution $\phi^{(1)}$ can be expanded using the eigenvectors and also the successive iterative steps:

$$\begin{aligned} \phi^{(1)} &= \sum_{j=1} k_j a_j \\ \phi^{(k+1)} &= H\psi^{(k)} = H^k \psi^{(1)} = \sum_{j=1} k_j a_j \\ \phi^{(k+1)} &= k_1 (\lambda_1)^k \left[a_1 + \frac{k_2}{k_1} (\frac{\lambda_2}{\lambda_1})^k a_2 + \frac{k_3}{k_1} (\frac{\lambda_3}{\lambda_1})^k a_3 + ... \right] \end{aligned} \tag{3.21}$$

Due to the ordering of the eigenvalues:

$$\begin{aligned} 0 < \left| \frac{\lambda_{j+1}}{\lambda_1} \right| < \left| \frac{\lambda_j}{\lambda_1} \right| < 1\ , for\ j = 2, 3, 4, ... \\ \lim_{k->+\infty} \frac{k_j}{k_1} (\frac{\lambda_j}{\lambda_1})^k a_j = 0\ , for\ j = 2, 3, 4, ... \end{aligned} \tag{3.22}$$

From the Eq. (3.22) it can be appreciated that the first ratio λ_2/λ_1 is the largest and the

convergence rate of the MAGIC mainly depends on this ratio. To understand the gain using the MAGIC-GPS the analysis of the error in the flux distribution and the FOM is necessary. Assuming that error ϵ can be calculated for each iteration k, the error k-th is approximated as

$$\epsilon_k = \frac{\lambda_2}{\lambda_1} \cdot \epsilon_{k-1} = \rho \cdot \epsilon_{k-1} \tag{3.23}$$

ϵ is the standard deviation described in the MC theoretical background and it converges as $1/\sqrt{N}$ where N is the number of histories. If the population of particles P increases by factor q higher than 1 for each iteration k.

$$P_k = q \cdot P_{k-1} \tag{3.24}$$

The convergence rate of the error will increase as:

$$\frac{\epsilon_k^{'}}{\epsilon_{k-1}^{'}} = \frac{\epsilon_k}{\epsilon_{k-1}} \cdot \frac{\sqrt{P_{k-1}}}{\sqrt{P_k}} = \frac{\rho}{\sqrt{q}} < \rho = \frac{\epsilon_k}{\epsilon_{k-1}} \tag{3.25}$$

Where ϵ_k is the error for iteration k^{th} using the standard MAGIC, while $\epsilon_k^{'}$ is the error using the MAGIC-GPS. The last equation shows as the larger q factor is, the faster the convergence is.
Considering the gain, it is possible define the average Figure of Merit for each particle in k^{th} iteration (FOM_k) that is different by FOM. Assuming that the convergence can be achieved after I iterations, k = 1,2,...,I. The population simulated in the MAGIC is P_1 that represents the starting population of the MAGIC-GPS. The averaged FOM per particle simulated by the MAGIC method is evaluated as follows:

$$\eta_{MAGIC} = \frac{\sum_{k=1}^{I}(P_k \cdot FOM_k)}{\sum_{k=1}^{I}(P_k)} = \frac{\sum_{k=1}^{I}(P_1 \cdot FOM_k)}{\sum_{k=1}^{I}(P_1)} = \frac{P_1 \cdot \sum_{k=1}^{I}(FOM_k)}{I \cdot P_1} = \frac{\sum_{k=1}^{I}(FOM_k)}{I} \tag{3.26}$$

The same approach can be applied for the MAGIC-GPS:

$$\begin{aligned} &\eta_{MAGIC-GPS} = \frac{\sum_{k=1}^{I}(P_k \cdot FOM_k)}{\sum_{k=1}^{I}(P_k)} = \frac{\sum_{k=1}^{I}(P_1 \cdot q^{k-1} \cdot FOM_k)}{\sum_{k=1}^{I}(P_1 \cdot q^{k-1})} = \\ &\sum_{k=1}^{I}\left(\frac{q^{k-1}}{\sum_{k=1}^{I} q^{k-1}} \cdot FOM_k\right) > \frac{\sum_{k=1}^{I}(FOM_k)}{I} = \eta_{MAGIC} \end{aligned} \tag{3.27}$$

In conclusion the MAGIC-GPS has a higher efficiency than the standard MAGIC. Increasing the population through the factor q the efficiency improvement will increase. However if the value of q is too large the number of particles increases too fast, the computational time increases rapidly. After different test in the paper the recommended value for q is 2. During the thesis some simulations applying the MAGIC-GPS will be performed to verify if the mathematical considerations can be confirmed.

Chapter 4

Application of WW and MAGIC

The main objective of the thesis is to understand if the WW approach using the MAGIC in OpenMC is suitable for the *new*cleo purposes, for example to provide the flux distribution in the LFRs. However, before going into the details of the models used to test the VR technique, it is useful to introduce the cross-sections library, which is used in all models studied in continuous energy mode.

The library used is the ENDF/B-VIII.0 that includes incident neutron, photoatomic, atomic relaxation, and thermal scattering data from ENDF/B-VIII.0. It can be downloaded by the OpenMC official data libraries [13]. The use of this nuclear data gives the microscopic total, scattering, capture and fission cross-section for a large amount of nuclides/isotopes at six different temperatures: 250 K, 293.6 K, 600 K, 900 K, 1200 K, and 2500 K. Moreover it is possible calculate the cross sections for any temperature using the interpolation method.

4.1 Simulation Settings and WW parameters

The simulations of the particles in OpenMC are based on different parameters, and the settings are fundamental to provide reliable results. In this section a brief guide recommendations will be provided to compensate the lack of user experience.
These recommendations may not be completely reliable for every case study, but they have been collected after a large amount of simulations. The first parameter to choose in a MC run is the number of particles simulated that is strongly affected by the physics of the problem and by the dimension of the domain. In general the guidelines for the simulation settings are the following:

- The number of the particles used during the MAGIC iterative process is typically low because the goal is try to fill the entire domain. The typical choice is approximately in the order of thousands.
  Neutron flux attenuation is fundamental to the correct choice in systems with highly absorbing media, where a larger number of particles may be required to reach the entire domain.
  The number of particles in the AR and VR run is typically several order of magnitude higher than the number of particles simulated in MAGIC. This reduces the variance

associated with the neutron flux, bearing in mind that the variance is inversely proportional to the number of histories N.

- Number of splits over the entire life of a particle (Number of splits in a history). It is the total number of splits that can be performed by a particle, and it is different by N_{split} in Eq. (3.7). Also for the number of splits, the choice is strongly affected by the neutron flux attenuation and by the medium.
  In small domain in which the neutron flux attenuation is not high (order of magnitude $< 10^5$) the number of splits could be in the order of thousands. However, the choice of number depends entirely on the nature of the problem and the model being studied.

- *Number of batches*: it represents the number of times that the particles are simulated. The total number of histories (N) is the product between the number of batches and the number of particles.
  There is no evidence that the results are worse with a low number of batches (10) than with a higher number of batches. In the review by Munk and R. N. Slaybaugh[1] a correlation between the number of batches and the Central Limit Theorem suggest to use almost 30 batches in the simulation, but the test performed does not show any evidence

Also the weight windows and the MAGIC have different parameters that can affect the results:

- *Survival Ratio* (f_s), it is defined as ratio of the survival weight (w_s) to the lower weight window bound for rouletting. It is used in Eq. 3.8. and the default value in OpenMC is 3. The particles survived to roulettings stay inside the weight windows and continues their life. The use of the survival ratio is necessary to avoid a chain of successive roulettings. In case of survival ratio equal to 1, the weight of the survived particle is exactly equal to the lower weight window bound.

- Weight Cutoff (w_c): Weight threshold below which particle histories are stopped. The default value is 10^{-38}, which may be too low in some models. In section 3.1.3 it is explained that the weight window bounds follow the neutron flux value and profile.
  When the neutron flux attenuation is not large, the minimum WW lower bound could be very far away from the weight cut-off. The simulation of particles with a very low contribution in deep penetrations zones could increase the computational time. For this reason the weight cutoff should be calibrated in function of the neutron flux attenuation.

- Maximum number of particles from a split (N_{Max}), the default value is 10 and it is used in Eq. (3.7).

- Relative error MAGIC criteria/threshold (always ≤ 1). It represents the maximum value of relative standard deviation in a phase-space cell during the MAGIC iteration. If the relative standard deviation in a phase-space cell is higher than the user-defined parameter the weight windows are deactivated in the cell. The reason is leaded to the WW bounds: if the RSD is too high, the particles flux estimation is not correct

so the weight windows bounds could be not set correctly. The default value is 1, and if the value is 1 this criteria is not applied.

- Number of iterations, a low number could be noyt enough to get a full WW map. A large number could be lead to a higher computational time (the WW map is full but the iterative process continues).

The settings and the parameters presented are modifying and adapted in function of the model choice. The general approach is try to test WW and MAGIC in OpenMC v. 14.1 in a large set of models, in continuous and in multi-group mode. Tests were carried out by simulating photons and neutrons to study their propagation in different media. The implementation of the models is shown in the following sections.

4.2 1-D multi-layer model

The first idea to test the WW approach is try to replicate the Lead-cooled Fast Reactor (LFR) concept of *new*cleo. The LFRs, differently from the commercial Light Water Reactors, are cooled by liquid lead or a lead-bismuth alloy. They operate with fast neutrons at atmospheric pressure and high temperatures [36]. The shielding of the escaping neutrons and photons without a moderator is more difficult to achieve due to the high particle energy associated with high penetrating power. For this reason different layer of steel and concrete are placed to reduce the dose in the containment building.

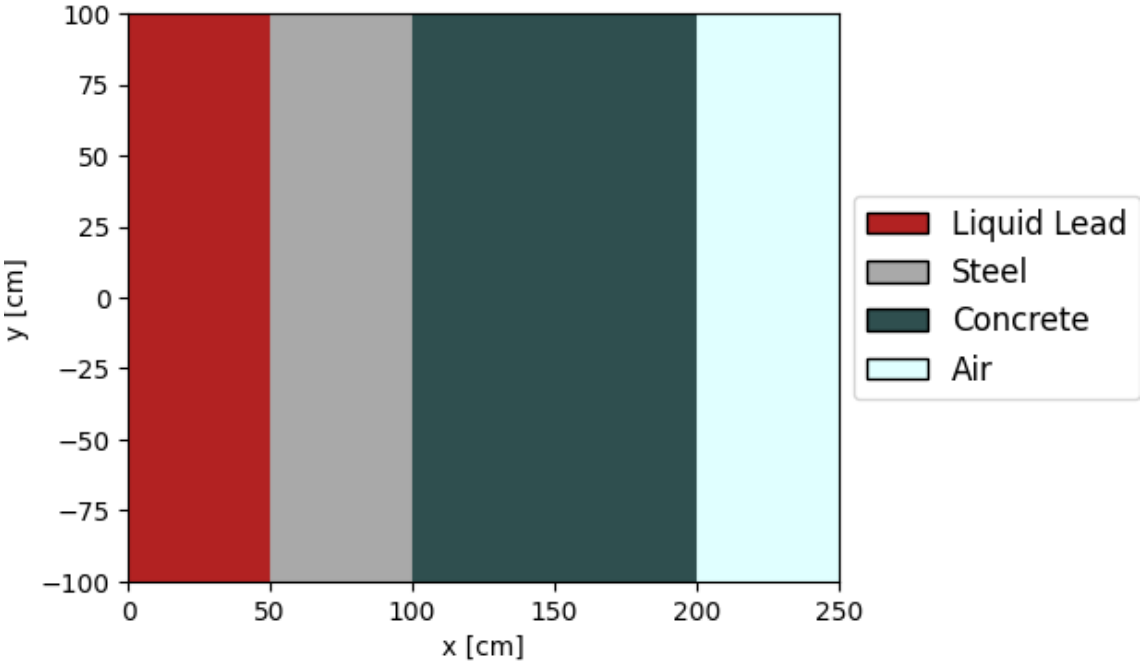

Figure 4.1: 1D multi-layer geometry view (x-y plane)

The geometry is a multi-layer slab studied in continuous-energy mode, the materials are shown in Figure 4.1. The motivation for this choice is related to the simplicity of the model. The study in 1 dimension is carried out with the intention of modifying the mesh used in the tally for the generation of the WW.

The red region contains liquid lead at 700 K, this layer is thick 50 cm. The material properties of Lead are provided using the lbh15[37][38], a Python package that implements the thermo-physical and the thermo-chemical properties of lead, bismuth and lead-bismuth eutectic (lbe) metal alloy available from the handbook edited by OECD/NEA.

Table 4.1: Liquid Lead composition

Lead Isotope	Weight Content
Pb-204	1.4 %
Pb-206	24.1 %
Pb-207	22.1 %
Pb-208	52.4 %

The light grey region thick 50 cm is composed by steel, and the dark grey region wide 100 cm is made of concrete with 16.9 % of hydrogen content and with 56.3 % of oxygen content in weight.
The last region in azure is filled by air, the dimension of the slab is 250 cm in the x-direction. The source is a box source thick 1 cm placed at the start of the liquid lead layer. It emits neutrons isotropically according to the Watt Distribution/Spectrum of U_{235}.
To implement a slab in OpenMC, it is necessary to define planes in the y and z directions, as the geometry must be finite in all direction. For this reason, the y and z planes are between -100 cm and 100 cm with reflective boundary conditions to be consistent with the infinite slab.
In x-direction reflective boundary condition is applied in the left side, while in the right side vacuum boundary condition is considered.
The model can be useful to understand if the neutrons can reach the air region and to quantify the variance or relative standard deviation in deep regions.

4.3 Becker-Larsen model

The Becker-Larsen model [39], proposed in 2011, was studied after the 1-D multi-layer analysis. The geometry is a 25 cm side homogeneous cube, as shown in Figure 4.2, with a 1 cm cubic source in the corner, symmetric boundary conditions at the planes intersecting the source and vacuum boundaries at the external planes.
The model was studied in MG mode with 3 energy group structure. The choice was mainly motivated to study the WW map generation in the Multi-Group (MG) mode.
In the paper, the energy subdivision is not given, then an assumption has been considered, using the CASMO 3-group structure [40]. The macroscopic cross sections of the region was given for each energy group:

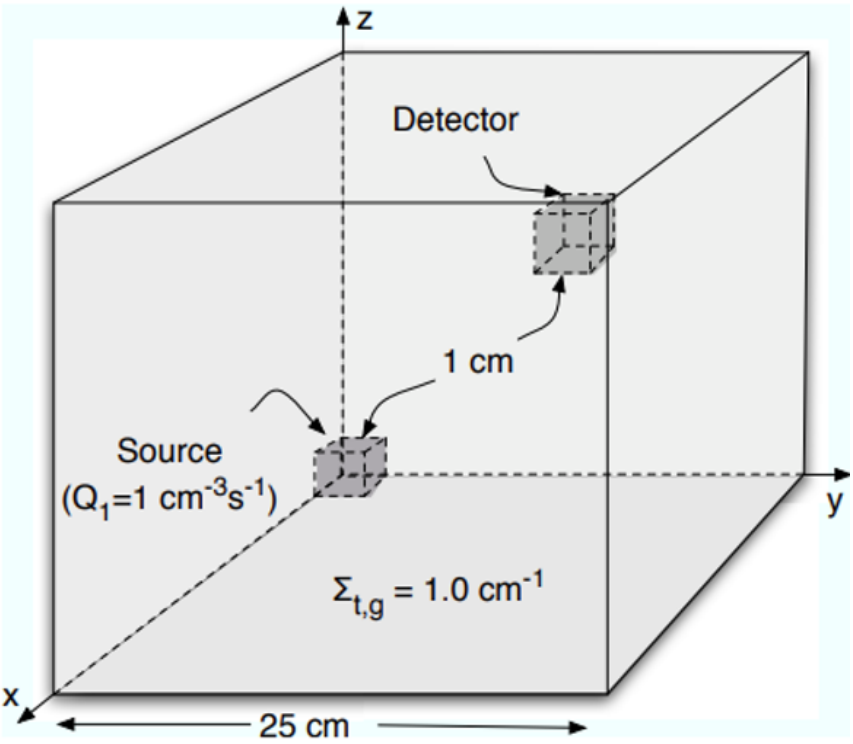

Figure 4.2: Larsen Benchmark geometry

Table 4.2: Cross sections and source data

Data	Energy groups		
	1	2	3
Energy [MeV]	$[10^7, 8.21 \cdot 10^5]$	$[8.21 \cdot 10^5, 6.25 \cdot 10^{-1}]$	$[6.25 \cdot 10^{-1}, 10^{-5}]$
$\Sigma_{t,g}$ $[cm^{-1}]$	1.0	1.0	1.0
$\Sigma_{s,g\longrightarrow 1}$ $[cm^{-1}]$	0.6	0.0	0.0
$\Sigma_{s,g\longrightarrow 2}$ $[cm^{-1}]$	0.1	0.7	0.0
$\Sigma_{s,g\longrightarrow 3}$ $[cm^{-1}]$	0.05	0.1	0.8
Q_g $[\mathrm{cm}^{-3}\ \mathrm{s}^{-1}]$	1.0	0.0	0.0

As shown in section 4.3, the source data is also provided. The source emits neutrons isotropically only in the first group.
Moreover, the possibility of modifying the cross section by the user gives a series of test that can be carried out to represent a very absorbing medium. These tests are called stress tests and are used to check the effectiveness of the WW and MAGIC in very extreme cases.

4.4 Structure holding nuclear fuel

A more realistic nuclear problem was studied using the model suggested by Wagner, Peplow and Mosher [41][42].

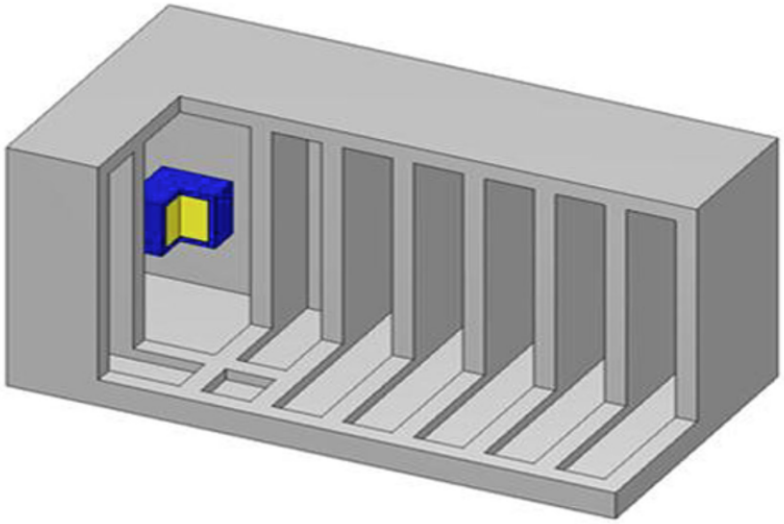

Figure 4.3: 3-D Structure view [41]

The structure has dimensions of 860x460x460 cm and is made up of different regions with different materials:

- The source box (80x80x80 cm) is placed in the centre of an air region of 200x200x200 cm. It consists of a homogenised mixture of uranium dioxide (UO_2) and water.
- A layer of steel (10 cm thick) surrounds the source for structural reasons.
- Concrete (30 cm thick), walls are distributed in the geometry and they are separated by an air gap of 70 cm between them.

The material properties, nuclides and weight concentrations implemented in OpenMC are the same as those used by the authors during their study. The source emits neutrons according to Watt's spectrum [10], isotropically and the total strength is 1 Ci as presented in the article. The choice of the total strength represents an assumption because the activity is the number of radioactive transformations per second that occur in a particular radionuclide. The strength of the source is typically provided in particles emitted per second.
The simulations performed are in Continuos-Energy mode but to generate the WW map, the SCALE-27[43] group energy structure is used. During the test performed by Wagner, Peplow and Mosher different MC and VR methods have been investigated:

1. *Analog method*: (with implicit capture on; weight cutoff of 10^{-16});
2. *Cooper and Larsen's method*: it is described in section 3.1.3. The weight windows bounds are generated using the scalar flux from the quasi-diffusion model.

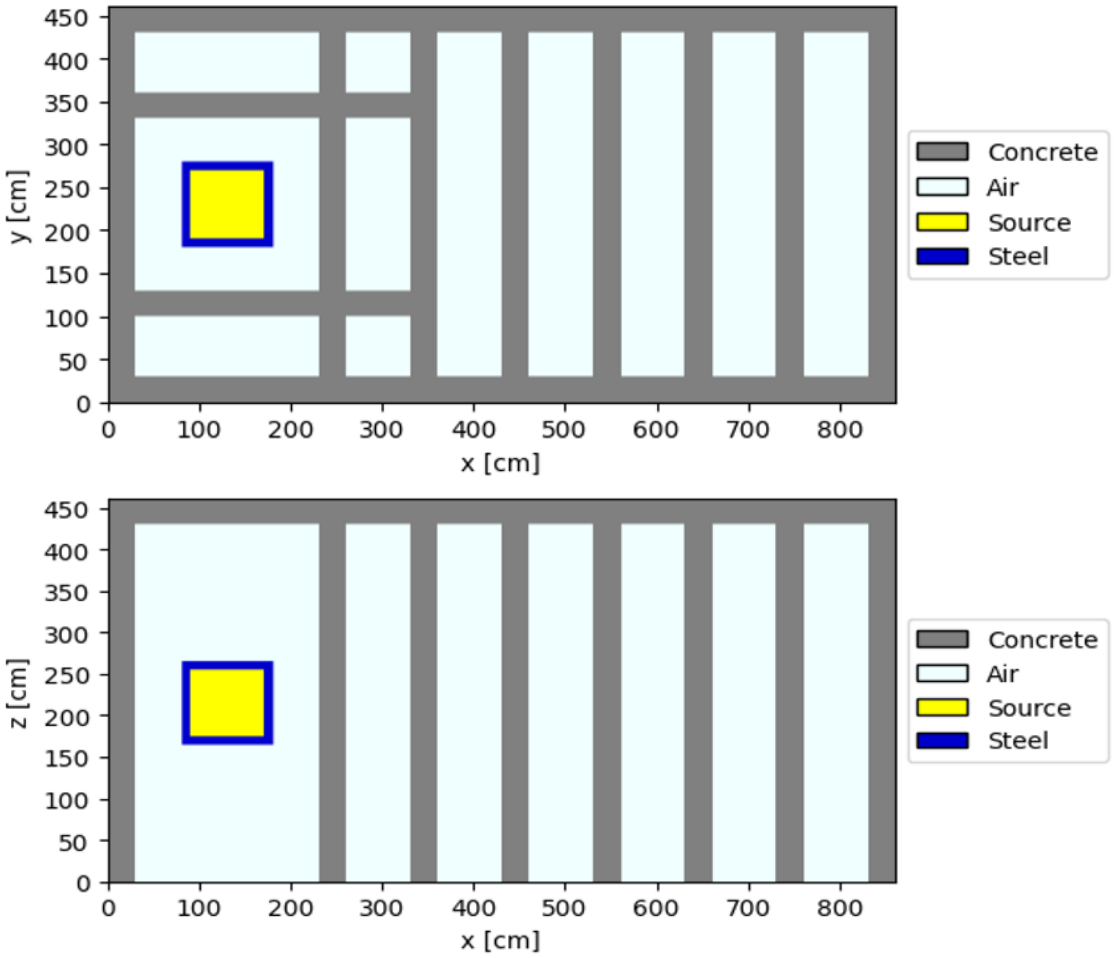

Figure 4.4: Geometry visualization at z = 215 cm (First Figure) and at y = 230 cm (Second Figure)

3. *GFWW/GRWW methods* [44]: they are based on the global estimation of the flux in the whole domain. GRWW method is Global Response Weight Windows and the weight windows are set throught the response to the introduction of an external source. For the GFWW and GRWW methods, no adjoint sources are required since only forward estimates of the flux over the entire geometry are required.

4. *Becker's method* [45]: it defines a different adjoint source distribution as a function of the desired response for the calculation[1].

5. *FW-CADIS* [46],[47]: (Forward-Weighted Consistent Adjoint Driven Importance Sampling) method uses and distributed the adjoint source across mesh cells as an inverse relation to the forward response of the cell. The FW-CADIS [48] was developed in 2007 by Peplow that proposed different CADIS methods.

The paper offers many results for the comparison in a realistic problem between MAGIC method and the other methods that use deterministic or adjoint solutions to set the weight windows bounds.

4.5 Application with photons

The LFR design takes into account also the radiation transported through the photons. There are three main ways in which photon (gamma-ray) radiation interacts with lead [49]:

- The photoelectric effect (at low energies)
- Compton scattering (at medium energies)
- Pair production (at high energies, above 1.02 MeV).

These interactions are less probable and less energetic than the neutron interactions. Lead is a very dense material with a high atomic number. It is therefore effective in attenuating high energy photons, but requires a relatively greater thickness than neutron shielding.
If the interactions are less probable, this can represent an issue for the WW. The particle's weight is compared for each collision, then the population control using the WW is applied less frequently and, thus, it is less efficient. Consequently, the photon flux estimation in deep regions could not be reliable due to the lack of statistical information.
To fix these issues, the "surface setting" is activated when photons are simulated: the weight comparison is also performed when a particle crosses a surface implemented in the model. The surfaces are planes defined during the implementation of the geometry in OpenMC, the number is completely arbitrary but has to be in the order of hundreds when the photons are simulated.

The geometry (Figure 4.5) is a multilayer slab 50 cm thick in with 4 layers composed/filled by different material:

1. A 10 cm thick slab composed by steel
2. Liquid lead layer thick 25 cm. The temperature of the lead is assumed at 700 K, in which the propagation of the neutrons is very difficult
3. A thin steel liner (5 cm) that simulate the wall thickness of the reactor pressure vessel (RPV). The thickness is very small because a LFR operating at atmospheric pressure, then the stress on the vessel are lower than the PWR/BWR.
4. At the end of the slab there 5 cm gap filled by air

The source of the model is a slab 1 cm thick at the start of the geometry. It emits photons isotropically according to the emission spectrum of Cobalt-60 in activated materials.

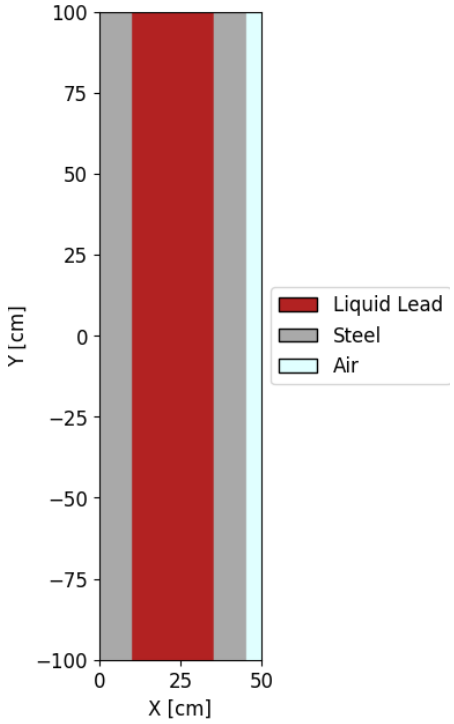

Figure 4.5: Geometry for photon test

Chapter 5

Results

5.1 New stopping criteria for the MAGIC method

The stopping criterion of the MAGIC method is entirely at the discretion of the users, who usually set an *a priori* number of iterations. The number of iterations performed by the MAGIC method clearly affects the performances of the calculation. If the number of iterations is not sufficient, the weight windows may not cover the whole domain, resulting in a reduced effectiveness of the variance reduction method. Conversely, if the number of iterations is excessively large, the WW might be set appropriately before the last iteration, resulting in superfluous iterations and, consequently, in a waste of computational time. The solution proposed in this work is the introduction of automatic stopping criteria to overcome these issues. The stopping criteria are based on the so-called Coverage Ratio (ζ), defined in [41] as,

$$\zeta = \frac{\text{Number of cells with non-zero flux score}}{\text{Total number of cells}}. \tag{5.1}$$

At the end of each iteration, the coverage ratio is computed and compared with a user-defined threshold. If the WWs are defined on a spatial mesh disregarding the particles energy, the iterative process is arrested when ζ overcomes a certain threshold τ. A set of tests performed on different study cases suggests that a good value for τ is around 0.99. If the WW are defined on a space-energy mesh, ζ is evaluated for each energy group g,

$$\zeta_g = \frac{\text{Number of cells with non zero flux score in g}}{\text{Total number of cells}}. \tag{5.2}$$

In the multi-group case, the simulation terminates when at least one of the following stopping criteria are satisfied:

1. the coverage ratio exceeds 0.99 for each energy group,

$$\zeta_g > \tau. \tag{5.3}$$

2. The difference of the group-wise coverage ratio between two successive iterates is lower than a certain user-defined tolerance

$$|\zeta_g^i - \zeta_g^{i-1}| < \varepsilon, \tag{5.4}$$

where i is the number of the MAGIC iteration. Despite ζ_g is supposed to increase monotonically in the iteration process, its value can have small statistical fluctuations. Hence, the absolute value is used to get a more robust stopping criterion.

While the first criterion is the natural extension of the previous criterion to the multi-group framework, the second one is introduced to deal with the possible missing convergence of ζ_g in some energy groups and is independent of the verification of the first criterion. Clearly, the evolution of the group-wise coverage ratio is linked to the emission spectrum of the source. For instance, if the source emits neutrons below a certain energy threshold, say E_{thresh}, the flux score in the groups above E_{thresh} is absent. In such cases, the coverage ratio of these groups may be significantly low or even approaching 0. Conversely, when the source emits fast neutrons, ζ_g in lower energy groups depends on the slowing down capabilities of the system. Hence, low energy groups may present a small ζ_g. The introduction of the second criterion is essential to overcome these issues. However, the check is only operated when the number of groups with $\zeta > 0.99$ exceeds a designated percentage of the total number of groups. Once the second stopping criterion is satisfied, the MAGIC iterative process terminates since, due to the nature of the source, further increases in the coverage ratio are no longer possible and additional iterations would just increase the computational burden. The appropriate percentage should be chosen on the basis of the emission spectrum of the source and the energy group structure employed. The introduction of stopping criteria reduces the computational time to provide a full WW map. For some purposes is useful compare the performance of the MAGIC with the same number of iterations, then the stopping criteria in some models could be not introduced. During the presentation of the results, the stopping criteria will be mentioned for any test.

5.2 1-D multi-layer

The first simulation was performed to understand if the WW and the MAGIC works correctly in OpenMC 14.1 and to enhance the gain compared to an Analog Run.
The spatial mesh is used to define the tally for the generation of the WW. The simulation is in continuous energy and no energy filter was introduced in the tally. The number of cells in x-direction chosen is 100, each cell is thick 2.5 cm.

Table 5.1: Settings and performances of the MAGIC calculation carried out in OpenMC.

Particles/batch	# of batches	max # of splits	Stopping criteria	# of iterations
$2.5 \cdot 10^4$	10	$4 \cdot 10^3$	No	5

In Figure 5.1 the neutron flux evolution is shown with the associated relative standard deviation (RSD). The first iteration shows that the neutron flux profile is not scored in all the domain.
In regions far from the source (the end of the concrete layer and the air layer) the flux score is not present. The MAGIC iterative process is necessary, and for the model studied at the third iteration the neutron flux map is full.

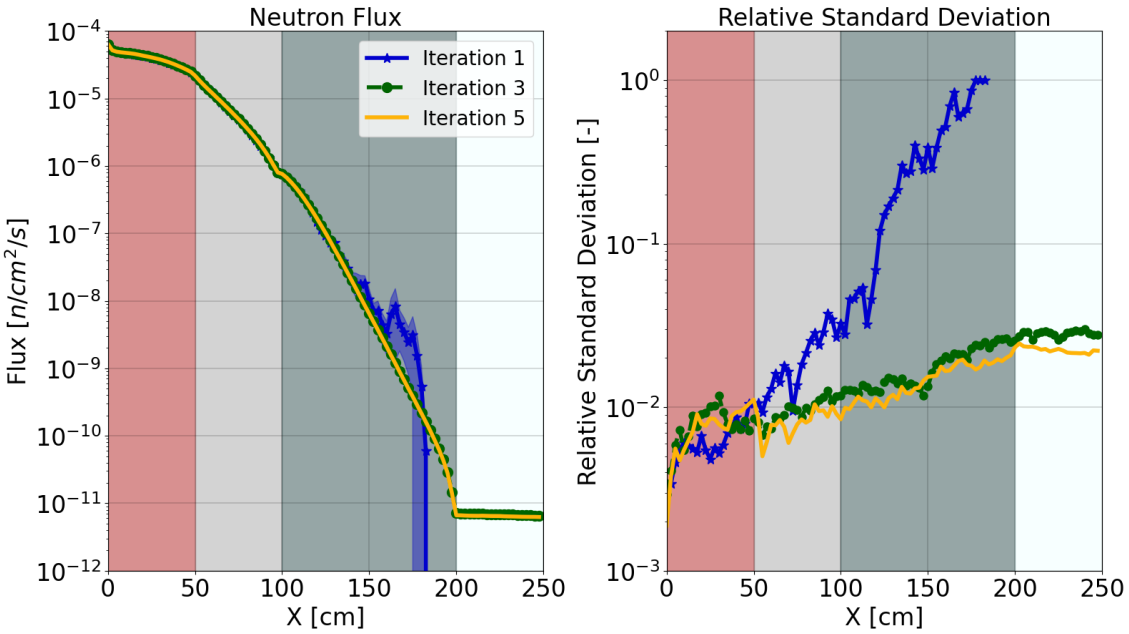

Figure 5.1: Neutron flux and Relative standard deviation evolution during the MAGIC iterations

The last iterations could only be necessary to reduce the relative standard deviation without further populating the map. The WW map of the last iteration (5^{th} iteration) will be used as input in the VR run increasing the number of particles to reduce the relative standard deviation.

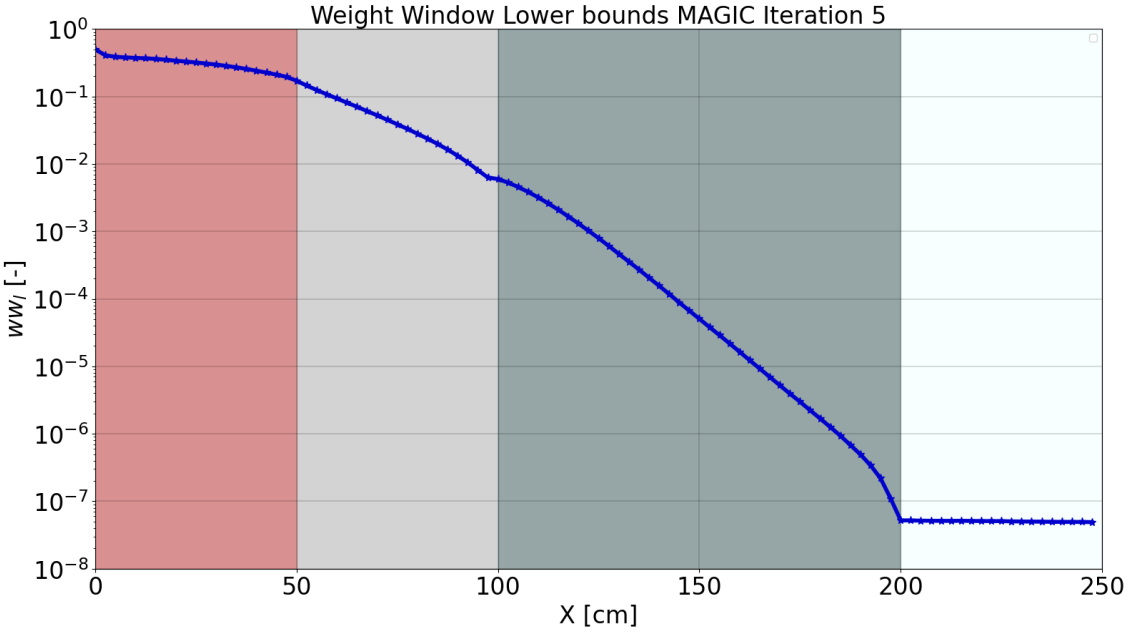

Figure 5.2: Weight Window lower bound Iteration #5

In Figure 5.2, the weight windows lower bounds are plotted. In OpenMC the weight windows lower bounds consider the Cooper and Larsen idea [3] (Eq. (3.14)), however the

implementation is different:

$$ww_l(\vec{r}) = \frac{\phi(\vec{r})}{2 \cdot max\ \phi(\vec{r})} \tag{5.5}$$

The ratio between lower to upper bounds of WW is 5 according to the suggestion of Booth in 1984. Consequently the center of the weight windows contains a factor 3/2:

$$ww_{center}(\vec{r}) = \frac{3}{2}\frac{\phi(\vec{r})}{max\ \phi(\vec{r})} \tag{5.6}$$

Thus, at the source position, the WW lower bound is 1/2 because flux $\phi(\vec{r})$ is the maximum flux, as shown in Figure 5.2.

Table 5.2: AR and VR run settings

Simulation	Particles/batch	# of batches	max # of splits
Analog (AR)	$5 \cdot 10^5$	10	-
Variance Reduction (VR)	$5 \cdot 10^5$	10	$4 \cdot 10^3$

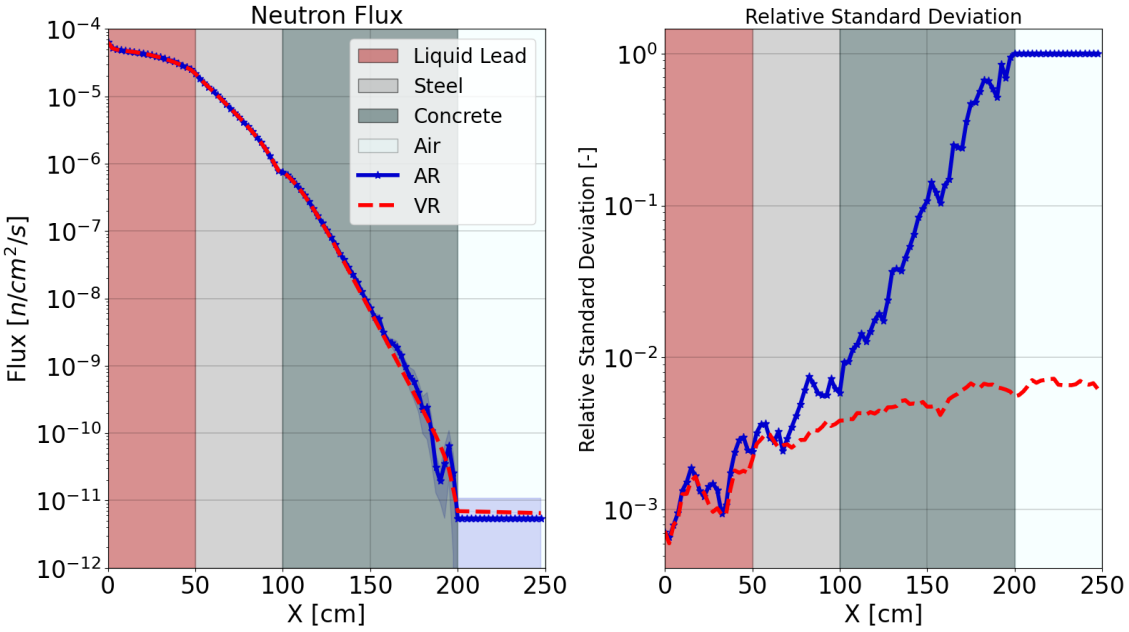

Figure 5.3: Neutron flux in Analog and in VR run

Figure 5.3 shows the neutron flux along the direction of the slab. The flux score is present in the entire domain but the Relative Standard Deviation (RSD) in the AR is very high in deep regions (close to the 100 %).

The WWs generated through the MAGIC are used in the VR run (the red curve) and it gives a better estimation of the neutron flux.
The reduction of the RSD is very evident in deep regions like in the concrete and in air layer.

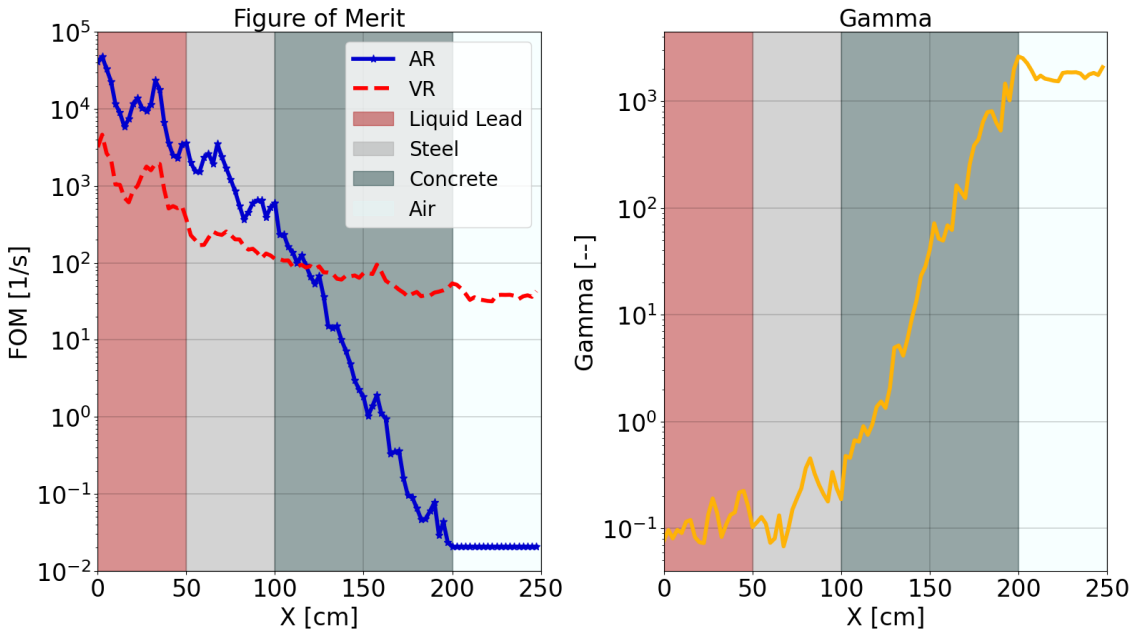

Figure 5.4: Figure of Merit and Gamma in Analog and in VR run

Figure of Merit (Eq. (3.15)) shown in Figure 5.4 is the quantity to evaluate the gain in terms of performance.
For the VR run the computational time used in the FOM calculation is the sum of computational time of MAGIC and the computational time of VR run.
In the first half of the domain the FOM is lower for the VR run because the variance is not reduced but the computational time is higher. In deep regions the variance is reduced and the FOM increases. The gain is calculated using Gamma parameter:

$$\Gamma = \frac{FOM_{VR}}{FOM_{AR}} \tag{5.7}$$

5.2.1 Mesh Refinement

The spatial mesh is one of the choices of the user in the simulation. The number of cells and their distribution could have an impact on the results. The results shown in the in Figures 5.3, 5.4 was performed using a equally spaced mesh with 100 cells. Different mesh will be tested based on:

1. Total number of cells and the minimum number of cells to get reliable results.

2. Distribution of the cells based on the neutron flux attenuation and equally flux ratio.

For the mesh refinement stopping criteria were introduced: the MAGIC ends when coverage ratio is >0.99 and when the mean relative standard deviation is < 0.05 (5 %). All the simulations have the same settings proposed in Table 5.1, 5.2 and the MAGIC ends in 3 iterations for each case study. The total number of cells is tested with 4 different simulations presented in the following table:

Table 5.3: Spatial mesh for the generation of the WW

Simulation name	# of cells	Cell's dimension in X-direction [cm]
VR 10 Cells	10	25
VR 20 Cells	20	12.5
VR 50 Cells	50	5
VR 100 Cells	100	2.5

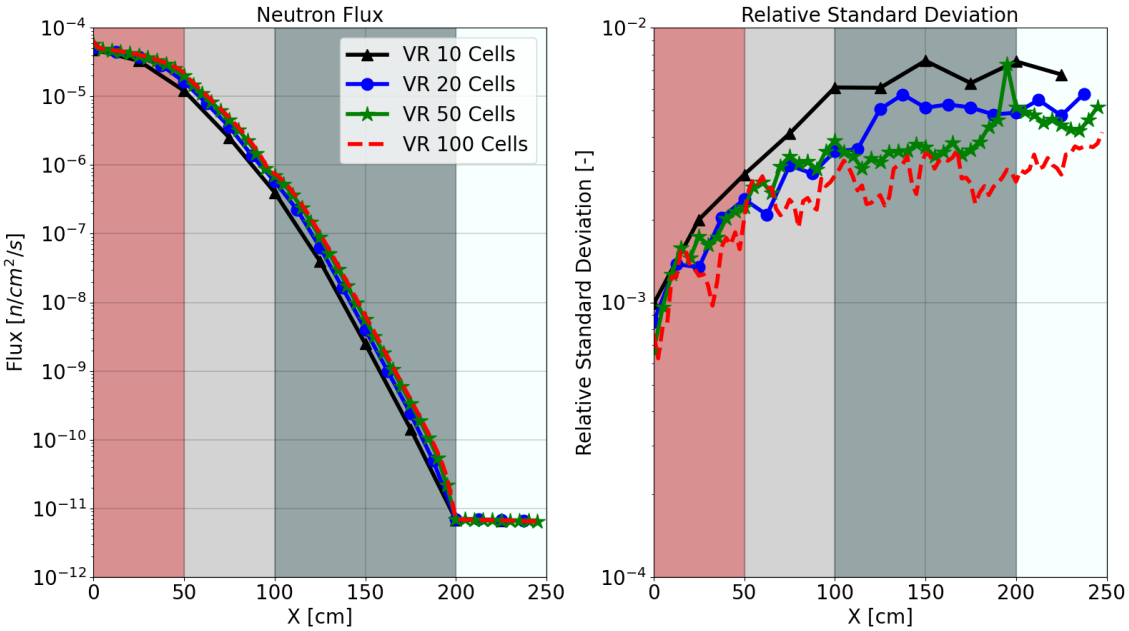

Figure 5.5: Neutron flux with different number of cells

As shown in Figure 5.5, 5.6 for this simple model also 10 Cells are sufficient to provide reliable results.
Considering the relative standard deviation in all the domain is lower than 1 % and increasing the number of cells decreases the overall RSD. The increase of computational time is smaller than the decrease of RSD, FOM results higher with higher number of cells.

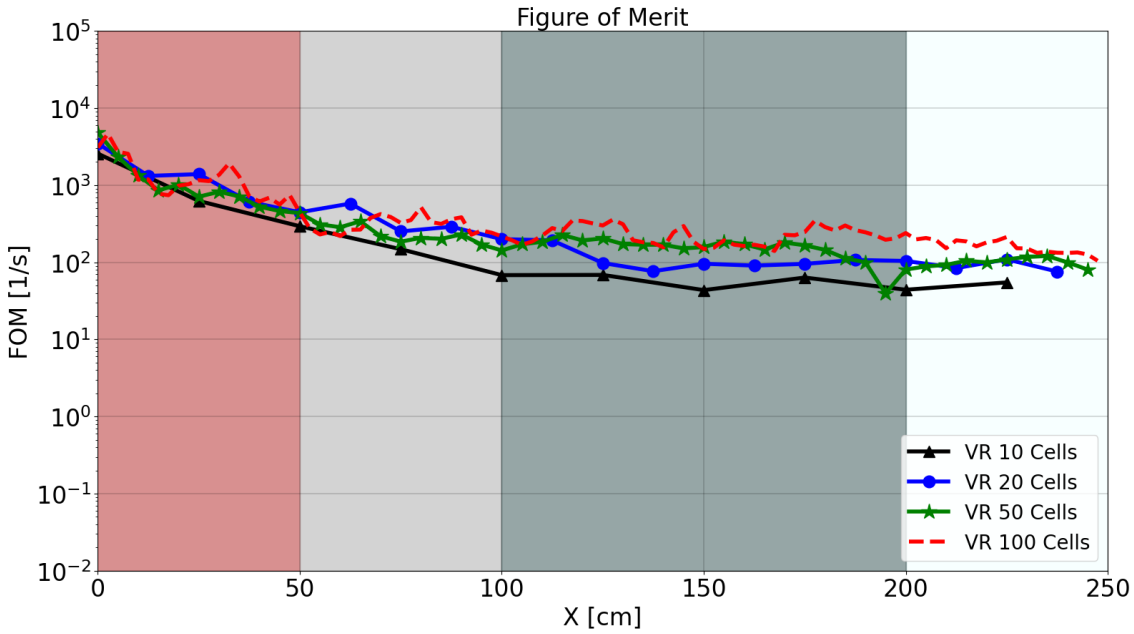

Figure 5.6: FOM with different number of cells

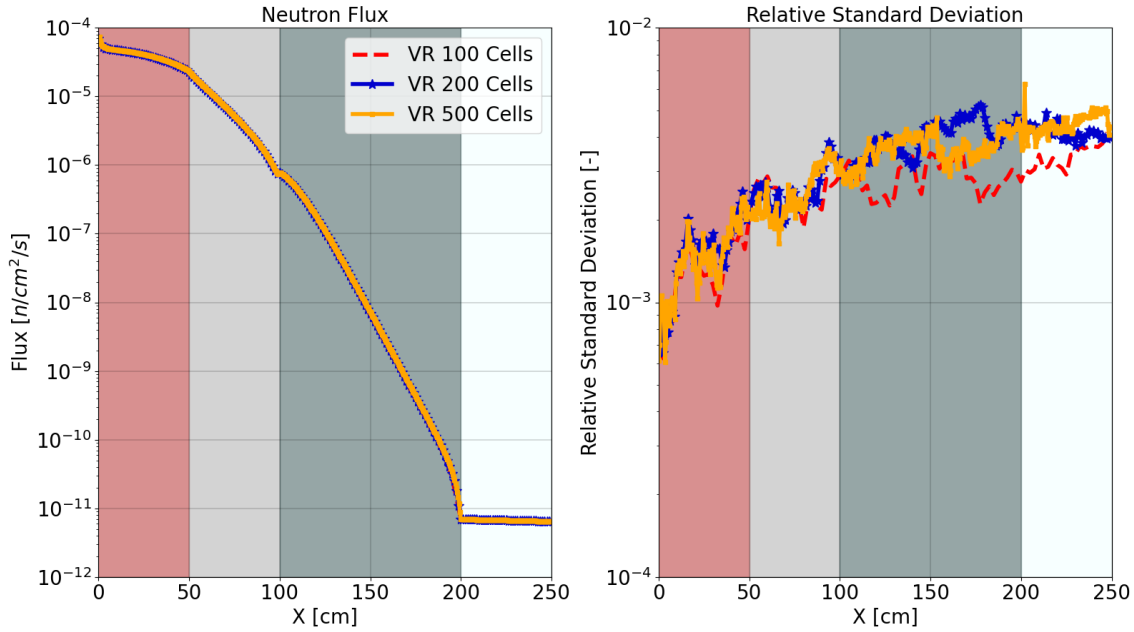

Figure 5.7: Neutron Flux profile 100-200-500 Cells

In Figure 5.7 a saturation trend is reached. If the number of cells is 200 or 500 the relative standard deviation is very similar to the case with 100 cells. However the FOM in Figure 5.8 shows a decrease due to higher computational time.
In this model the saturation trend is reached for around 100 Cells. Using the results obtained by the ”VR 100 Cells simulation”, further analysis were performed.

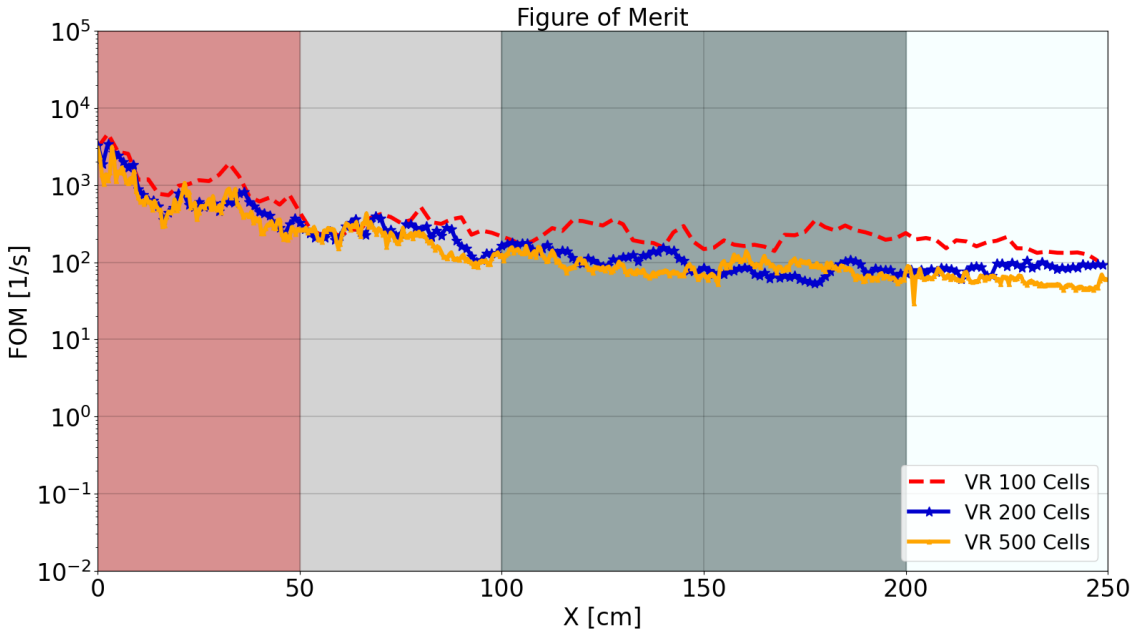

Figure 5.8: FOM 100-200-500 Cells

The Neutron flux attenuation in each layer "i" (Λ_i) was calculated as follows:

$$\Lambda_i = \frac{\phi_i^{beginning}}{\phi_i^{end}}, \tag{5.8}$$

where $\phi_i^{beginning}$ and ϕ_i^{end} are the flux calculated for each material "i". Moreover the flux ratio between adjacent cells (k_i) and $\Delta\phi_i$ were calculated as follows:

$$k_i = \frac{\phi_i^k}{\phi_i^{k+1}} \tag{5.9}$$

$$\Delta\phi_i = \frac{\phi_i^k - \phi_i^{k+1}}{\phi_i^k} \tag{5.10}$$

The flux ratio in fig. 5.9 shows that 50 cells are sufficient to provide a uniform flux ratio. The flux ratio needs to be as uniform as possible as Booth recommends and the weight windows ratio should not be higher than 4 for the whole domain [23][24].
Figure 5.10 shows that the cells are not correctly distributed. However $\Delta\phi_i$ is not uniform because it depends on the neutron flux attenuation in layer i.
In the air region, for instance, a high number of cells is not necessary because the neutron flux has a low attenuation (table 5.4).

A new mesh for VR 50 cells was proposed. The idea is try to distribute the number of cells based on the neutron flux order of magnitude in each material:
The modified mesh has the same number of cells but the dimension of the cells in each material is different:
The choice is based on the order of magnitudes presented in table 5.4. As shown in the

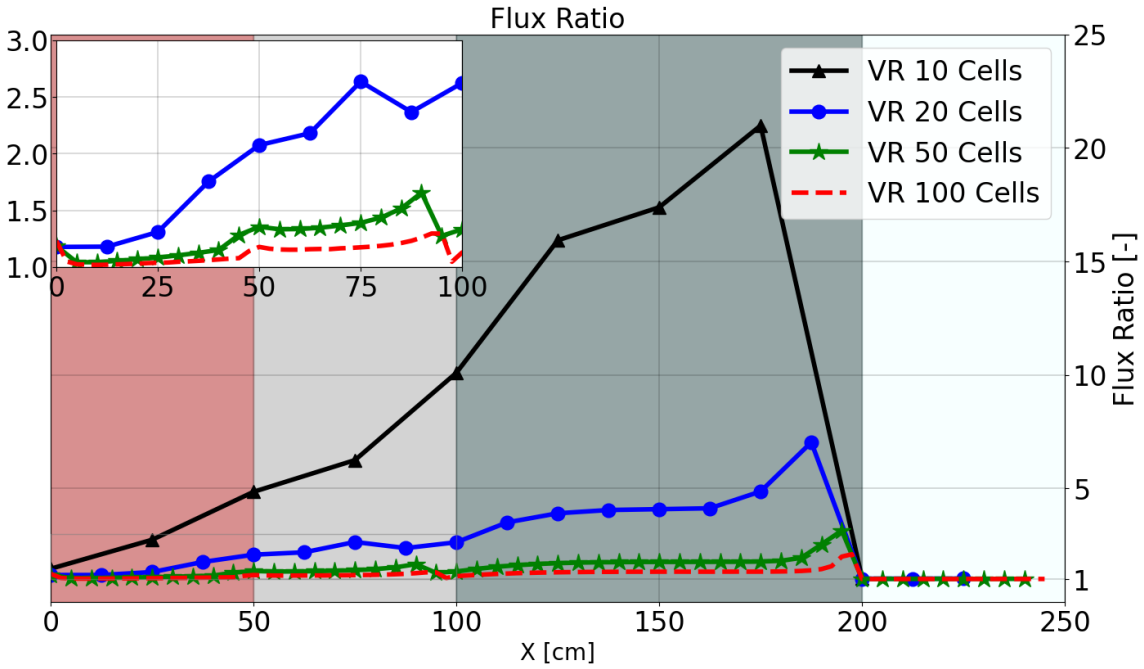

Figure 5.9: Flux ratio for different number of cells

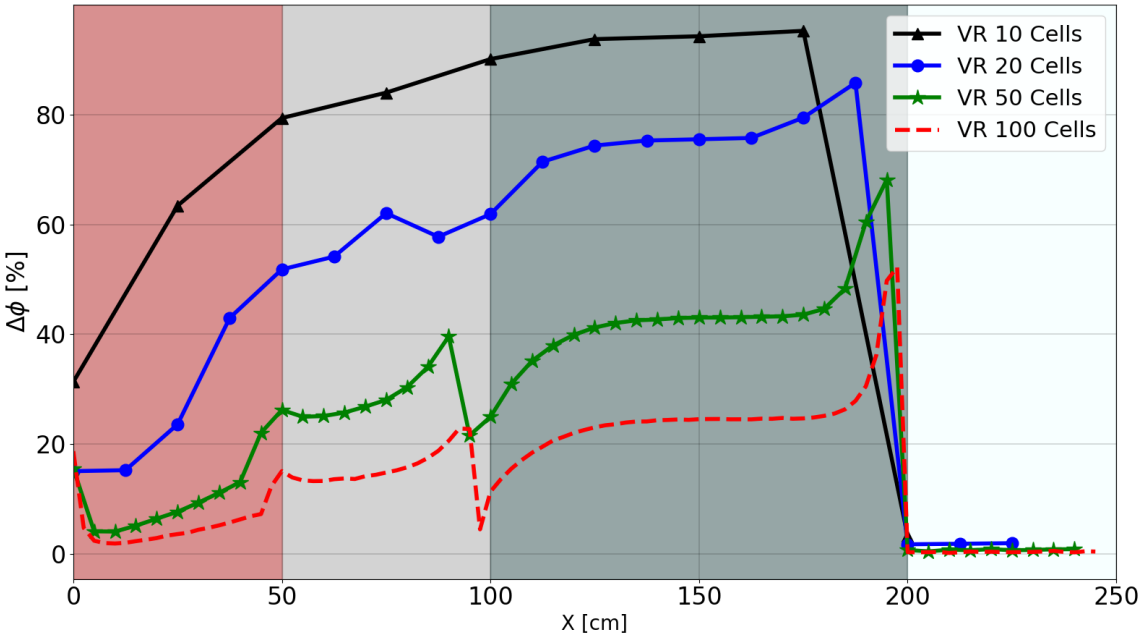

Figure 5.10: $\Delta\phi_i$ for different number of cells

liquid lead and in the air region the neutron flux attenuation is small, then the number of cells chosen is low.
The larger the neutron flux attenuation is, the higher number of cells is used in the concrete. The number of cells chosen for each layer is user-defined, and the experience of the user is useful to avoid a small number of cells that are not sufficient to give reliable results. The choice should also take into account the saturation problems highlighted in Figure 5.7.
No gain is shown using this configuration. Different arrangements were tested, varying the

Table 5.4: Neutron flux attenuation in materials (Simulation "VR 100 Cells")

Material	Neutron flux order of magnitude
Liquid Lead	2.57
Steel	$3.14 \cdot 10^1$
Concrete	$5.49 \cdot 10^4$
Air	1.07

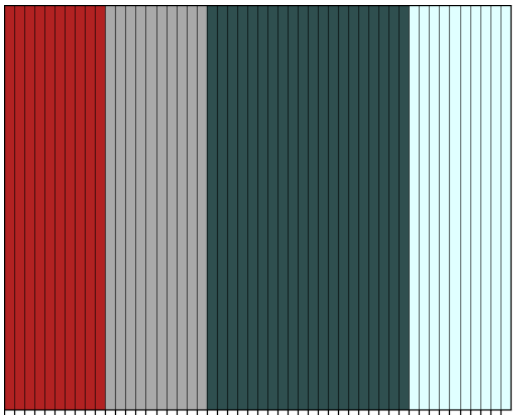

Figure 5.11: Starting mesh with 50 cells

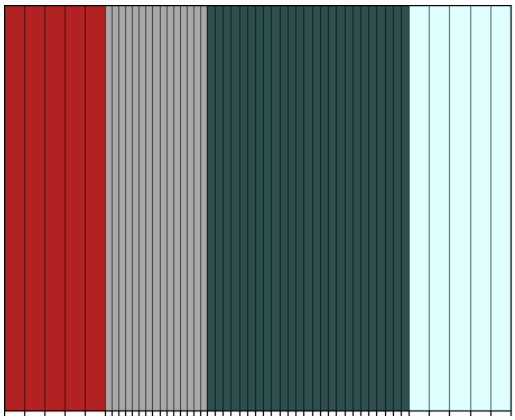

Figure 5.12: Modified mesh with 50 cells

Table 5.5: Modified mesh settings

Material	# of cells	Cell's dimension in X-direction [cm]
Liquid Lead	5	10
Steel	10	5
Concrete	30	3.33
Air	5	10

number of cells and their distribution in the materials. For the 1D model under analysis, the choice of an evenly spaced mesh appears to be the best option.

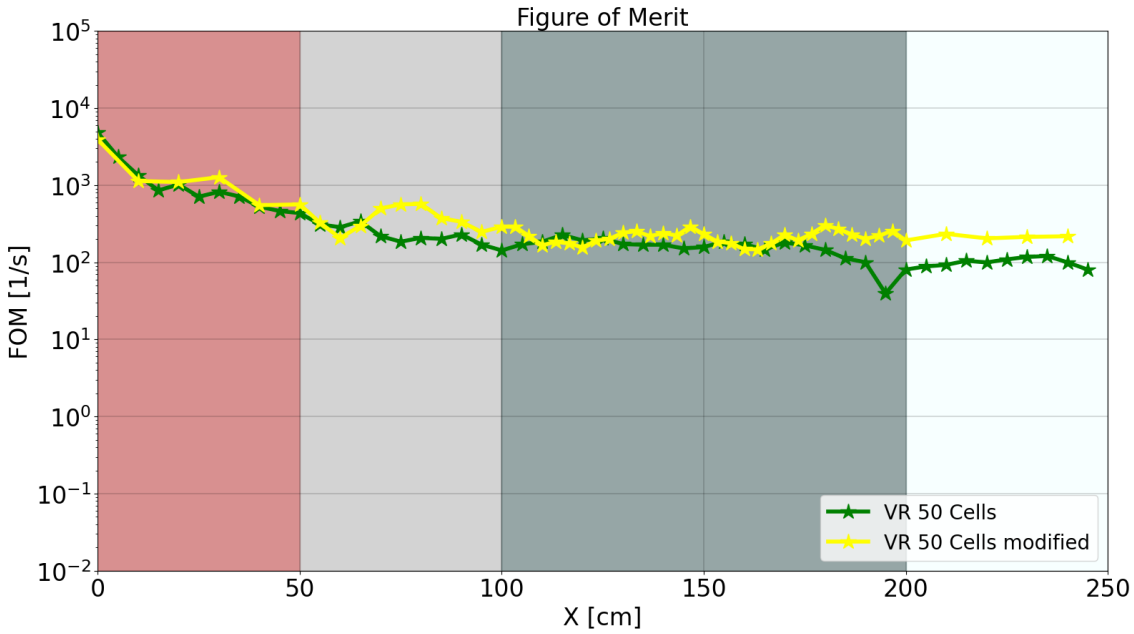

Figure 5.13: FOM comparison mesh modified

5.3 Analysis in MG mode

The Becker-Larsen model was studied to understand the effectiveness of WW and MAGIC in Multi-Group mode (MG). The WWs were generated with a spatial-energy mesh, the energy bins in the tally are the same of the CASMO 3-GROUP for the simulation in the MG mode. As mentioned in section 3.1.2, the total number of the weight windows is the cartesian product between spatial mesh dimension and energy groups.
Differently by the 1D slab multi-layer the simulation is in multi-group mode as described in section 4.3.

Table 5.6: Settings and performances of the MAGIC calculation carried out in OpenMC.

Particles/batch	# of batches	max # of splits	# of iterations	Threshold
10^3	10	10^6	5	0.7

Table 5.7: Analog Run and VR run settings

Simulation	Particles/batch	# of batches	max # of splits
Analog (AR)	10^8	10	-
Variance Reduction (VR)	10^8	10	10^5

The model is 3-dimensional and the mesh used in the analysis is 25x25x25. Each cell has

a volume of 1 cm^3.
The main purpose of the model is to test the WW in multi-group mode and the surface settings is enabled in case (paragraph 4.5).
The surfaces are implemented in the geometry definition and may not match the mesh cells used as filters in the tallies. In general, the mesh cells are different from the surfaces defined by planes in OpenMC, but in this model they are defined exactly in the same way as the mesh cells (each 1 cm in each direction there is a plane).

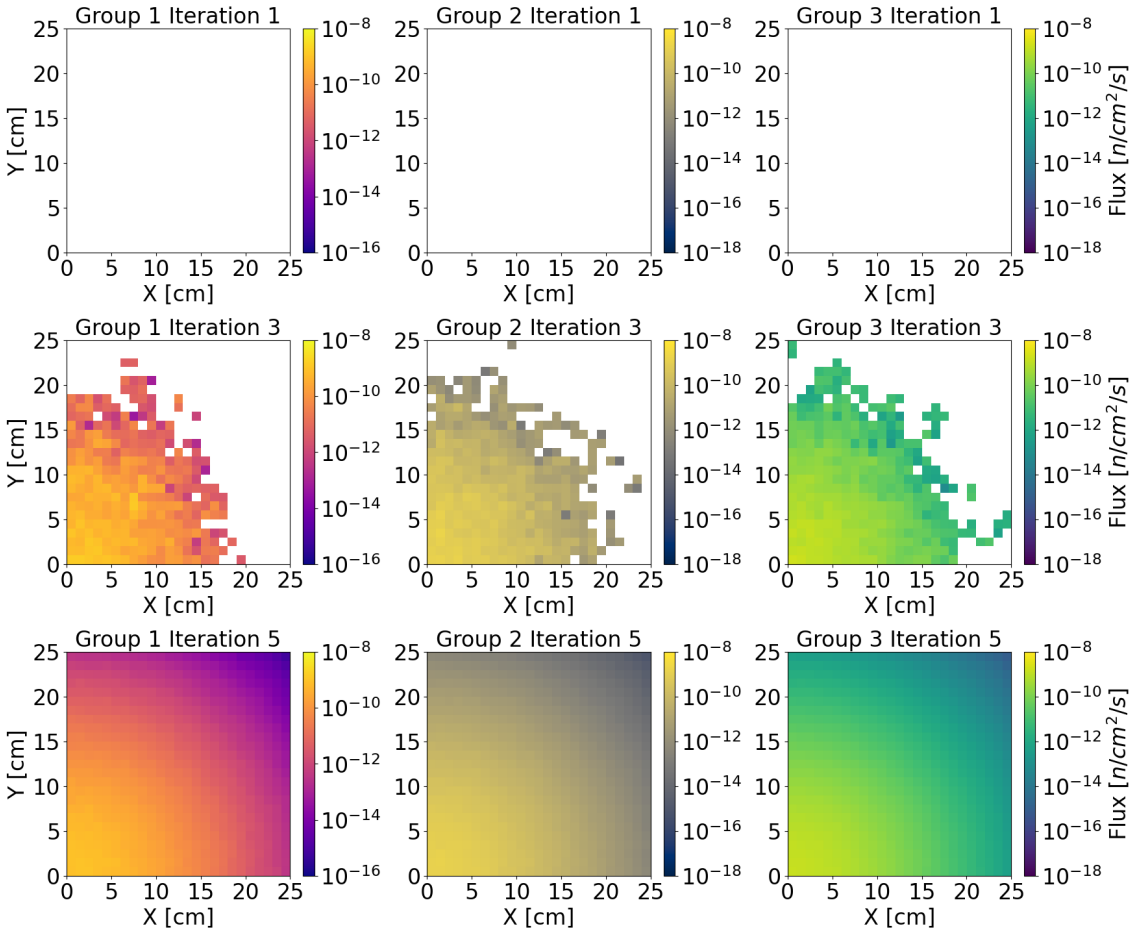

Figure 5.14: Neutron Flux during MAGIC iterations at z = 25 cm

Figure 5.14 shows the group neutron flux at the top of the cube. In the first iteration the flux score is 0 in any mesh cell because the particles particles are not able to reach the top of the cube due to the characteristics of the problem and for the settings chosen. If the number of particles and the number of splits are too low, the simulation also using the MAGIC could be not give reliable results.
During the iterative process the coverage ratio of the WW map increases, and the filling rate is different for each energy group.

Furthermore, for the next investigation, the study along the diagonal from the lower left corner to the upper right corner will be considered.
A focus on the iterative process for the first neutron flux group shows a high variance in also in the last WW map. As mentioned above, the flux score on the roof of the geometry

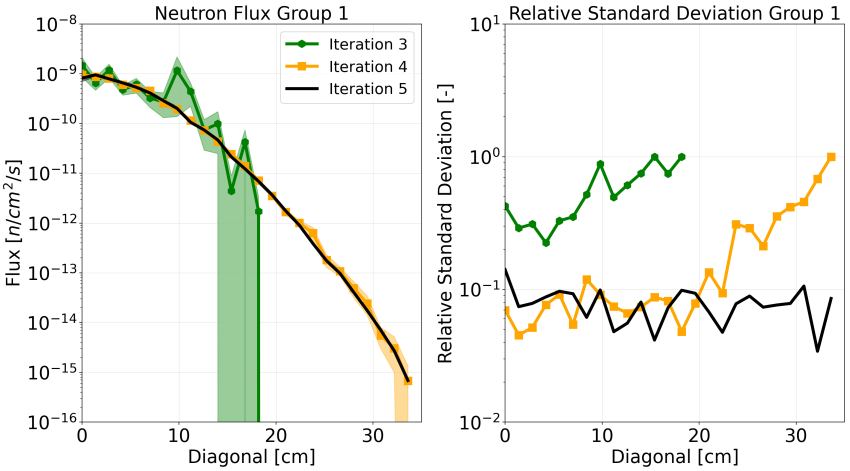

Figure 5.15: Neutron flux Group 1 along the diagonal z = 25 cm

could be very poor or completely lacking. For each z-plane the flux score is present along the diagonal as presented in Figure 5.15.

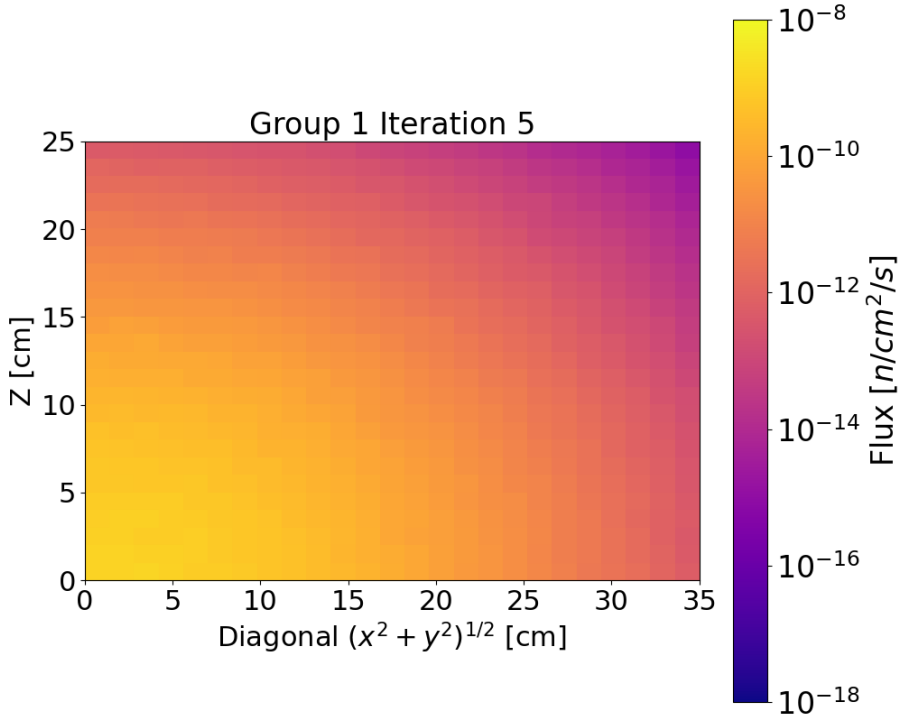

Figure 5.16: Neutron flux Group 1 along the diagonal

Considering the small number of particles, the MAGIC works correctly in the model presented. The relative standard deviation is high in Figure 5.15, but the main objective of MAGIC is to fill the WW map for the VR run.

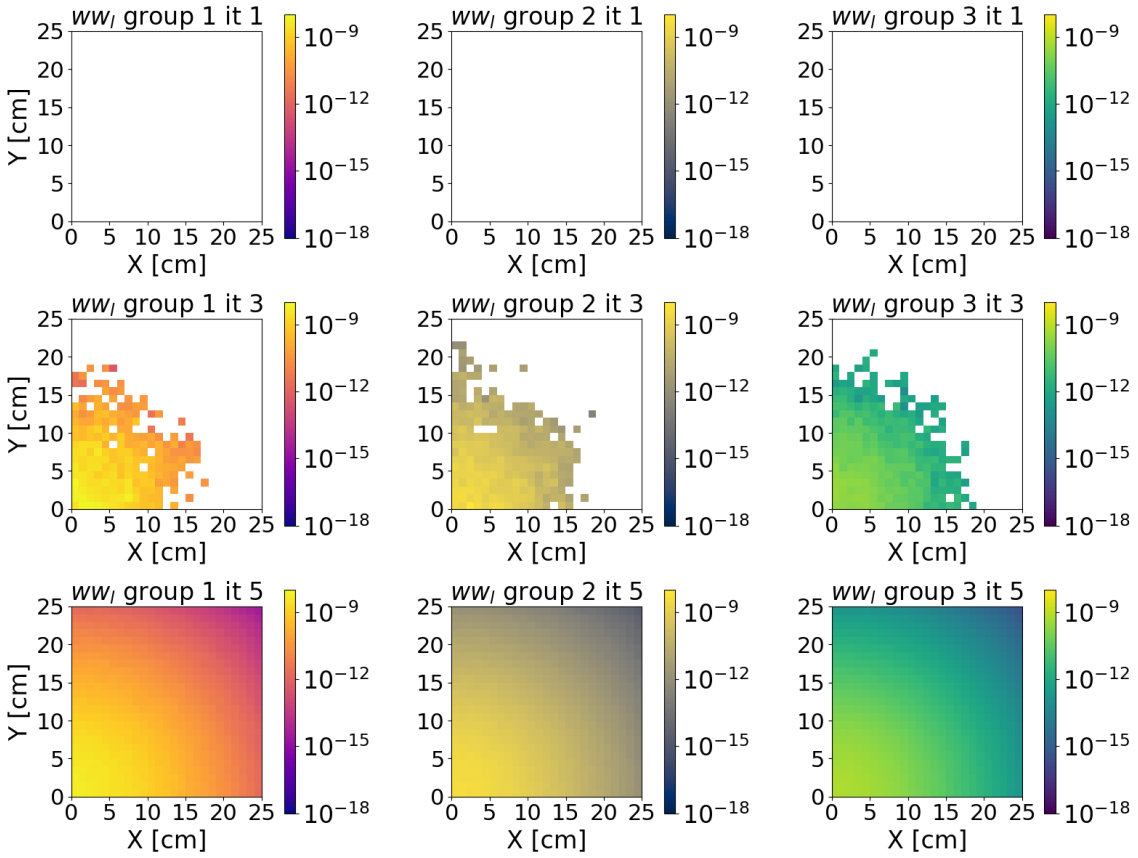

Figure 5.17: Weight Window lower bounds MAGIC Iterations at z = 25 cm

Figure 5.17 is useful to check the ”threshold” option (section. 4.1)of the WW. It can be seen that the weight window lower bounds in Figure do not properly follow the neutron flux value shown in Figure 5.15.
The activation of the threshold (0.7 for this model) set the WW lower bounds to -1 (de-activation value) where the RSD is higher than the threshold. When a particle enters in a phase space region where the WW lower bound is -1, it continues its life like in the AR (section 3.2). The third iteration in all groups shows that in half of the domain the flux value is present but the variance is too high.
In a z-plane at z = 1 cm the flux score is not present in all diagonals in AR as shown in Figure 5.18. The use of the weight windows and MAGIC is essential to obtain results in these regions. The main objective of the GVR methods is to populate the whole domain uniformly with the same low variance and this can be appreciated in the FOM profile for the VR run.

5.3.1 A Stress Test

A Stress test is typically used to verify the effectiveness of a method when the problem becomes very difficult to solve. In the Becker-Larsen model, the choice is to modify the scattering cross section to obtain a more absorbing medium. In this way the flux score is not favoured as the particles are quickly absorbed and the convergence of the MAGIC and

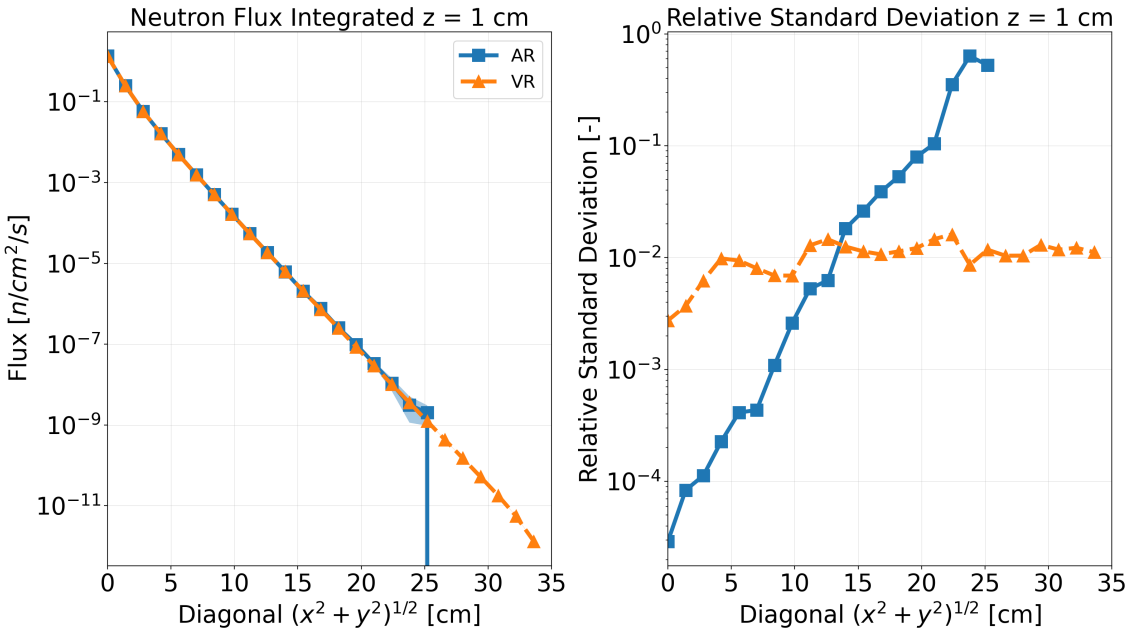

Figure 5.18: AR and VR run along the diagonal at z = 1 cm

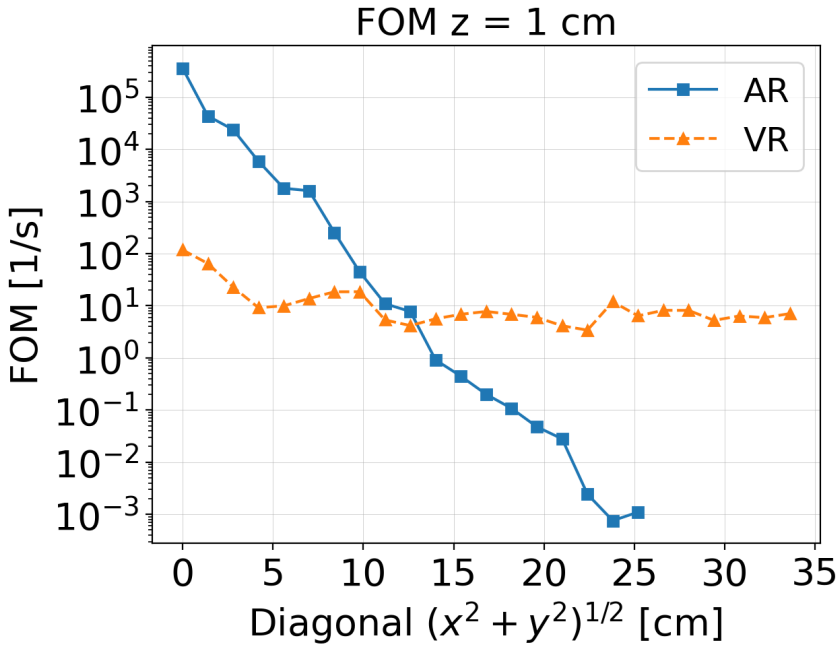

Figure 5.19: FOM along the diagonal at z = 1 cm

VR runs can be tested.
As shown in Figure 5.20 the absorption cross section is 99 % of the total. The weight adjustment through Eq. (3.6) is modified. The higher absorption is traduced in a reduction of the particle weight for each collision.
In this way the particles reach the weight cutoff before than the standard scattering matrix case and their histories end sooner than the standard model. Figure 5.21 compares the standard case with the modified case.

$\Sigma_{s,g\to1}\,[cm^{-1}]$	0.6	0.0	0.0
$\Sigma_{s,g\to2}\,[cm^{-1}]$	0.1	0.7	0.0
$\Sigma_{s,g\to3}\,[cm^{-1}]$	0.05	0.1	0.8

→

$\Sigma_{s,g\to1}\,[cm^{-1}]$	0.01	0.0	0.0
$\Sigma_{s,g\to2}\,[cm^{-1}]$	0.005	0.005	0.0
$\Sigma_{s,g\to3}\,[cm^{-1}]$	0.0	0.005	0.005

Figure 5.20: Standard and Modified Scattering Matrix

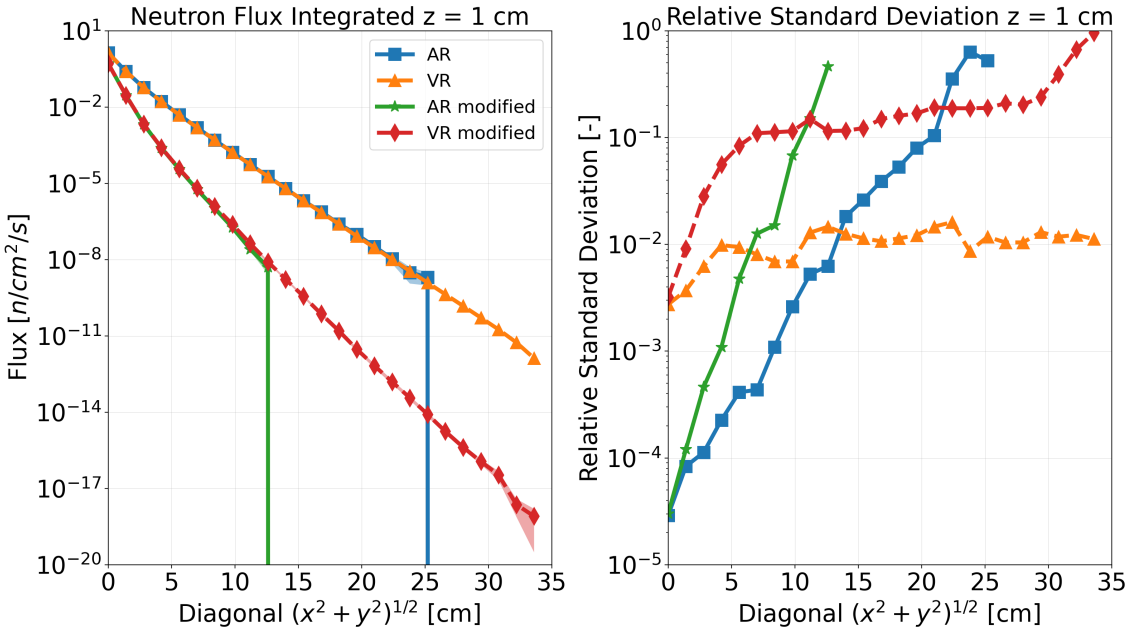

Figure 5.21: AR and VR run along the diagonal at z = 1 cm modified scattering matrix

The ”AR modified” compared with the ”AR” is able to score the neutron flux until 25 cm along the diagonal. The ”VR modified run” shows that the medium attenuates the neutrons better than the standard ”VR run” due to the lower weight of the particles in the deep regions.
The Relative Standard Deviation (RSD) comparison shows an increase in the VR modified run with respect to the VR run because less particles are able to reach the detectors in the deep regions of the geometry and to contribute to the variance estimation.
The FOM (Figure 5.22) in the modified VR is lower than in the default case due to the higher RSD. The increase in RSD is the main contributor to the higher FOM, in fact the computational time is lower because the particle histories end earlier.
The plots are considered in the z-plane at the top of the source, but it can be useful to understand if the flux is scored in the upper right corner at the top of the cube (z = 25 cm):

Figure 5.23 shows that in the default scattering matrix the AR is able to score the flux in a small portion of the plane. The VR profile is completely full in the default case with a low variance.
On the other hand, in the modified scattering matrix case (Figure 5.24) the AR is not able to score any particles because they are killed due to the higher absorption probability. The

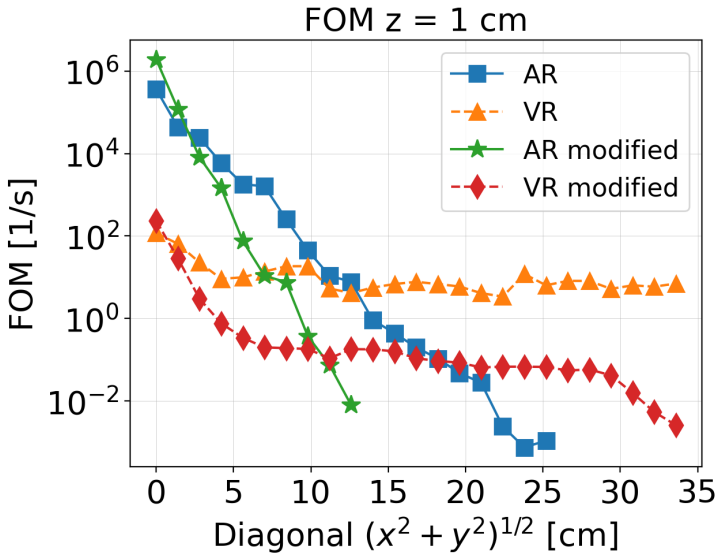

Figure 5.22: FOM comparison with modified scattering matrix

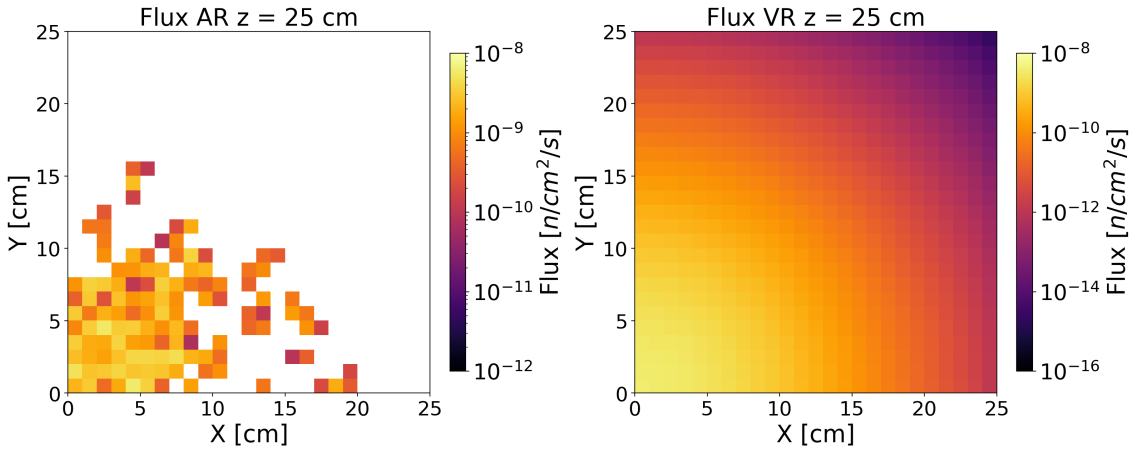

Figure 5.23: Neutron flux at z = 25 cm AR and VR (Default scattering matrix)

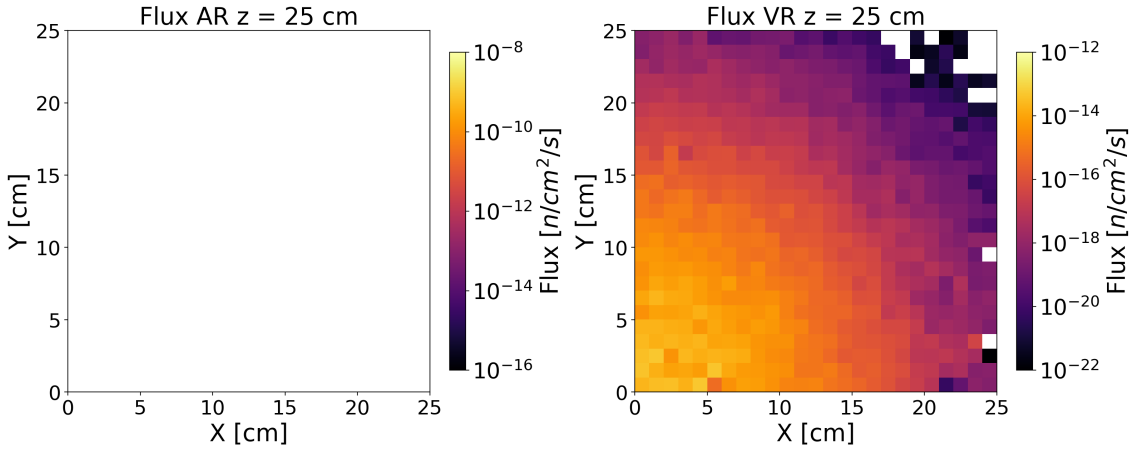

Figure 5.24: Neutron flux at z = 25 cm AR and VR (Modified scattering matrix)

VR run is not able to score the neutron flux in the whole domain and in deep regions the variance is very high. The only way to solve these problems is to increase the number of simulated particles or to increase the number of splits and consequently increases the computational effort.

5.4 Verification of MAGIC in a structure holding nuclear fuel

The estimation of the neutron flux in a structure containing nuclear fuel was performed using the stopping criteria described in section 5.1. The spatial mesh used during the analysis is the mesh proposed by article 86x46x46 cells where each cell has a volume of 10 cm^3.

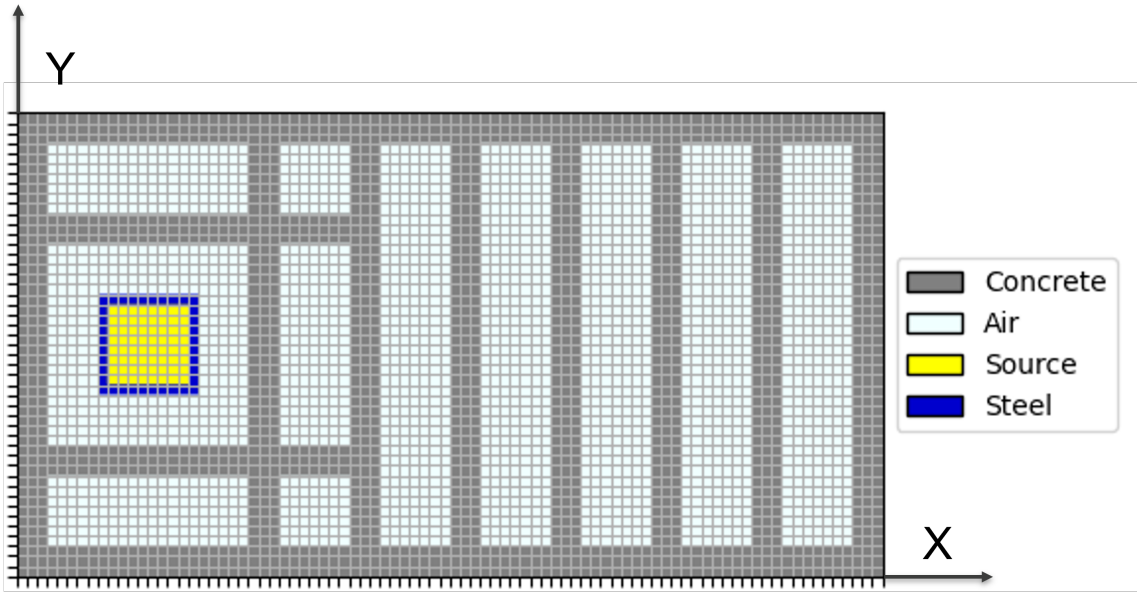

Figure 5.25: Regular Spatial mesh at z = 215 cm

One of the main points of interest for the model is the convergence of the WW map during the MAGIC iterations for each group. In the following table there are settings for the MAGIC method are reported.

Table 5.8: Settings and performances of the MAGIC calculation carried out in OpenMC.

Particles/batch	# of batches	max # of splits	Stopping criteria	# of iterations	Time [min]
10^4	10	10^5	Yes	12	48.71

With the introduction of the stopping criteria the MAGIC process ends after 12 iterations. The coverage ratio was plot for each group during the iterations as shown in Figure 5.26. The convergence rate of the groups is very different and the coverage ratio in the high

energy groups is very low (first group 6.37, 20 MeV). The main reason is the nature of the source, in fact the Watt's energy spectrum[10] for the U-235 has a low chance of emitting neutrons at high energy and the collisions during their history reduce the neutron energy.

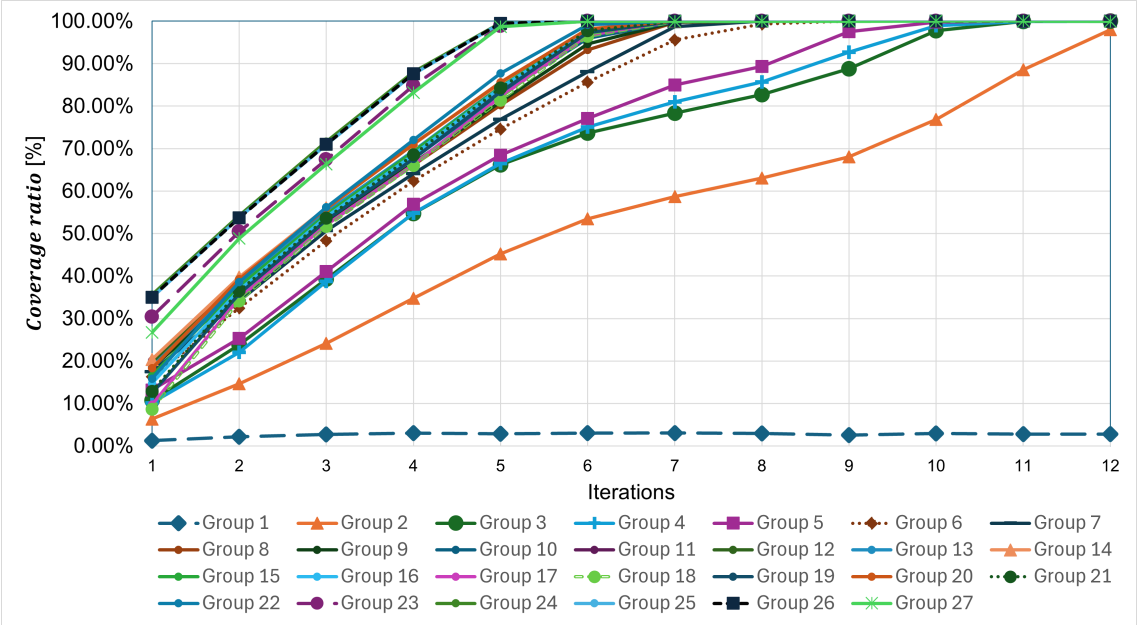

Figure 5.26: Coverage Ratio convergence trend, for the different energy groups, with respect to the number of MAGIC iterations

The average coverage ratio during the iterations is shown in table 5.9. The coverage

Table 5.9: Average Coverage Ratio

Iteration	1	2	3	4	5	6	7	8	9	10	11	12
Average ζ [%]	17.86	36.10	51.94	66.32	79.73	89.27	92.57	93.44	94.43	95.42	95.97	96.32

ratio has an increasing trend thanks to the use of the previous WW map as input. The last WW map has many energy groups completely filled (CR equal to one) and only the first and the second group are not filled.

Figure 5.27 shows the WW filling during the iterations in a plane at z = 215 cm (the center of the source). In the first iterations the shape of the source is easily identifiable. The particles can not reach the deep penetrations regions but the MAGIC uses the map to score the neutron flux in the whole domain as shown in the iteration 12, even if the neutron flux attenuation is very high (16 order of magnitudes between the source and the end of the structure). The iterative process is fundamental to get the flux score and the splits allows to the particles to reach the regions far from the emission point. The analysis of the neutron flux in the group 5 is motivated to compare the results with the literature [41].

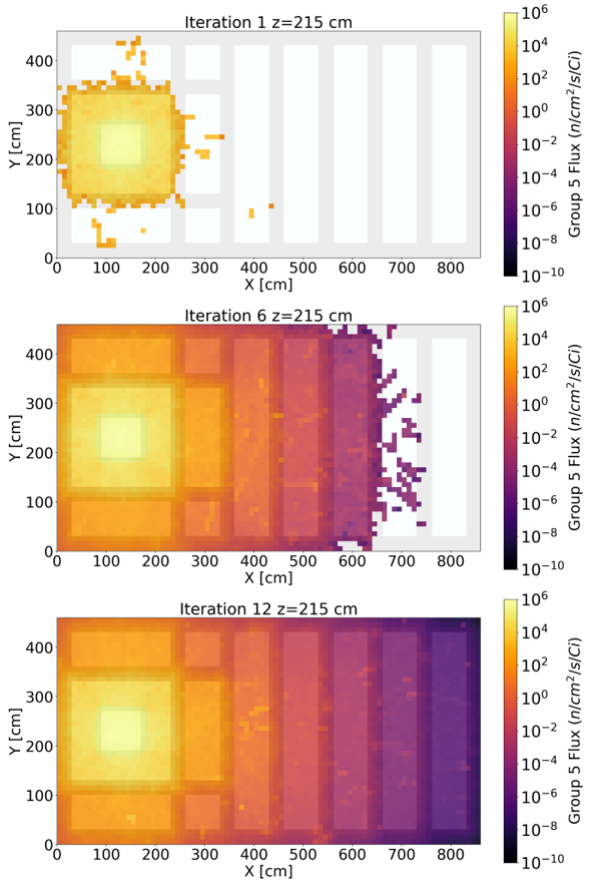

Figure 5.27: Group 5 neutron flux (0.9 to 1.4 MeV) during the MAGIC

The settings for the AR and the VR run are presented in the following table:

Table 5.10: Analog Run and VR run settings

Simulation	Particles/batch	# of batches	max # of splits
Analog (AR)	$2 \cdot 10^7$	10	-
Variance Reduction (VR)	$2 \cdot 10^6$	10	10^5

Figures 5.28, 5.29 show that the AR is not able to fill the flux map. The VR run with the use of the WW is necessary to get the score value in the whole domain.
The possibility to compare the results with other VR methods is the motivation for the choice of the Wagner-Peplow-Mosher model to test MAGIC with stopping criteria.

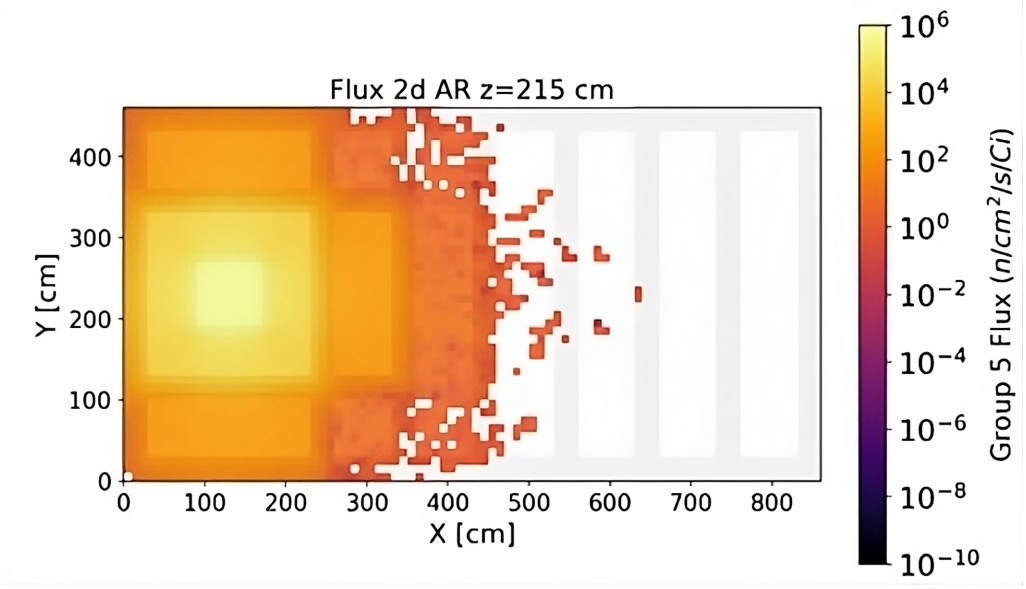

Figure 5.28: Group 5 neutron flux (0.9 to 1.4 MeV) AR at z = 215 cm

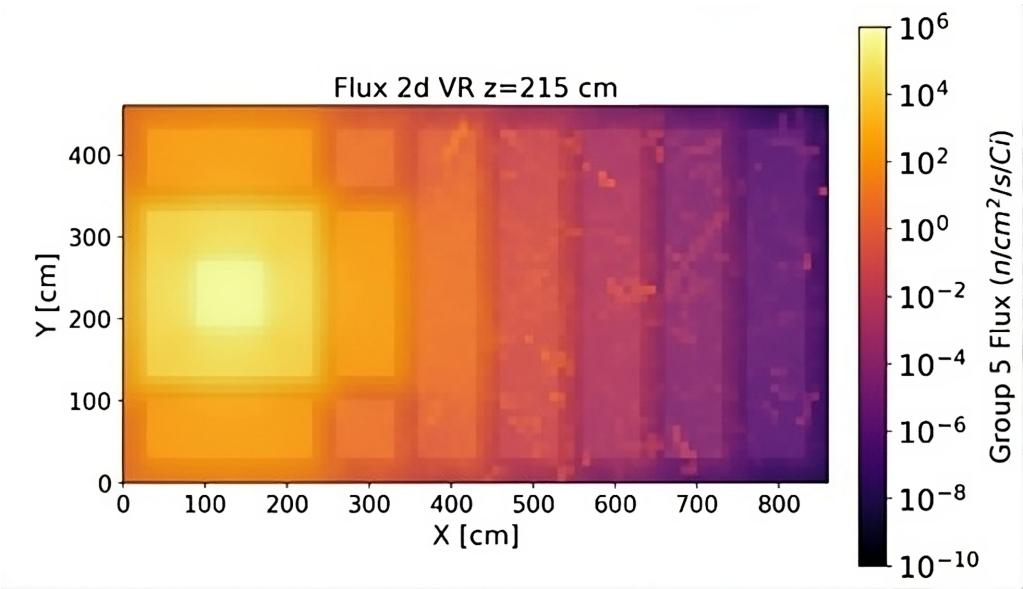

Figure 5.29: Group 5 neutron flux (0.9 to 1.4 MeV) VR at z = 215 cm

The other VR methods are very close in estimation shows in Figure 5.30.
In the AR the profile is not complete along the x-direction, while in the VR the complete flux estimation is evaluated. In deep regions in the neighbourhood of concrete walls, the RSD is higher because the particles collide more frequently.

The particles can be rouleted more easily and their history end If a large number of

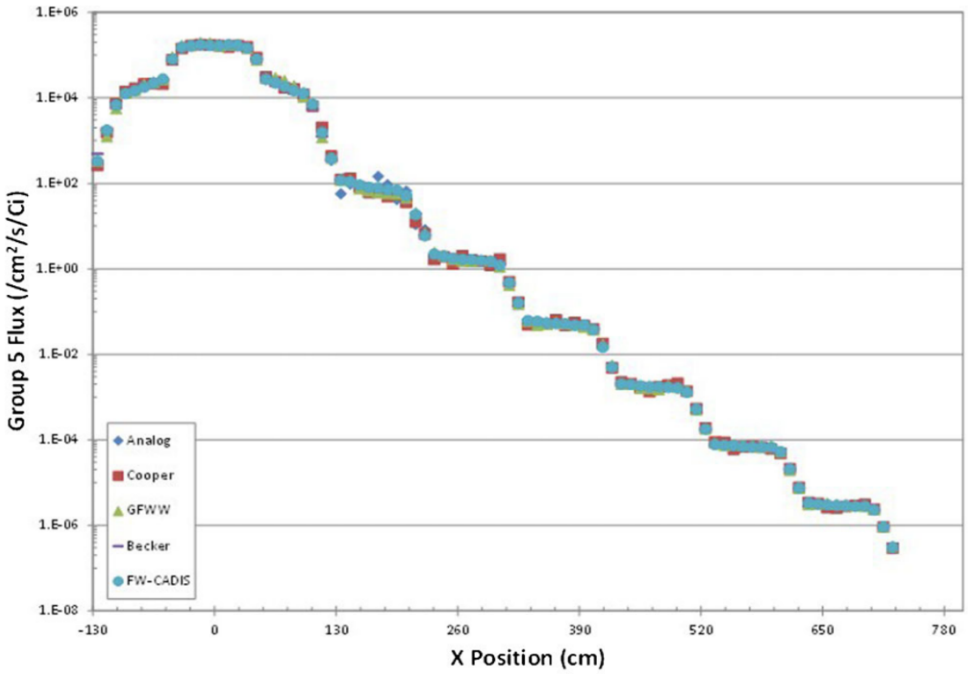

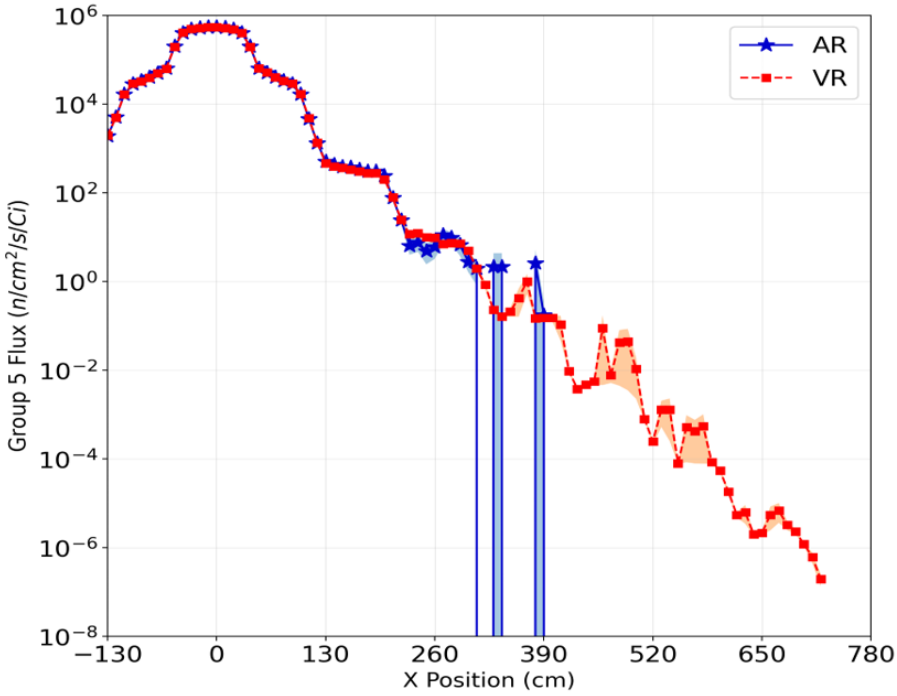

Figure 5.30: Group 5 neutron fluxes (0.9 to 1.4 MeV) along x direction in the center of source z=215 cm, y=230 cm. First Figure Paper Results, Second Figure OpenMC Results.

particles lose the roulette game, the contribution in the detectors region is lower and consequently the variance and RSD will be higher. In the next section the comparison between the mean RSD and the coverage ratio will be analysed in more detail.
Table 5.11 compares the different methods taken from the reference [41] with the OpenMC calculation using MAGIC. The calculations with the different VR method are compared

Table 5.11: Comparison among the performances of the MAGIC compared to the other techniques employed in the reference

Method	Histories	Time (min)	ζ	Mean RSD	Cells with <10 % RSD [Fraction]
Analog	16 986 000	1444	0.4589	2.14E-01	0.1
Cooper and Larsen	375 000	1415	0.9921	2.03E-01	0.23
GRWW	166 750	1419	1.0000	1.37E-01	0.4
Becker's Global	1 417 800	1383	0.9997	1.27E-01	0.51
FW-CADIS	29 610 000	1391	1.0000	9.33E-02	0.67
MAGIC	20 000 000	1326	1.0000	5.43E-02	0.87

on the basis of different parameters, which are: the number of particle histories, the overall computational time, the coverage ratio ζ, the mean RSD and the fraction of cells with an RSD < 10%. The spatial mesh used in the reference [41] was employed in the MAGIC calculation as well, comparing different parameters. The coverage ratio (ζ) is calculated using the neutron flux integrated on the entire energy spectrum, while the "mean RSD" appearing in the table is the average relative uncertainty calculated across all the spatial cells in the geometry.
The table shows that some methods, like the standard calculation and the method proposed by Cooper and Larsen, are not able to provide estimations over the entire domain. While the mean RSD is quite similar for the first four methods, the number of cells with an RSD below 10 % shows a notable discrepancy. In comparison to FW-CADIS, which employs an adjoint flux to determine the weight windows, the results obtained with MAGIC are similar. However, the mean RSD in MAGIC is the lowest, and the proportion of cells with lower uncertainty is markedly higher when MAGIC is used.
The performance of the different VR methods cannot rely on the comparisons of Figure of Merits since different computer architecture were used. However, it can be appreciated that, for a similar number of particle histories simulated using MAGIC and FW-CADIS, MAGIC provided a smaller value of the average RSD and a larger number of regions having RSD below 10%.

5.4.1 Non-Regular mesh test

Mesh refinement test performed in the 1-D multi layer model show saturation issues. To verify the difference between a non-regular and a regular mesh, a new evaluation was performed for this model. The idea is modify the distribution of the cells in the materials maintaining the same number of cells (181 976).

The mesh is modified as presented in Figure 5.31, 5.32. The distribution of the cells

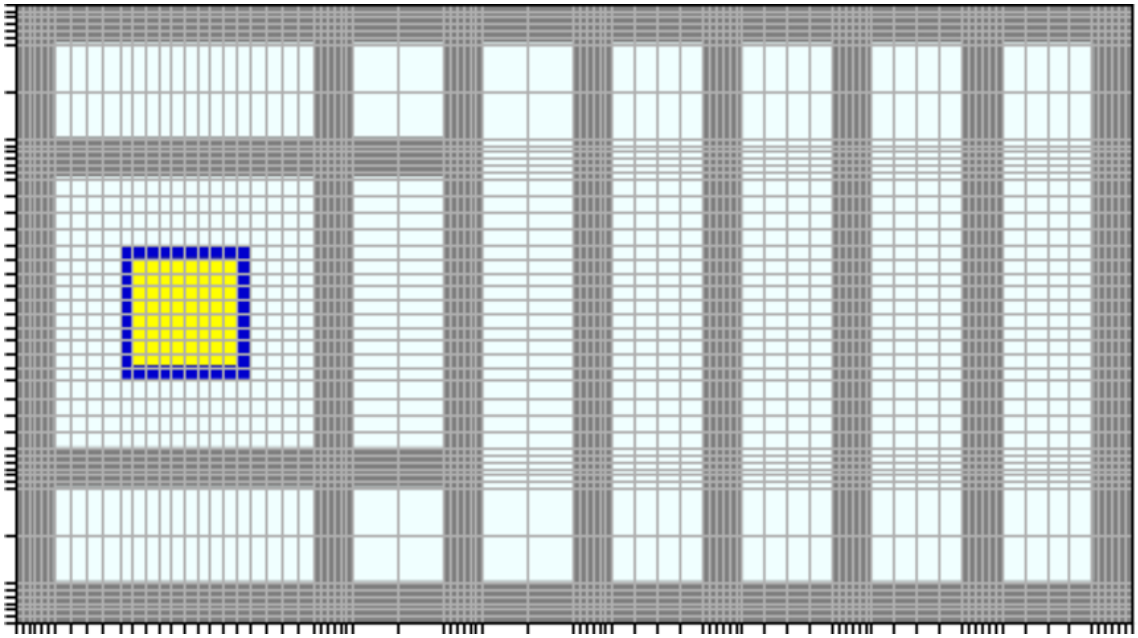

Figure 5.31: Non-regular spatial mesh at z = 215 cm

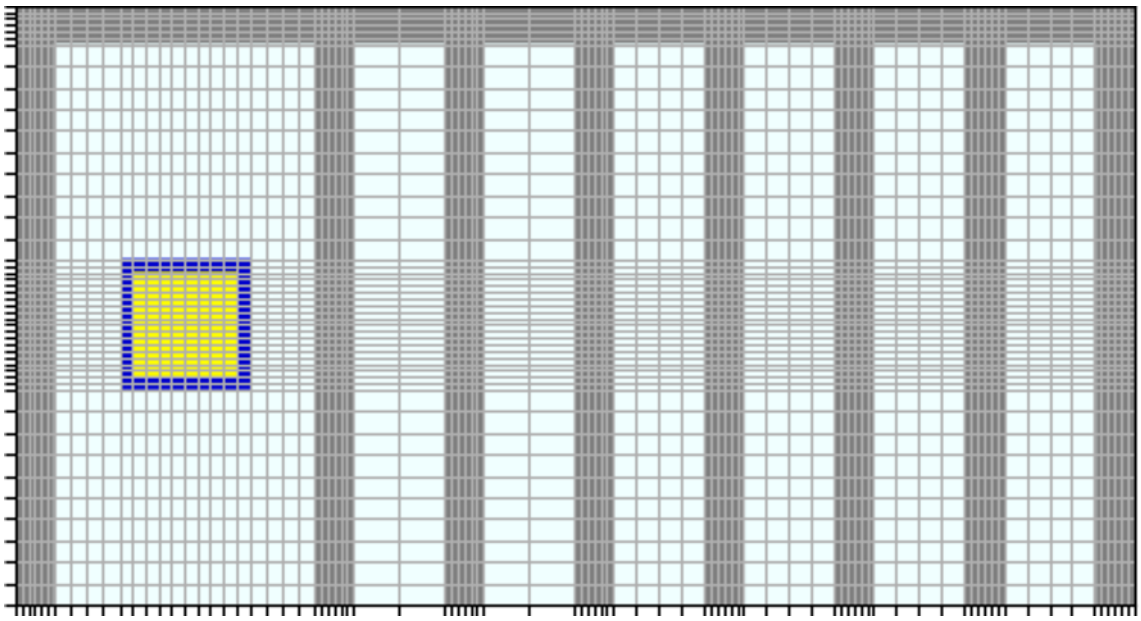

Figure 5.32: Non-regular spatial mesh at y = 230 cm

is made in order to have a higher number of cells in the concrete walls. However the choice in each material and in each region is arbitrary. The number of cells close to the source is high to split faster the particles with a high weight. The final goal is understand if this configuration could enhance the performance of the method.

The results presented in table 5.12 show that the non-regular mesh in this model does not improve the performance. The mean RSD is higher than the regular mesh test and the computational time is also bigger. Consequently the FOM is lower even if the Coverage

Table 5.12: Comparison between the VR methods

Method	Histories	Time (min)	ζ	Mean RSD	Cells with <10 % RSD [Fraction]	FOM [1/min]
MAGIC Regular Mesh	20 000 000	1326	1.0000	5.43E-02	0.87	1.80E+01
MAGIC Non-Regular Mesh	20 000 000	2210	1.0000	6.39E-02	0.85	1.20E+01

ratio and the fraction of cells with RSD < 10 % are approximately the same. The regular mesh seems to be the best option also for the structure holding nuclear fuel.
A second test was carried out on the mesh, reducing the number of cells to generate the WW.
Using the knowledge gained from the mesh refinement analysis on the 1-D multi-layer model, a new mesh 72x40x24 was proposed (table 5.13, 5.14):

Table 5.13: Variable mesh regions (X-Y direction)

Region	Dimension [cm]	# of cells	Δ x [cm]
Concrete wall	30	6	5
Air gap	70	2	35
2 Air regions Source-Concrete walls (X-Y)	100	2	50
Source region (X-Y)	100	8	12.5

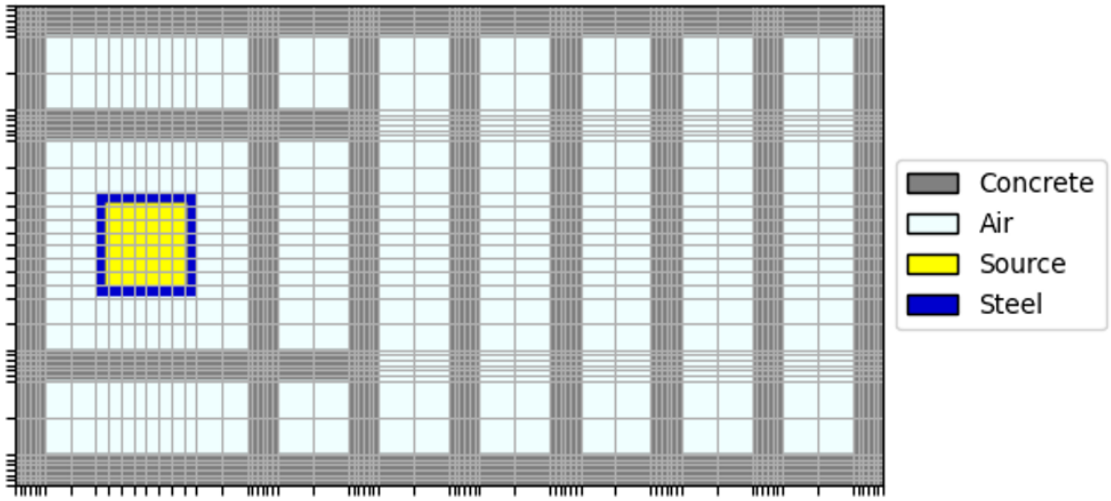

Figure 5.33: Variable mesh regions (X-Y direction)

The new mesh is less dense and the cells are distributed according to the neutron flux

attenuation through the different materials.

Table 5.14: Variable mesh regions (Z direction)

Region	Dimension [cm]	# of cells	Δz [cm]
Concrete wall	30	6	5
Air region below the source	165	5	33
Air region above the source	165	5	33
Source region (Z direction)	100	8	12.5

Table 5.15: Setting and performances of MAGIC with the new mesh.

Particles/batch	# of batches	max # of splits	Stopping criteria	# of iterations	Time [min]
10^4	10	10^5	Yes	9	26.02

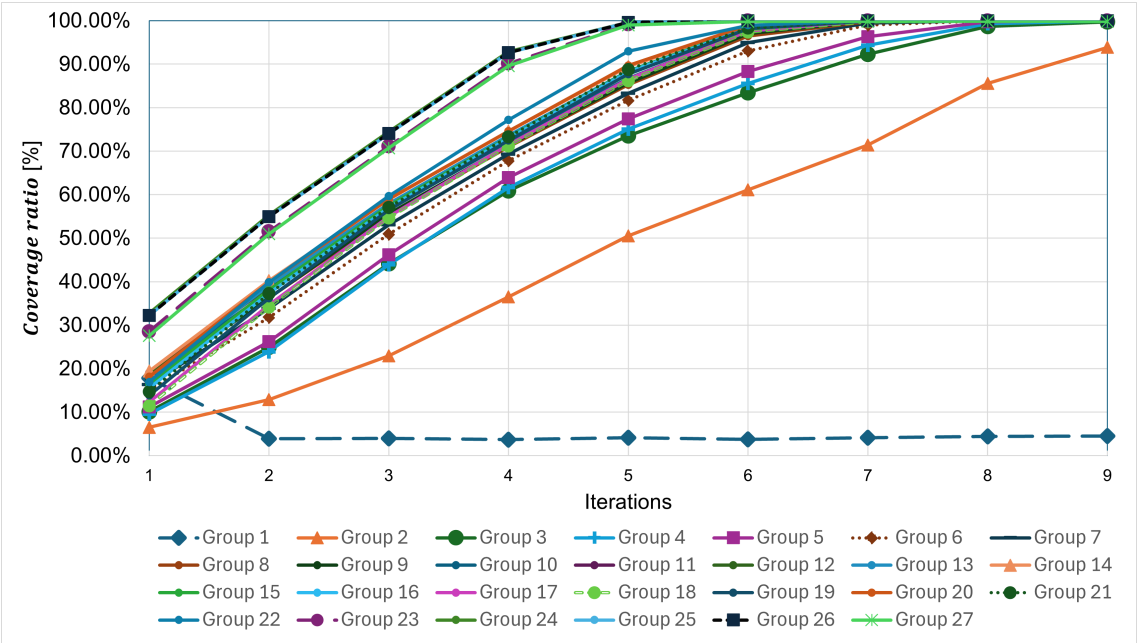

Figure 5.34: Coverage Ratio convergence trend, for the different energy groups, with respect to the number of MAGIC iterations with tuned mesh

The number of required iterations using the tuned mesh is reduced from 12 to 9. This is mainly due to the lower number of cells where the flux should be scored, which means that the stopping criteria is reached sooner. Despite the coarser WW mesh, the coverage ratio

Table 5.16: Average Coverage Ratio with respect to the number of MAGIC iterations using the tuned mesh

Iteration	1	2	3	4	5	6	7	8	9
Average ζ [%]	18.06	36.67	55.01	71.00	83.79	91.87	94.66	95.83	96.21

at the 9th iteration (see table 5.16) is very similar to the one of the final iteration shown in table 5.9. Moreover, a gain of about 26 min in the computational time was achieved.

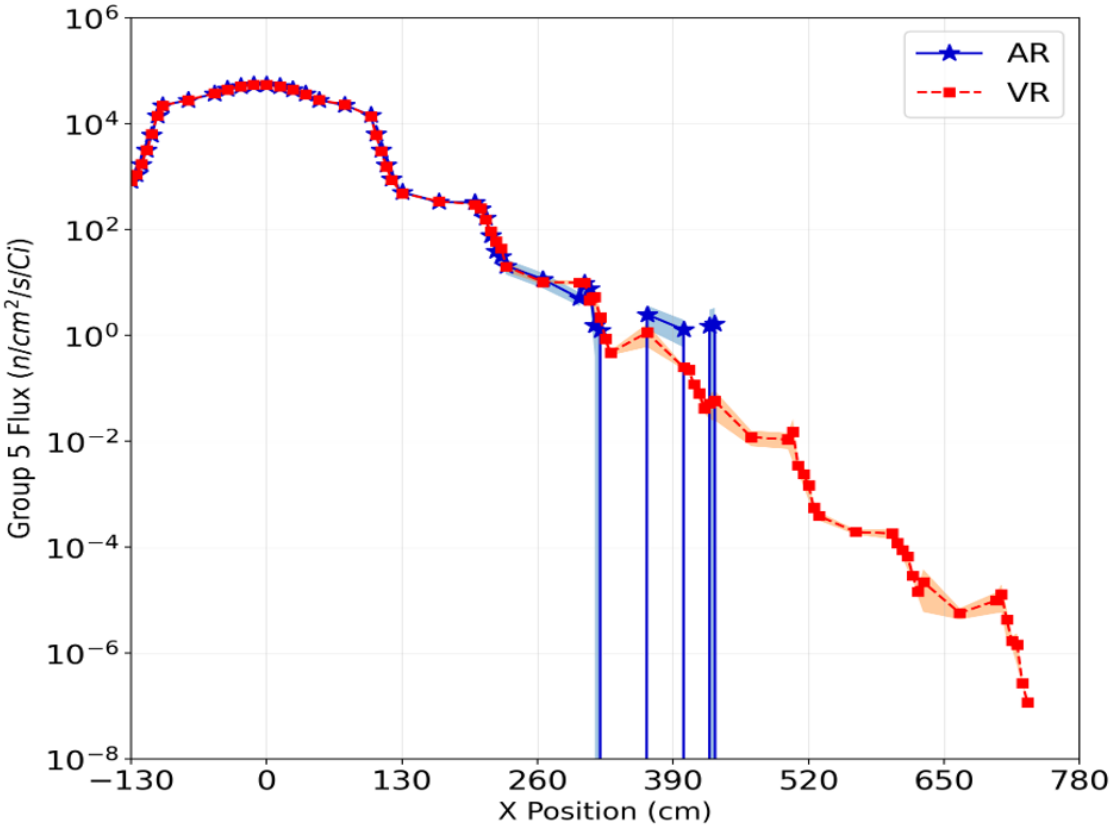

Figure 5.35: Group 5 neutron fluxes (0.9 to 1.4 MeV) along x direction in the center of source z=215 cm, y=230 cm new mesh

The VR run shows that the neutron flux profile is similar to that shown in Figure 5.30, but the shape near the source is distorted and the peak is not the same as in the previous case. If the goal is estimate the neutron flux to perform a dose rate assessment in deep regions the results seems to be reliable.
The results in Table 5.17 show that the computational time is reduced by 200 minutes. The mean RSD is the same, but we have a small gain in terms of FOM. However, in relative terms it could be useful when the number of particles is higher.

Table 5.17: Comparison between the VR methods

Method	Histories	Time (min)	ζ	Mean RSD	Cells with <10 % RSD [Fraction]	FOM [1/min]
MAGIC Regular Mesh	20 000 000	1326	1.0000	5.43E-02	0.87	1.80E+01
MAGIC New mesh	20 000 000	1112	1.0000	5.36E-02	0.88	2.20E+01

5.5 Photons test

The main motivation for carrying out this test is to analyse the MAGIC and to find out the difference between the photon test and the neutron test. The surface setting is enabled for these test for the reason explained in section 4.5. For our model the surfaces are implemented in 0.1 cm increments. The total number of surfaces is 500 and the weight is compared each time that a particle crosses a surface. The following table shows the MAGIC settings:

Table 5.18: Settings and performances of the MAGIC calculation carried out in OpenMC.

Particles/batch	# of batches	max # of splits	Stopping criteria	# of iterations	Time [min]
10^5	5	10^6	Yes	4	4.64

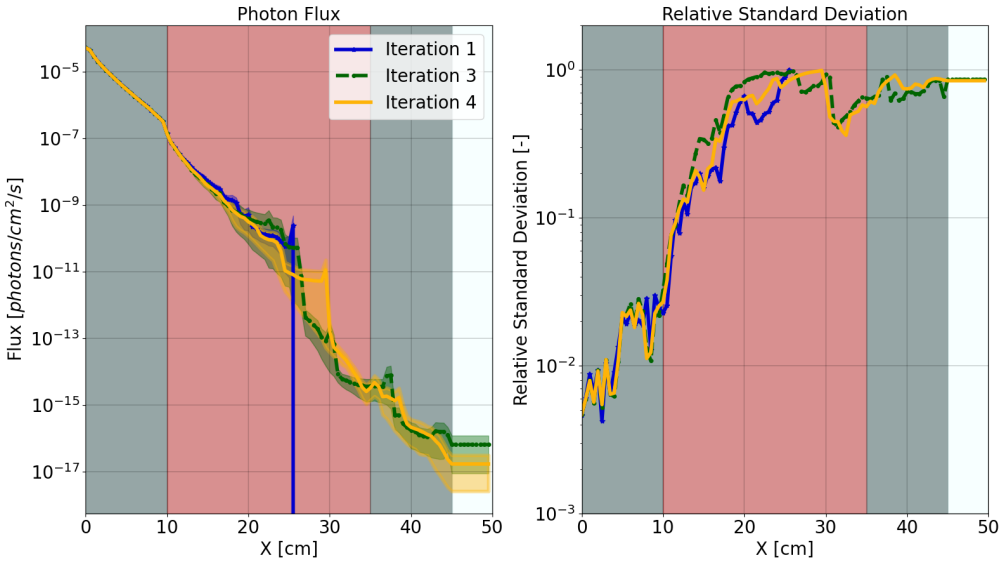

Figure 5.36: Photon flux during MAGIC iterations

The MAGIC iterations show a different behaviour to that obtained during the neutron test. The WW map is filled during the iterations, but the RSD remains very high even when the map is complete. The reason is that, as mentioned above, the photons collide less than neutrons and they are not able to reach deep regions easily. The surface settings try to

compensate these problems, but the number of photons reaching the end of the geometry is still very low, even with a high number of splits. Two tests were performed increasing the number of particles in AR and VR run with the same MAGIC settings.

Table 5.19: Analog Run and VR run settings Test 1

Simulation	Particles/batch	# of batches	max # of splits
Analog (AR)	10^5	5	-
Variance Reduction (VR)	10^7	5	10^4

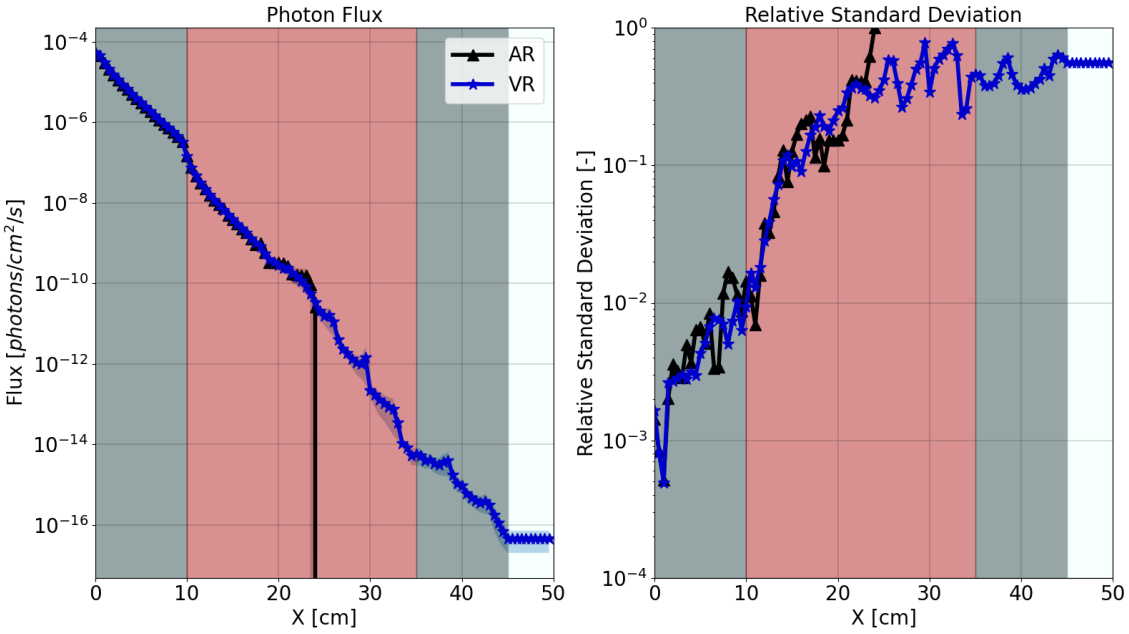

Figure 5.37: AR and VR run Photon flux

Also in the VR run there is a difference with respect to the neutrons test. In fact, the RSD with a very high number of photons simulated is close to 100 % in deep regions. The variance reduction for photons calculations seems to be more difficult than the one performed simulating neutrons.
To verify the issues with the VR for the photons the number of particles was increased and a new test performed.

Figure 5.38 shows how the variance reduction becomes less efficient compared to the neutron test as the number of histories increases. With an increase of 2 orders of magnitude in the number of particles simulated in the AR, the profile is not complete in the whole domain. The FOM comparison cannot be performed efficiently because in deep regions (where the gain of the VR is higher) the flux value is not provided by the simulation.

Table 5.20: Analog Run and VR run settings Test 2

Simulation	Particles/batch	# of batches	max # of splits
Analog (AR)	10^7	5	-
Variance Reduction (VR)	10^8	5	10^6

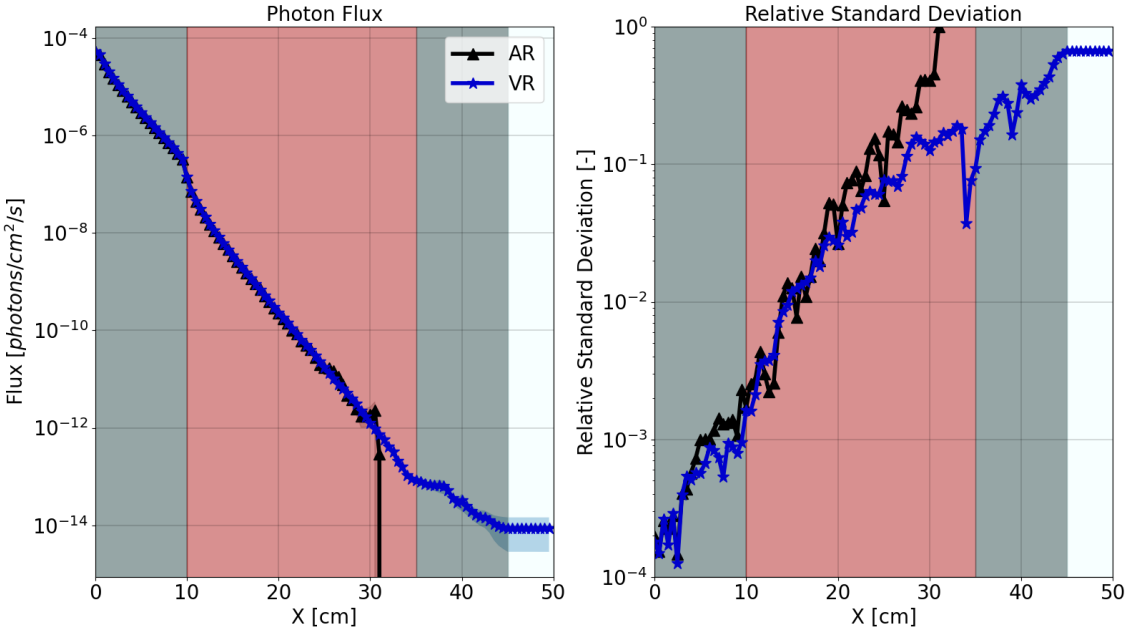

Figure 5.38: AR and VR run Photon flux Test 2

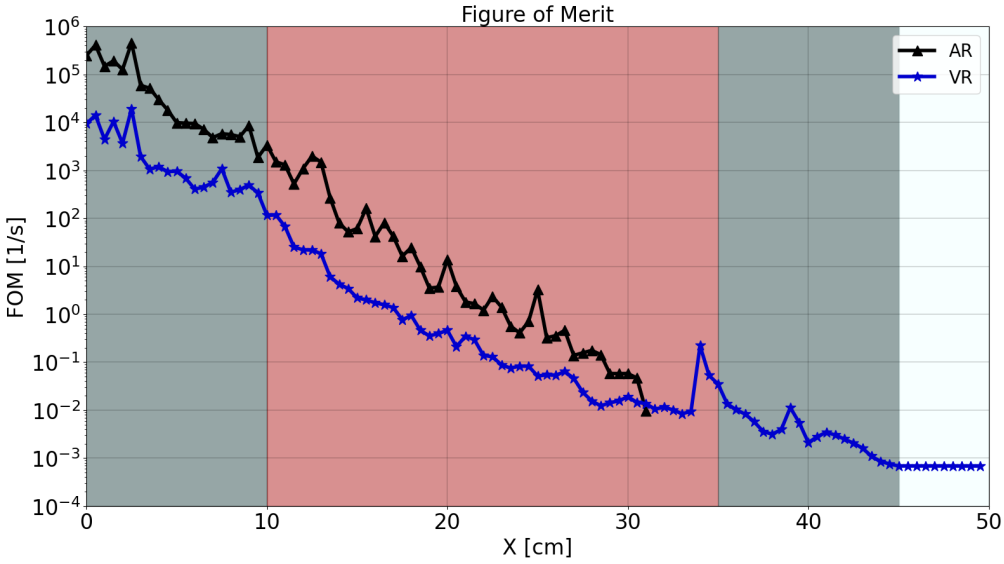

Figure 5.39: FOM Test 2 with photons

5.6 MAGIC-GPS Test

Different tests were performed to verify the effectiveness of the MAGIC-GPS method. The model chosen is the structure holding nuclear fuel presented by Wagner, Peplow and Mosher [41]. For all the tests the initial population of particles simulated during the MAGIC is equal. Moreover the same stopping criteria has been considered during the test.

Table 5.21: MAGIC and MAGIC-GPS settings and performances

Simulation	Method	Initial Population	# of batches	max # of splits	q factor	# of iterations
Test 1	MAGIC	10^3	10	10^5	1	14
Test 2	MAGIC-GPS	10^3	10	10^5	1.25	10
Test 3	MAGIC-GPS	10^4	10	10^5	2	7

Each test was performed with 2 different population for VR run (Test X.1 1E4 particles, Test X.2 1E5 particles). In the next table we analyse the results comparing:

1. The computational time necessary to fill the WW map (considering the stopping criteria)
2. The computational time of the VR run (in min)
3. The fraction of cells with a nonzero flux score (Coverage Ratio) calculated on the integrated neutron flux in the VR run
4. The fraction of cells with a relative uncertainty < 10% calculated using the Group 5 neutron flux in the VR run
5. The mean relative standard deviation (RSD) calculated using the Group 5 neutron flux in the VR run
6. The average FOM of the simulation. It is calculated using the total time (MAGIC process+VR run time) and the mean relative standard deviation

The results show that as q factor increases, the computational time of the MAGIC also increases. The trend depends on the number of particles simulated, which increases for each iteration as q factor increases. The FOM decreases following the increase of the q factor, but it is compensated by the fact that the CR increases.
The Coverage Ratio plot in Figure 5.40 shows a very slow convergence of the WW map in some groups. At the end of the MAGIC iteration process, the groups have converged, but the average coverage ratio is very low (78.15 %). Considering the main objective of MAGIC, the WW map should be as complete as possible. The use of this WW map

Table 5.22: Results Comparison

Simulation	Time MAGIC [min]	Time VR [min]	ζ[%]	Cells with RSD < 10%[%]	Mean RSD	Average FOM
1.1	8.07	16.20	34	0.39	0.559	1.32E-01
2.1	16.22	60.52	69	0.37	0.342	1.12E-01
3.1	54.40	3.62	80	0.36	0.449	8.56E-02

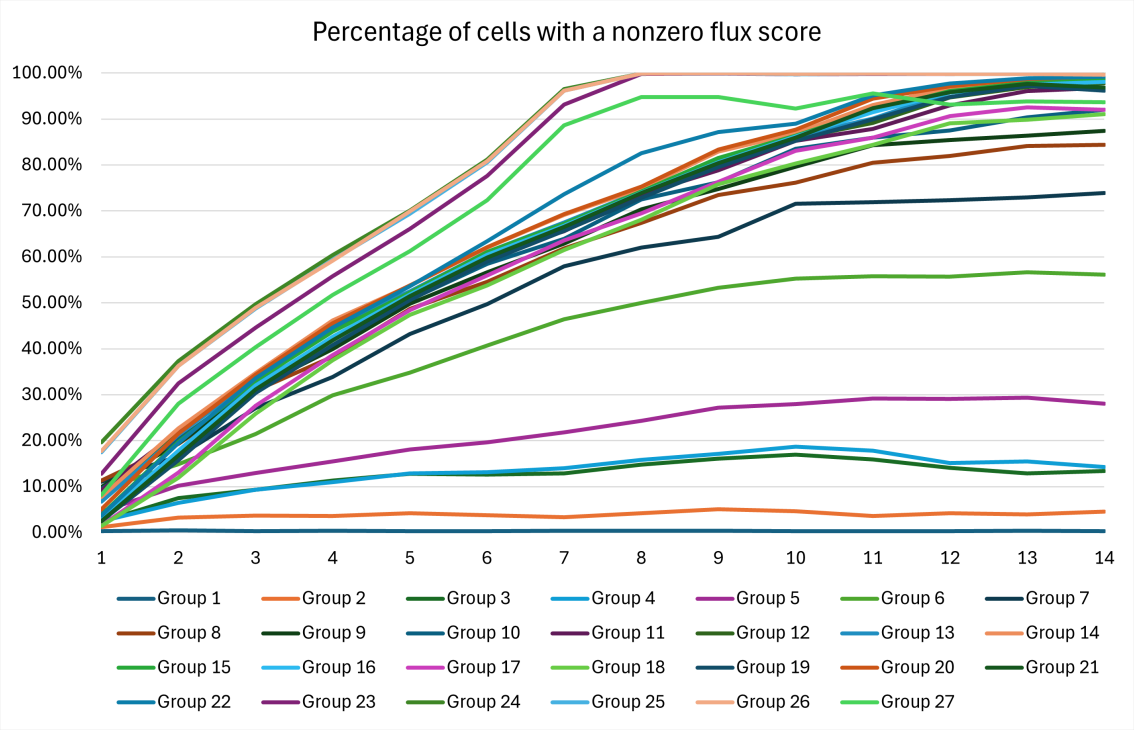

Figure 5.40: Coverage Ratio evolution during Test 1.1

might not be sufficient to obtain reliable results in the VR run. Even if the computational performance in terms of FOM is better, the flux score is not present in a very large part of the domain, as shown in Table 5.22.

The evolution of the coverage ratio in Test 2.1 shows a gain compared to the Test 1.1. In fact, the number of iterations decreases and the average coverage ratio increases to 89.03 %.
The advantage of using MAGIC-GPS is very clear in Table 5.22. The computational time is higher in the VR run, but the mean RSD is lower compared to the standard MAGIC. The Test 3.1 with a q factor equal to 2 (as recommended in [4]) shows a very high coverage, close to 80 %. Also in this case, the FOM decreases, but the flux value is present in a larger part of the domain. The reliability of this estimation can be obtained by increasing the number of particles in the VR run.
The gain is very important as it increases the number of particles in the VR run. As shown in table 5.23, the time of the VR run increases between the standard MAGIC and the

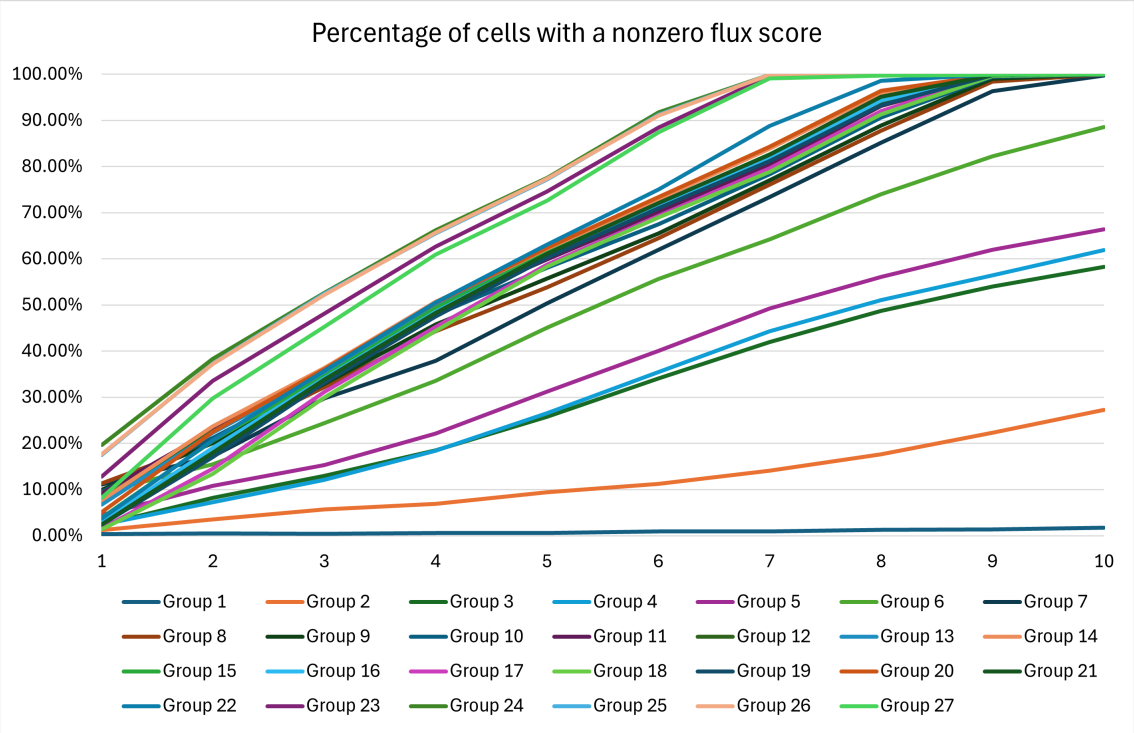

Figure 5.41: Coverage Ratio evolution during Test 2.1

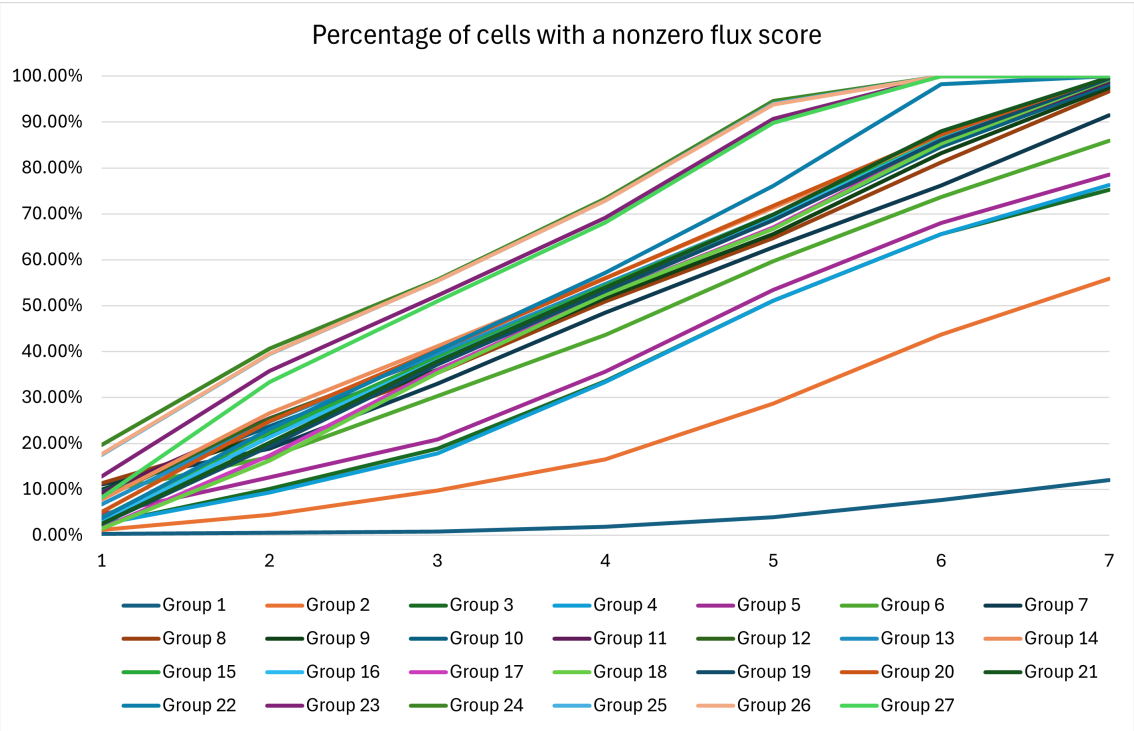

Figure 5.42: Coverage Ratio evolution during Test 3.1

MAGIC GPS with q equal to 1.25 (test 2.2). However, when the WW maps have a higher average CR, the VR run is more efficient from a computational point of view.
The time VR in test 3.2 shows that the simulation is faster than the other two tests.

Table 5.23: Results Comparison with higher number of particles

Simulation	Time MAGIC [min]	Time VR [min]	ζ[%]	Cells with RSD < 10%[%]	Mean RSD	Average FOM
1.2	8.07	174.35	43	6.74	0.461	2.57E-02
2.2	16.22	230.90	90.46	2.92	0.342	3.46E-02
3.2	54.40	44.17	100	38.19	0.181	2.63E-01

For the CR (ζ) the gain is even more evident. The test with a q factor equal to 2 allows to obtain a full flux map for the group 5, and the estimation is also more accurate. The number of cells with a lower uncertainty is much higher in Test 3, and the overall mean RSD decreases. All these considerations are condensed in the FOM, which is higher by an order of magnitude in Test 3.2 as compared to Test 2.2 and Test 1.2.

Chapter 6

Conclusions

The goal of the thesis was the investigation of a popular GVR method combining the Weight Windows (WW) approach [2] and the so-called Method of Automatic Generation of Importances by Calculation (MAGIC) method [33], with the ultimate goal of improving the performances of the calculations. The reduction of the variance in the estimation takes a key role to ensure a good quality of results and, consequently, a high degree of reliability. In this work, different models were prepared and tested (either new ones or taken from the literature) to test different problem (with neutrons and photons) that may be encountered to estimate the particle fluxes in the reactor.

The first model studied is a 1-D multi-layer structure to investigate the neutron propagation in different media, in continuous-energy mode. The results show that the WW approach using MAGIC is necessary to obtain a reliable estimate of the neutron flux profile with a low variance. Also from the computational point of view, the results show a gain through the FOM evaluation (Figure 5.4). In addition, the mesh refinement analysis was useful in highlighting saturation phenomena related to the number of spatial cells chosen for the WW generation. The tests on the mesh were also considered in relation to the distribution of cells in the different regions. However, the final FOM values suggest that the equally spaced mesh seems to be the best option for the 1D multi-layer model.

After this simple model in CE mode, the model introduced by Larsen and Becker in [45] was studied in multi-group mode (MG). The flux score is not present in a very large portion of the domain performing the AR, but the MAGIC shows an evident gain in populating the whole domain also in MG case. The modification of the scattering matrix was modified to increase the neutron absorption of the medium in order to test MAGIC algorithm in limit case. The results show that MAGIC provides reliable estimates even in this was very extreme case.

Another useful outcome of these calculations that MAGIC results seem to be dependent on the number of iterations employed. The choice of this parameter is primarily based on user experience. To mitigate the impact of this dependency on the results, a new set of stopping criteria was introduced to automatically terminate the MAGIC iterations (paragraph 5.1). To verify the effective gain in terms of computational time, a structure holding nuclear fuel was studied (paragraph 5.4). The results on the convergence of the

groups demonstrate that the filling rate is dependent on the nature of the source. Furthermore, the comparison between the MAGIC and the other VR methods considered by the authors in the literature shows a suitable match between the neutron flux estimations. The stopping criteria was tested on different mesh using the knowledge acquired in the 1-D model mesh refinement (paragraph 5.2.1), and further analysis shows that the mesh and the distribution of cells influence the convergence of the WW maps and also the number of iterations necessary to get a flux score complete in the whole domain.
In conclusion the introduction of the stopping criteria enhance the performance of the MAGIC, the iterative process converges more rapidly and tests in more complex could improve considerably the computational time necessary to generate the flux map.

The analysis considers also the transport of photons, that are relevant in the context of LFR design and licensing. The results obtained by WW and MAGIC in a new 1D model indicate that the reliability of estimation is limited due to the intrinsic physical characteristics of the photons and the methodologies employed for the weight comparison (paragraph 5.5). The Variance Reduction is less efficient as compared to the neutron test and also in terms of FOM the gain as compared to the corresponding Analog Run is lower than the previous case study. In contrast to the neutron tests, the increment in the number of particles demonstrates a minimal reduction in the RSD. This suggests that, with regard to photons, the number of histories must be slightly higher, resulting in an increase in the computational time. The reliability of the photon flux estimation occupies a fundamental role in the dose rate assessment. As a future perspective, these methods should be improved to work properly with photons as well

The improvement of the new stopping criteria is really important in the test performed. In the literature, another innovative proposal to enhance the performances of the MAGIC was considered, called MAGIC-GPS [4]. The thesis reviewed the mathematical proof of the MAGIC-GPS presented by the authors of the methodology (paragraph 3.3). The objective of the tests is to verify the effective gain of the MAGIC-GPS in a realistic problem scenario (Wagner, Peplow and Mosher model), and to determine if the coupling between the stopping criteria and the MAGIC-GPS is a chain improvement. The MAGIC-GPS improvement is based on the q factor variation, a parameter that increases the particles population at each iteration. The test is performed with the same stopping criteria but the number of iterations is very different (Table 5.22). The results in paragraph 5.6 highlight that the CR is markedly distinct between the MAGIC and the MAGIC-GPS. By elevating the q factor, a larger number of groups are populated. Consequently, the final WW map employed in the VR run is more exhaustive, and it provides more reliable flux estimation in terms of Average FOM and Mean RSD. The recommended value of the q factor mentioned in the literature is 2 [4] and the tests performed on the structure holding nuclear fuel confirm the recommendation. In conclusion the MAGIC-GPS applied with the stopping criteria improve the results and the estimation of the particle flux. Specifically, future extensions of this work will assess the sensitivity of the tolerance thresholds used in the stopping criteria to different systems and energy spectra. Another relevant aspect that should be investigated is the optimisation of the weight windows mesh generation, which could adaptively generated according to the physical characteristics of the system. Specifically, future extensions of this work will assess the sensitivity of the tolerance

thresholds used in the stopping criteria to different systems and energy spectra. Another relevant aspect that should be investigated is the optimisation of the weight windows mesh generation, which could adaptively generated according to the physical characteristics of the system. Moreover more detailed test should be performed with the photons in a more realistic problem, i.e. the reactor vessel analysis.

Bibliography

[1] M. Munk and R. N. Slaybaugh. Review of hybrid methods for deep-penetration neutron transport. 2019.

[2] R. A. Forster and T. N. K. Godfrey. Mcnp—a general monte carlo code for neutron and photon transport. Technical report, Los Alamos National Laboratory, 1981.

[3] M. A. Cooper and E. W. Larsen. Automated weight windows for global monte carlo particle transport calculations. *Nuclear Science and Engineering*, 2001.

[4] Qingquan Pan; Huanwen Lv; Songqian Tang; Xiaojing Liu. Magic-gps global variance reduction method for large-scale shielding calculation. *Nuclear Engineering and Design Volume 414*, 2023.

[5] G. I. Bell and S. Glasstone. *Nuclear Reactor Theory*. 1970.

[6] Maurizio Spurio Sylvie Braibant, Giorgio Giacomelli. *Particles and Fundamental Interactions: An Introduction to Particle Physics (1st ed.)*. Springer, 2012.

[7] Teresa Kulikowska. An introduction to the neutron transport phenomena. Technical report, Institute of Atomic Energy, Swierk, Poland, 2000.

[8] Charles F. Golub, Gene H.; Van Loan. *Matrix Computations (3rd ed.)*. Baltimore: Johns Hopkins, 1996.

[9] Wm. J. Garland. Reactor physics: Multigroup diffusion. Technical report, Department of Engineering Physics, McMaster University, Hamilton, Ontario, Canada, 2002.

[10] A. Haghighat. *Monte Carlo Methods for Particle Transport Second Edition*. CRC Press, 2021.

[11] C. J. Everett E. Cashwell. A practical manual on the monte carlo method for random walk problems. Technical report, Physics, Mathematics Mathematics of Computation, July 1960.

[12] F. B. Brown. Fundamentals of monte carlo particle transport. Technical report, Los Alamos National Laboratory, 2005.

[13] Bryan R. Herman Adam G. Nelson Benoit Forget Paul K. Romano, Nicholas E. Horelik and Kord Smith. Openmc: A state-of-the-art monte carlo code for research and development. In *Ann. Nucl. Energy, 82, 90–97*, 2015.

[14] T. E. Booth and J. S. Hendricks. Importance estimation in forward monte carlo calculations, nuclear technology - fusion. 1984.

[15] J. Spanier and E. M. Gelbard. *Monte Carlo Principles and Neutron Transport Problems*. Wesley Publishing Co, 1969.

[16] J. L. Macdonald. Investigation of pattern recognition techniques for the identification of splitting surfaces in monte carlo particle transport calculations. Technical report, Los Alamos National Laboratory, 1975.

[17] J. L. Macdonald and E. D. Cashewell. The application of artificial intelligence techniques to the acceleration of monte carlo transport calculations. Technical report, Los Alamos National Laboratory, 1978.

[18] O. L. Deutsch and L. L. Carter. Simultaneous global calculation of flux and importance with forward monte carlo.

[19] T. E. Booth and J. S. Hendricks. Deep penetration by monte carlo. Technical report, Trans. Am. Nucl. Soc., 43, 609, 2009.

[20] J. S. Hendricks. A code-generated monte carlo importance function. Technical report, Trans. Am. Nucl. Soc., 41, 307, 1982.

[21] T. E. Booth. Automatic importance estimation in forward monte carlo calculations. Technical report, Trans. Am. Nucl. Soc.,41, 308, 1982.

[22] T. E. Booth. A weight window/importance generator for monte carlo streaming problems. 1983.

[23] T. E. Booth. Genesis of the weight window and the weight window generator in mcnp-a personal history. Technical report, Los Alamos National Laboratory, 2006.

[24] W. L. Thompson; O. L. Deutsch; and T. E. Booth. A review of the theory and application of monte carlo methods. In *Proceedings of a Seminar-Workshop, Oak Ridge Tennessee*, 1980.

[25] X-5 Monte Carlo Team. Mcnp-a general monte carlo n-particle transport code, version 5. Technical report, Los Alamos National Laboratory, 2003.

[26] V. Ya. Gol'din. A quasi-diffusion method for solving the kinetic equation. 1964.

[27] M. M. Miften and E. W. Larsen. *The Quasi-Diffusion Method for Transport Problems in Multidimensional Geometries*. PhD thesis, PhD The University of Michigan, Department of Nuclear Engineering and Radiological Sciences, 1994.

[28] J. C. Wagner and A. Haghighat. Automatic variance reduction for monte carlo shielding calculations with the discrete ordinates adjoint function. In *Proc. Joint Int. Conf. Mathematical Methods and Supercomputing for Nuclear Application*, 1997.

[29] J. C. Wagner and A. Haghighat. Automated variance reduction of monte carlo shielding calculations using the discrete ordinates adjoint function. Technical report, Nucl. Sci. Eng, 1998.

[30] D. E. Peplow; E. D. Blakeman; and J. C. Wagner. Advanced variance reduction strategies for optimizing mesh tallies in mavric. Technical report, Trans. Am. Nucl. Soc, 2007.

[31] D. E. Peplow; E. D. Blakeman; and J. C. Wagner. "forward-weighted cadis method for global variance reduction. Technical report, Trans. Am. Nucl. Soc, 2007.

[32] D. E. Peplow; E. D. Blakeman; and J. C. Wagner. Forward-weighted cadis method for variance reduction of monte carlo calculations of distributions and multiple localized quantities. In *Proc. Int. Conf. Advances in Mathematics, Computational Methods, and Reactor Physics (ANS)*, 2009.

[33] A. Davis and A. Turner. Application of novel global variance reduction methods to fusion radiation transport problems. In *International Conference on Mathematics and Computational Methods Applied to Nuclear Science and Engineering (MC) Rio de Janeiro*, 2011.

[34] A. Davis and A. Turner. Comparison of global variance reduction methods for monte carlo radiation transport simulations of iter. In *In Proceedings of the 26th Symposium on Fusion Technology - SOFT-26*, 2010.

[35] A. Davis and A. Turner. Comparison of global variance reduction techniques for monte carlo radiation transport simulations of iter. *Fusion Engineering and Design Volume 86, Issues 9–11*, October 2011.

[36] Tanju Sofu. Overview of lead-cooled fast reactor (lfr) technology. Technical report, Argonne National Laboratoy, 2019.

[37] Daniele Panico and Daniele Tomatis. lbh15: a Python package implementing lead, bismuth, and lead-bismuth eutectic thermophysical properties for fast reactor applications. In ANS, editor, *Proc. of 20th International Topical Meeting on Nuclear Reactor Thermal Hydraulics (NURETH-20), Washington DC, USA*, pages 1–12, Aug 20–25 2023.

[38] Gabriele Ottino, Daniele Panico, Daniele Tomatis, and Pierre-Alexandre Pantel. lbh15: a python package for standard use and implementation of physical data of heavy liquid metals used in nuclear reactors. *Journal of Open Source Software*, 9(96):6383, 2024.

[39] T.L. Becker and E.W. Larsen. A general transform for variance reduction in monte carlo simulations. In *International Conference on Mathematics and Computational Methods Applied to Nuclear Science and Engineering. Rio de Janeiro, RJ, Brazil*, 2011.

[40] J. Leppänen; M. Pusa; T. Viitanen; V. Valtavirta; and T. Kaltiaisenaho. The serpent monte carlo code: Status, development and applications in 2013 casmo 3-group-structure. available online: https://serpent.vtt.fi/mediawiki/index.php/casmo_3-group_structure. *Ann. Nucl. Energy, 82*, 2011.

[41] J. C. Wagner; D. E. Peplow; and S. W. Mosher. Fw-cadis method for global and regional variance reduction of monte carlo radiation transport calculations. *Nuclear Science and Engineering : 176, 37–57*, 2014.

[42] D. E. Peplow. Comparison of hybrid methods for global variance reduction in shielding calculations. In *MC 2013, Sun Valley, Idaho, May 5-9*, 2013.

[43] M. A. Jessee W. A. Wieselquis, R. A. Lefebvre. Scale code system. Technical report, OAK RIDGE NATIONAL LABORATORY, 2020.

[44] E. W. Larsen T. L. Becker. The application of weight windows to 'global' monte carlo problems. In *ANS Math. Comp. Top. Meeting, Saratoga Springs, New York, May 3-7*, 2009.

[45] T. L. Becker. Hybrid monte carlo/deterministic methods for deep-penetration problems. Technical report, Doctoral Dissertation, University of Michigan, 2009.

[46] D. E. Peplow; E. D. Blakeman and J. C. Wagner. Advanced variance reduction strategies for optimizing mesh tallies in mavric. Technical report, Transactions of the ANS 97, 595-597, 2007.

[47] J. C. Wagner; D. E. Peplow and S. W. Mosher. Fw-cadis method for global and semi-global variance reduction of monte carlo radiation transport calculations. Technical report, Nuclear Science and Engineering, 2013.

[48] D. E. Peplow; E. D. Blakeman; and J. C. Wagner. Advanced variance reduction strategies for optimizing mesh tallies in mavric. *Trans. Am. Nucl. Soc., 97, 595*, 2007.

[49] J. K. Shultis e R. E. Faw. *Radiation Shielding*. Published by the American Nuclear Society, Inc. La Grange Park, Illinois 60526 USA, 2000.